Organisation for Economic Co-operation and Development

ENV/JM/MONO(2020)21/ANN3

Unclassified English - Or. English

24 September 2020

ENVIRONMENT DIRECTORATE
JOINT MEETING OF THE CHEMICALS COMMITTEE AND THE WORKING PARTY ON CHEMICALS, PESTICIDES AND BIOTECHNOLOGY

ANNEX III: In silico models - detailed description of methods and generated data WITHIN CASE STUDY ON THE USE OF INTEGRATED APPROACHES TO TESTING AND ASSESSMENT FORREAD-ACROSS BASED FILLING OF DEVELOPMENTAL TOXICITY DATA GAP FOR METHYL HEXANOIC ACID

Series on Testing and Assessment
No. 325

The corresponding annexes are available under the following cotes:
ENV/JM/MONO(2020)21

JT03465710

This document, as well as any data and map included herein, are without prejudice to the status of or sovereignty over any territory, to the delimitation of international frontiers and boundaries and to the name of any territory, city or area.

Annex III. In vitro models - detailed description of methods and generated data

HDAC-1: QPRF HDAC inhibition

TK-1: TK model description for ZET

TK-2: TK model descriptions CALUX

TK-3: TK model description for mEST & UKN1

PBPK-1: PBPK model description for mouse

PBPK-1: PBPK model description for human

Class-1: Dempster-Schafer Classification model description

Class-2: Bayesian Automatic Classification model description

Class-3: Biological Fingerprint Classification model description

1. HDAC-1: QPRF HDAC inhibition

Predicting the Likelihood of Induction of Exencephaly in Rodents

1. Substance

- Compound name: 2-Methylhexanoic acid
- CAS. No: 4536-23-6
- EC Number: 224-883-9
- Structural smile: CCCCC(C)C(=O)O
- InChl: 1S/C7H14O2/c1-3-4-5-6(2)7(8)9/h6H,3-5H2,1-2H3,(H,8,9)
- Structural formula: C7H14O2
- 2D structure:

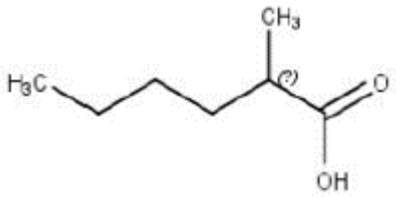

2. General information

2.1 Date of QPRF: 01 September 2017".

2.2 QPRF author and contact details:

Jaffar Kisitu

jaffar.kisitu@uni-konstanz.de

AG.Leist, Konstanz Research School of Chemical Biology

3. Prediction

3.1 Endpoint (OECD Principle 1)

a. Endpoint: *induction of exencephaly*

b. Dependent *variable: Teratogenic potential*

This parameter is a three-level factor i.e. teratogens (> ++), borderline-teratogens (+) and Non-teratogens (0). The + is a scale derived in the Nau-protocol based study in mice on the rate of induction of exencephaly. This measure scales the dose administered to the rate of induction of exencephaly. The scales spans between 0 and +++++ in increasing order of the rate of induction of exencephaly at deceasing dose levels.

3.2 Algorithm (OECD Principle 2)

a. Model or submodel name:

LDA-Developmental toxicity potential

b. Reference to QMRF:

This model has been newly compiled.

c. Table.2. Predicted value (model result):

Compound Name	*In vivo* behaviour	Predicted behaviour
2-Propylheptanoic Acid)	Teratogenic	Teratogenic
2-Propypentanoic Acid	Teratogenic	Teratogenic
2-Propyl-4-pentenoic Acid	Teratogenic	Teratogenic
2-Ethylhexanoic acid	Teratogenic	Teratogenic
4-Pentenoic Acid	Non-Teratogenic	Non-Teratogenic
2-Methylhexanoic Acid	Non-Teratogenic	Non-Teratogenic
2-Methylpentanoic Acid	Unknown	Non-Teratogenic
2-Ethylbutanoic Acid	Non-Teratogenic	Borderline-Teratogen
Hexanoic Acid	Unknown	Non-Teratogenic
2,2-dimethylpentanoic Acid	Non-Teratogenic	Non-Teratogenic

These compounds were tested according to the Nau-protocol for exencephaly and graded according to their teratogenic potential to generate values between 0 to +++++. This was generated by taking into account the rate of induction of exencephaly and dose of the administered analogue. In this prediction, Teratogens were those analogues with teratogenic potential > ++, borderline-teratogens (+) and non-teratogens (0). The output from the model is a probability of belonging to any of the three groups and the final categorisation for a particular analogue is based on maximum likelihood based on the probability.

d. Predicted value (comments):

The predicted value of the analogues used in this prediction model is a semi-quantitative output generated as a posterior probability of an analogue being able to induce a certain level of exencephaly in rodent embryos at or below a specified dose.

e. Descriptor values:

For the analogues used in developing the prediction model, see table 3. The descriptors used in developing the prediction model are qualitative structure-activity relationships features for the model compounds derived from *in vivo* observations. These were text mined from literature in which model compounds had been tested in *in vivo* studied. Such descriptors included:

- whether the analogue was branched
- had an unsaturated bond
- any other branching apart from the C2 branch
- the branch length and
- Whether the analogue exists in enantiomeric forms.

The other features were physicochemical parameters considered based on the fact that this group of compounds are weak electrolytes and that their toxicokinetics is very much dependent on such parameters.

These included:

- the number of carbon atoms (molecular weight)
- LogP
- pKa and
- LogD at pH 7.7.

The pH 7.7 simulated the embryonic pH on days 11 and 8 of neural tube closure in rats and mice respectively.

The last descriptor added to the prediction model was the respective EC50 value for HDAC inhibition. This was added as a biological layer to strengthen the prediction and embody any unconsidered relevant biological factors.

3.3 Applicability domain (OECD principle 3)

a. Domains:

i. descriptor domain :

The chemicals onto which the prediction model was applied belong to the same chemical class i.e. carboxylic acids. The descriptors used in this prediction model were parameterised (transformed into numbers) qualitative structural features seen from *in vivo* studies of this compound group and concluded to be associated with the teratogenic effects including exencephaly, the target endpoint for this prediction model. The other descriptor added along to these structural features is a biological layer of histone deacetylase inhibition (HDACi). This biological endpoint has been pinpointed as the molecular initiating event in the adverse outcome pathway for the development of neural tube defects as a result of exposure to this compound group. It was therefore added as a layer to bridge any unconsidered relevant biological phenomena. The descriptors therefore used in this model fit for all compounds for which predictions are made i.e. this model was built specifically for this compound class.

ii. structural fragment domain

All model compounds belong to the same chemical class. The analogues in the training set contain the same structural features as those in the test set. The predicted compounds, therefore, share the same structural fragments as other analogues used in building the prediction model.

b. Structural analogues:

See table 3 below

Table.3. Structural analogues used in the development of the prediction model

Analogue	CAS.No	Smile Structure	Source	Experimental observation
2-Propylpentanoic acid	99-66-1	CCCC(CCC)C(=O)O	Training	Positive
2-Propyloctanoic acid	31080-41-8	CCCCCCC(CCC)C(=O)O	Training	Positive
2-Propylheptanoic acid	31080-39-4	CCCCCC(CCC)C(=O)O	Training	Positive
2-Propylhexanoic acid	3274-28-0	CCCCC(CCC)C(=O)O	Training	Positive
2-Propyl-4-pentenoic acid	1575-72-0	CCCC(CC=C)C(=O)O	Training	Positive
2-Propyl-2-pentenoic acid	60218-41-9	CCCC(=CCC)C(=O)O	Training	Negative
2-Ethyl-4-methylpentanoic acid	108-81-6	CCC(CC(C)C)C(=O)O	Training	Negative
2-Ethylhexanoic acid	149-57-5	CCCCC(CC)C(=O)O	Training	Positive
2-Methyl-2-propypentanoic acid	31113-56-1	CCCC(C)(CCC)C(=O)O	Training	Positive
2-Methyl-2-pentenoic acid	3142-72-1	CCC=C(C)C(=O)O	Training	Negative
2-Ethyl-3-methylpentanoic acid	22414-77-3	CCC(C)C(CC)C(=O)O	Training	Negative
2-Isopropylpentanoic acid	62391-99-5	CCCC(C(C)C)C(=O)O	Training	Negative
2-Methylpentanoic	20225-24-5	CCCC(CC)C(=O)O	Test	Unknown
2,2-Dimethylpentanoic acid	3115-28-4	CCCCC(CCCC)C(=O)O	Test	Negative
2-Ethylbutanoic acid	88-09-5	CCC(CC)C(=O)O	Test	Negative
Hexanoic acid	97-61-0	CCCCCC(=O)O	Test	Unknown

c. Considerations on structural analogues:

For those compounds with *in vivo* data, the model predictions are in line with reported observations such that active analogues are predicted as so and inactive analogues likewise save for 2-ethylbutanoic acid, an *in vivo* inactive analogue that is predicted to have weak teratogenicity. For the target analogue, 2-methylhexanoic acid, the prediction model just like the *in vivo* studies deem this compound as a non-teratogen at a dose less than 3mmoles/Kg of body weight in mice, on the dose-exencephaly rate scale. However, other studies have reported this analogue not to induce Valproic acid like effects at doses greater than 6mmoles/Kg of body weight in rodents. For the predictions of the other case study compounds, refer to the table under section 3b.

3.4 The uncertainty of the prediction (OECD principle 4)

The teratogenic effects of valproic acid and its analogues is attributed to the parent compound and not the metabolites. Therefore, this prediction model assumes that all analogues are able to reach the embryo but only a selected set turns out to be actively teratogenic. The uncertainty in this respect lies in the fact that some analogues may be metabolised faster than others, which renders them inactive. Additionally, enterohepatic circulation has not been reported for all analogues. Therefore, this prediction includes a

small uncertainty due to non-consideration of the rate of metabolism. However, this is considered in the overall interpretation of the model.

3.5 The chemical and biological mechanisms according to the model underpinning the predicted result (OECD principle 5).

The proposed adverse outcome pathway for the induction of neural tube defects due to the exposure to valproic acid and its analogues points to the inhibition of histone deacetylase (HDAC) enzymes as the molecular initiating event. In most cases, save for the unbranched analogues, potent HDAC inhibitors induce high rates of exencephaly in rodents. Such analogues additionally have a branched structure at the second carbon atom of at least 2 carbon atoms and with the carbon chain being ≥ 5 carbon atoms. The introduction of unsaturated bonds specifically in the C4-C5 position and more so the triple bond, leads to enhanced HDAC inhibition and hence more teratogenicity.

4. Adequacy

4.1 Regulatory purpose:

Currently, there is no regulatory application of the prediction model. However, in the event that it should be fixed for use, the model could be used as inclusions in drug leaflets and box warnings of the possible adverse effects likely to arise from excessive exposure to any of the analogues deemed to teratogenic.

4.2 Approach for regulatory interpretation of the model result:

Branched-chain carboxylic acid like valproic acid analogues may present some degree of teratogenic effects.

4.3 Outcome:

The interpretation of the model is that unsaturated valproic acid analogues with a branched chain structure and which are potent HDAC inhibitors have a high probability of inducing teratogenic effects.

4.4 Conclusion:

The prediction provided in this model though supported by biological data may not be adequate in a situation where an analogue is predicted to have weak teratogenic effects. In this situation, additional redress may be sought by applying an *in vitro* method that is able to assess the DART effects of this group of compounds.

2. TK-1: TK model description for ZET

PBPK modelling of zebrafish embryo for reprotoxicity assessment of valproic acid and some of its analogues

Siméon S[1], Brotzmann K[2], Fisher C[3], Gardner I[3], Maclennan R[4], Bois F[1]

[1]INERIS, METO unit, Parc ALATA BP2, Verneuil en Halatte, France

[2]University of Heidelberg, Aquatic Ecology and Toxicology, Centre for Organismal Studies (COS), Im Neuenheimer Feld 504, D-69120 Heidelberg, Germany

[3]Simcyp Ltd., Blades Enterprise Centre, John Street, Sheffield S2 4SU, United Kingdom

[4]Cyprotex Discovery Ltd., BioHub at Alderley Park, Ardeley Edge, Cheshire, SK10 4TG, United Kingdom some of its analogs

Introduction

Understanding and predicting chemicals' effects on development and reproduction is a complex challenge in toxicology. In the European project *Eu-ToxRisk*, *in silico* and *in vitro* tools are being developed for toxicity read-across, and exercised in specific case studies. One of those case-studies focuses on the developmental toxicity of valproic acid (VPA) and nine of its analogues: 2,2-dimethylvaleric acid, 2-ethylbutyric acid, 2-ethylhexanoic acid, 2-methylhexanoic acid, 2-methylpentanoic acid, 2-propylheptanoic acid, 4-ene-valproic acid, 4-pentenoic acid and hexanoic acid.

VPA is an antiepileptic and a thymoregulator prescribed during manic episodes of bipolar disorder. It exerts its pharmacological effects mainly in the central nervous system, but its mechanism of action is not well known (Sztajnkrycer 2002). It is a notorious teratogen, inducing neural tube defects (Phiel *et al.* 2001). Chemicals with similar structure can be inferred to have similar hazardous properties, but this should be backed-up at least by *in silico* and *in vitro* evidence.

Among the *in vitro* test systems available to us, the zebrafish embryo is a real asset, for various reasons. First, its transparency allows to detect morphological malformations visually, without interrupting development or invasive interventions (Bernut, Lutfalla, and Kremer 2015). Second, the number of eggs laid is high and their development time is short (120 hours) (Goldsmith and Jobin 2012). Third, it is a small organism, easy to husband in the laboratory (Hill *et al.* 2005). Finally, gene homologies between zebrafish and humans, at the amino acid sequence level and at the messenger RNA distribution level, have been shown. This suggests that specific genes play similar roles during development and that evidence obtained with zebrafish embryos should be transposable humans (Ekker and Akimento 1991) (Howe *et al.* 2013). One important step in such inter-species or *in vitro* to *in vivo* extrapolations is to account for differences in pharmacokinetics between the systems studied and the target species (Quignot, Hamon, and Bois 2014). Those differences translate into differences in target organ concentrations for the same systemic exposure dose.

Physiologically-based pharmacokinetic (PBPK) models are *in silico* modelling tools specifically designed to estimate target organ concentrations of therapeutic drugs or toxicants (Feng *et al.* 2018). PBPK models connect anatomy, physiology, and biochemistry

processes to understand a chemical's fate in the body, using physiological parameters. They allow predictions of chemicals' concentration–time profiles in experimentally inaccessible organs from minimal data. In doing so, they provide mechanistic insight into toxicity and reduce the time, cost and need for experimental animal studies (Khazaee and Ng 2018).

To better explain, predict, and extrapolate developmental toxicity observed in zebrafish embryo, we developed a PBPK model which integrates organ volume changes during development and hepatic metabolism. Our zebrafish embryo model is based on Péry *et al.* (2014) adult zebrafish model and on the Simcyp® virtual *in vitro* intracellular distribution (VIVD) model (Fisher *et al.*, submitted). The model assumes quasi steady-state distribution between various zebrafish cell types (tissues). The partition coefficients between the various organs and organelles considered by the model (yolk, liver, gut, muscle, skeleton, eye, brain, heart, skin, other tissues, lysosomes, and mitochondria) and the culture medium, are conditioned by the chemical of interest physiochemical properties (*pH* acidic, basic, neutral or amphoteric character of the molecule, *etc*.)

We describe here the model and demonstrate, for VPA and its analogues, how the model can be used to base toxic effect measures, such as EC_{10}, on internal concentrations.

Materials and methods

Chemicals

The chemicals studied are valproic acid and nine analogues; 2,2-dimethylvaleric acid, 2-ethylbutyric acid, 2-ethylhexanoic acid, 2-methylhexanoic acid, 2-methylpentanoic acid, 2-propylheptanoic acid, 4-enevalproic acid, 4-pentenoic acid and hexanoic acid.

Zebrafish experiments

The zebrafish embryo experiments were carried out according to the OECD test guideline 236 (2013) on fish embryo acute toxicity testing of chemicals. Briefly, test duration was 120 hours post fertilization (hpf) with malformation observations at 24, 48, 72, 96 and 120 hpf. Two to eight concentrations were tested per chemical. The tests were performed on 24-well plates, with one embryo per well in 1 mL of culture medium, and with 4 control embryos per plate. The culture medium was replaced daily. Each test was performed twice or thrice with embryos from different spawns. Three reference plates were used: a negative control, a positive control and a plate with culture medium (containing 0.1% of DMSO).

The various nominal concentrations used are given in Table 2, in the Results section.

Analytical methods

Cyprotex® did chromatography concentration measurements in the embryo and in the culture medium 120 hpf, for the ten chemicals studied at different nominal concentrations.

PBPK model

Figure 1 presents the schematic structure of the zebrafish embryo we developed. Ten compartments are considered: yolk, liver, gut, eye, brain, heart, skin, muscles, other organs and tissues. Mitochondria and lysosomes in tissues (except the yolk) form two additional compartments (not represented on Figure 1). These organelles have a specific critical pH of 4.5 for lysosomes and 8 for mitochondria, leading 'ion trapping' (sequestration of compounds because of their differential ionization between organelles and cellular medium). Given the small size of the embryo, instantaneous diffusion is assumed.

Figure 1. Structure of zebrafish embryo model. Chemical partition between the various compartments and can metabolized in the liver.

Cl_{met} is the metabolic clearance.

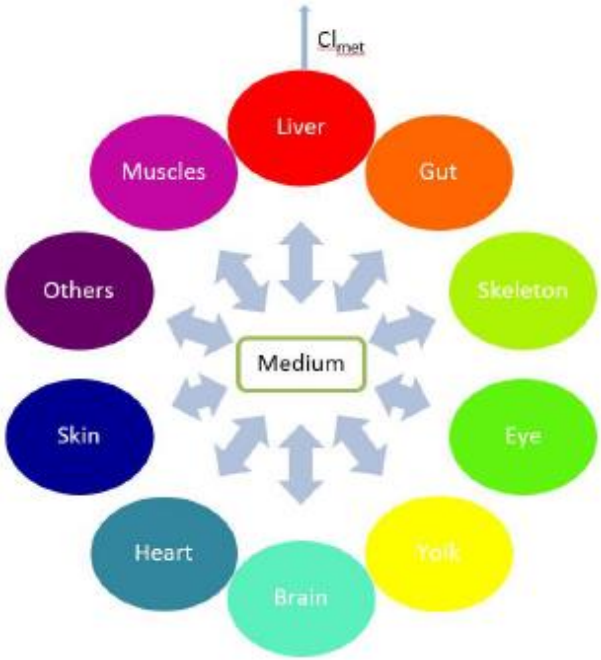

Model equations

The total quantity of parent molecules in the system (Q_{parent}) is a function of time, as is the quantity metabolized (Q_{met}), and computed as:

$$Q_{parent} = Dose - Q_{met} \quad (1)$$

where Dose is the quantity of parent chemical introduced in the test system at time zero or at medium replacement time.

Metabolism is assumed to be linear in the embryo. The total quantity of metabolites formed per unit time in system is proportional to the number of liver cells (N_{cell}), metabolic clearance per liver cell (Cl_{met}) and the chemical concentration in liver (C_{liver}).

$$\frac{Q_{met}}{dt} = N_{cells} \times K_{met} \times C_{liver} \quad (2)$$

N_{cell} is calculated from liver volume (V_{liver}) and hepatocyte volume (V_{hep}).

$$N_{cells} = \frac{V_{liver}}{V_{hep}} \quad (3)$$

Concentrations in organs, lysosomes and mitochondria (C_i), are assumed to be at any time proportional to the concentration unbound in medium ($C_{medium,u}$). The proportionality factors are the organs, yolk, lysosomes or mitochondria over medium unbound partition coefficients ($P_{mu:i}$):

$$C_i = P_{mu:i} \times C_{medium,u} \quad (4)$$

$C_{medium,u}$ is computed according to:

$$C_{medium,u} = \frac{Q_{parent}}{\frac{V_{medium}}{fu_{diluted}} + P_{a:w} \times fu_i \times V_{air} + P_{p:w} \times S_{medium} + \sum(P_{mu:j} \times V_j)} \quad (5)$$

where V_{medium} is the volume of culture medium, $fu_{diluted}$ the fraction unbound in medium corrected for serum dilution, fu_i the fraction unionized in medium, $P_{a:w}$ and $P_{p:w}$ are respectively air and plastic to water partition coefficient, V_{air} the volume of air in head space, S_{medium} the surface area of medium in contact with plastic. V_j includes the volumes of yolk, liver, gut, muscle, skeleton, eye, brain, heart, skin, and other tissues.

Finally, the total concentration in medium (C_{medium}) is:

$$C_{medium} = \frac{C_{medium,u}}{fu_{diluted}} \quad (6)$$

V_{air} is computed as the difference between well volume and medium, embryo and yolk volumes:

$$V_{air} = V_{well} - V_{medium} - V_{embryo} - V_{yolk} \quad (7)$$

We model the developing embryo and it is necessary to consider organ growth. The time-evolution of the volumes of liver, gut, muscle, skeleton, eye, brain, heart, skin, and other tissues (V_k) is computed using the following equation:

$$V_k = e^{K_{g,k} \times (t - \tau_k)} - 1 \quad (8)$$

where τk is the time of growth initiation of organ k. Before τk, organ volumes are equal to zero. The organ growth rates ($K_{g,k}$) were fitted to data on embryo volume time course:

Embryo volume without yolk (V_{embryo}) is computed as:

$$V_{embryo} = 0.005 \times 10^{-6} \times e^{+0.000750 \times t} \quad (9)$$

The yolk volume (V_{yolk}) is given by:

$$V_{yolk} = 0.268 \times 10^{-6} \times e^{-0.000417 \times t} \quad (10)$$

Muscle volume (V_{muscle}) is computed by the difference between the embryo volume and the sum of the volumes V_k.

$$V_{muscle} = V_{emvryo} - \sum V_k \quad (11)$$

The time-evolution of the various volumes is illustrated on Figure 2. After 100 hpf, muscles contribute in majority to the embryo growth.

Figure 2. Zebrafish embryo organ growth and total embryo growth (black line).

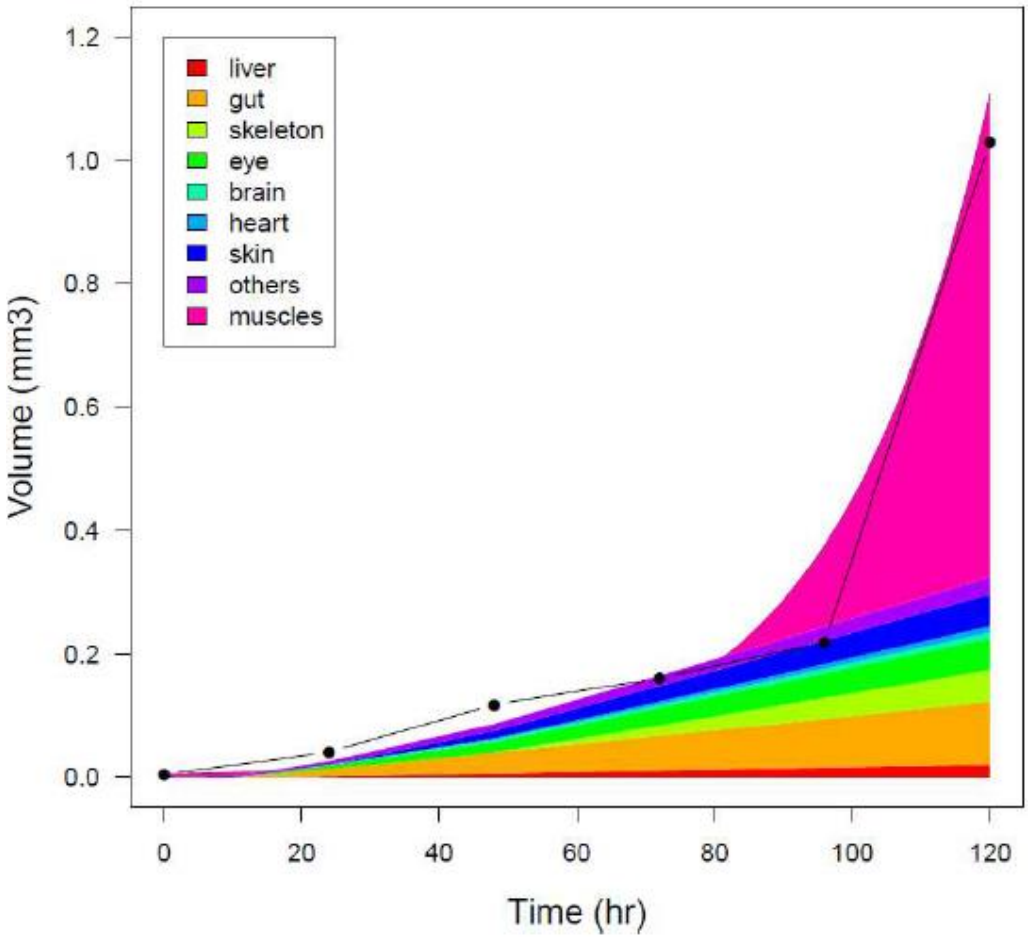

Air concentration depends on the air to water partition coefficient and fraction unionized in medium.

$$C_{air} = P_{a:w} \times C_{medium,u} \times fu_i \quad (12)$$

Similarly, plastic concentration depends on the plastic to medium unbound partition coefficient.

$$C_{plastic} = P_{p:w} \times C_{medium,u} \quad (13)$$

The quantity in medium (Q_{medium}) depends on concentration unbound in medium, adjusted by fraction unbound, corrected for serum dilution.

$$Q_{medium} = \frac{C_{medium,u}}{fu_{diluted} \times V_{medium}} \quad (14)$$

Quantities in organs, yolk and air (Q_i) are simply computed as:

$$Q_i = C_i \times V_i \quad (15)$$

The quantity on plastic ($Q_{plastic}$) is related to the surface area of medium in contact with plastic.

$$Q_{plastic} = C_{plastic} \times S_{medium} \quad (16)$$

The quantity in lysosomes (Q_{lyso}) and mitochondria (Q_{mito}) depend on the volume of the embryo and the fractions of lysosome (f_{lyso}) and mitochondria (f_{mito}) in cells, respectively.

$$Q_{lyso} = C_{lyso} \times V_{embryo} \times f_{lyso} \quad (17)$$

$$Q_{mito} = C_{mito} \times V_{embryo} \times f_{mito} \quad (18)$$

The length of the embryo was calibrated with data from Kimmel (Kimmel *et al.* 1995).

$$L_{embryo} = \mathrm{A} \times \frac{t^B}{C^B + t^B} + D \quad (19)$$

where A = 0.0260 dm, B = 4.397, C = 1617 minutes and D = 0.00755 dm.

Model parametrization

Experiments on zebrafish embryos were carried out in 24-well plates, and the substances studied were assumed partition instantaneously on plastic, in air and embryo. Partition coefficient are known to depend on the molecules' physicochemical properties (*logP*; Henry's constant; *pKa*; compound's character: mono or dibasic, mono or diacid, neutral, ampholyte; molecular weight; blood to plasma ratio and fraction unbound in bovine serum, *pH* and membrane potential. The Simcyp® VIVD model takes these properties into consideration to determine the partition coefficient of each molecule, namely: fraction unbound in medium, corrected for serum dilution ($fu_{diluted}$); fraction unionized in medium (fu_i), polymer to water partition coefficient ($P_{p:w}$); air to water partition coefficient ($P_{a:w}$); medium unbound to organs (liver, gut, muscle, skeleton, eye, brain, heart, skin, others), yolk, lysosomes and mitochondria partition coefficient ($P_{mu:i}$).

The Figure 3 shows the schema of VIVD model. It predicts the unbound concentration in culture media by calculating a hypothetical volume of distribution accounting for binding to serum components, binding to plastic, distribution into the air in the headspace above media and distribution into the cultured cells. The Henry's law constant describes distribution into the headspace. Binding to plastic is defined by a previously described model based on *logP* (Kramer *et al.* 2010).

Figure 3. Schematic representation of the *in vitro* distribution model.

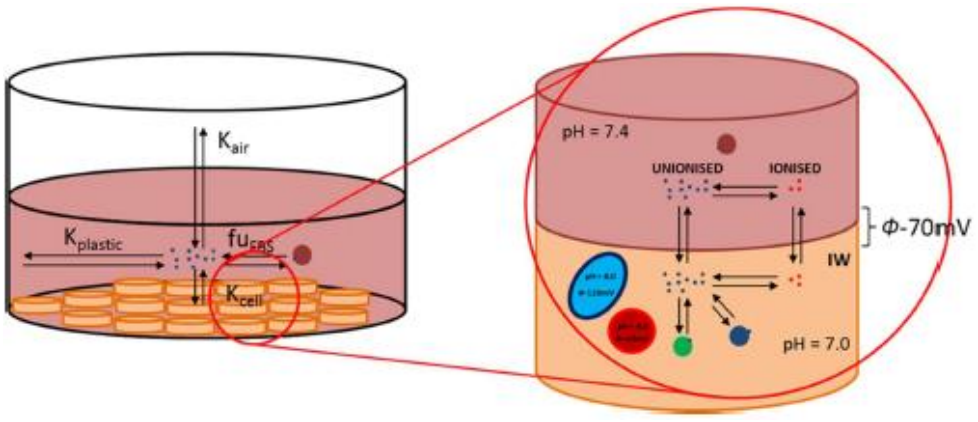

The other parameters are given in Table 1.

Table 1. Physiological parameter values of the model.

Parameters	Symbols	Units	Values	References
Initial organ growth time		Minutes		
Liver	T_{liver}		960	Brotzmann K
Gut	T_{gut}		600	-
Skeleton	$T_{skeleton}$		2880	-
Eyes	T_{eyes}		660	-
Brain	T_{brain}		540	-
Heart	T_{heart}		1800	-
Skin	T_{skin}		1440	-
Other tissues	T_{others}		0	-
Organ growth rate		$Minutes^{-1}$		
Liver	$k_{g, liver}$		3.35×10^{-6}	(adjusted)
Gut	$k_{g, gut}$		1.47×10^{-6}	-
Skeleton	$k_{g, skeleton}$		1.16×10^{-6}	-
Eyes	$k_{g, eyes}$		7.68×10^{-6}	-
Brain	$k_{g, brain}$		1.40×10^{-6}	-
Heart	$k_{g, heart}$		1.90×10^{-6}	-
Skin	$k_{g, skin}$		8.72×10^{-6}	-
Other tissues	$k_{g, others}$		3.75×10^{-6}	-
Volume of culture well	V_{well}	L	0.034	OECD
Volume of culture medium	V_{medium}	L	0.001	-
Volume of liver cell	$V_{cell\ liver}$	L	10^{-12}	
Fraction lysosome in cells	f_{lyso}	-	0.01	
Fraction mitochondria in cells	fmito	-	0.1	
Surface area of medium in contact with plastic	S_{medium}	dm^2	0.0513	

Estimation of metabolic clearance

The metabolic clearance of each compound was estimated by Markov Chain Monte Carlo (MCMC) simulations in Bayesian framework using data on culture medium and embryo concentration at 120 hpf (Smith and Roberts 1993).

The prior distribution of metabolic clearance was assumed to be uniform from 0 to 10^{-10} L/min except for 2-propylheptanoic acid and 4-ene-valproic acid for which the maximum had to be set at 10^{-9} L/min.

The data likelihood was assumed to be log-normal around the model prediction with geometric standard deviation σ (estimate of residual uncertainty). σ was assumed to be distributed normally around 1.5 ± 1.5 SD with a truncation from 1.5 to 10 (i.e a vague prior).

Two Markov chains were simulated and one in two samples were recorded. 10000 iterations were carried out for each chemical. Convergence of the two chains was assessed using Gelman and Rubin's Rhat convergence criterion (Gelman and Rubin 1992).

Software

The static model equations have been coded in R version 3.4.3 (R Development Core Team 2013) and used for computing partition coefficients, $fu_{diluted}$ and fu_i. All simulations, including MCMC simulations, of the dynamic model were performed with GNU MCSIM version 5.6.6 (Bois, F.Y. 2009).

Results

Kinetic data

The Table 2 shows the concentration measurement results in the embryo and medium at 120 hpf. For Valproic acid, a measurement was also made after 72 hpf.

Table 2. Nominal concentrations (µmol/L) used to study compound's kinetic, and embryo and medium concentrations (µmol/L) measured at 120 hpf.

Compound	Nominal concentration	Embryo concentration	Medium concentration
Valproic acid	6.25	0.779	4.471
	12.5	1.377	9.169
	25	1.728	19.1
	50	2.979	50.94
	100	4.469	66.34
	200	8.217	167.9
	400	8.082	238.3
	400*	84.43*	374.9*
2,2-dimethylvaleric acid	312.5	16.15	298.4
	500	48.38	556.3
2-ethylbutyric acid	100	0.5855	173.1
	200	2.329	87.6
	400	36.15	431.2
	800	55.84	586.4
2-ethylhexanoic acid	12.5	1.206	12.99
	25	1.425	29.79
	50	1.487	57.59
	100	3.542	93.66
	200	16.74	167.6
2-methylhexanoic acid	125	0.163	175.5
	250	0.3339	319.9
	500	39.94	638
2-methylpentanoic acid	177.7	0.7072	286.5
	266.6	1.805	371.7
	400	7.684	613.8
	600	93.53	761.6
2-propylheptanoic acid	12.5	0.7864	13.65
	25	1.231	26.59
	50	1.308	52.35
4-ene-valproic acid	200	14.95	271.2
	400	89.91	414
4-pentenoic acid	500	N/A	480.8
	1000	122.7	860.3
Hexanoic acid	520	0.6918	558.9
	625	218.8	500

* Measurements at 72 hpf.

Partition coefficient estimation

The parameter's value obtained with the VIVD model are given in the Table 3.

For each compound, the fraction unbound in medium corrected from serum dilution is high and comprised in the interval [75.5:99.6] percent. One exception for 2-propylheptanoic acid which has a low $fu_{diluted}$, 19.2%.

Each compound is in majority present under ionized form in the medium. 2,2-dimethylvaleric acid, 2-methylpentanoic acid and 4-pentenoic acid have the same fraction unionized in the medium (fu_i), 0.99%. 2-ethylbutyric acid and 4-ene-valproic acid have a fu_i equal to 0.315%. For 2-ethylhexanoic acid, 2-propylheptanoic acid and valproic acid the fu_i 0.627%. 1.24% for the 2-methylhexanoic acid and 0.788% for the Hexanoic acid.

The partition coefficient on plastic are difficult to interpret directly. It is better to compare the quantity bound to plastic and present in water. For a parent quantity of 1 µmol, the plastic quantity is about 2×10^{-3} µmol (0,2%). It is useful to check the low impact of materials used on the kinetic of the test chemical.

All compounds partition rather in yolk than in medium, except for 2-propylheptanoic acid.

All compounds have higher affinity for the other embryo tissues than for medium.

Affinity for lysosomes is ten or hundred higher than for the other compartments for all compounds, except for 2-propylheptanoic acid.

Table 3. Physicochemical parameter value predicted by the VIVD model, for VPA and nine analogues.

Parameter	Symbol	Value					
		Valproic acid	**2,2- dimethylvaleric acid**	**2-ethylbutyric acid**	**2-ethylhexanoic acid**	**2-methylhexanoic acid**	**2-methylpentanoic acid**
Fraction unbound in medium corrected from serum dilution	$fu_{diluted}$	7.55×10^{-01}	9.51×10^{-01}	8.80×10^{-01}	8.24×10^{-01}	9.25×10^{-01}	9.79×10^{-01}
Fraction unionized in medium	fu_i	6.27×10^{-03}	9.90×10^{-03}	3.15×10^{-03}	6.27×10^{-03}	1.24×10^{-02}	9.90×10^{-03}
Plastic/water partition coefficient*	$P_{p:w}$	5.20×10^{-04}	9.96×10^{-05}	2.38×10^{-04}	3.56×10^{-04}	1.49×10^{-04}	4.56×10^{-05}
Partition coefficients							
Air/water	$P_{a:w}$	2.52	1.84	5.84	2.52	1.97	1.66
Medium unbound/yolk	$P_{mu:yolk}$	3.74×10^{-01}	2.45×10^{-01}	1.67×10^{-01}	3.03×10^{-01}	3.21×10^{-01}	2.08×10^{-01}
Medium unbound/liver	$P_{mu:liver}$	2.90×10^{-01}	2.97×10^{-01}	2.07×10^{-01}	2.77×10^{-01}	3.28×10^{-01}	2.90×10^{-01}
Medium unbound/gut	$P_{mu:gut}$	2.54×10^{-01}	2.72×10^{-01}	1.89×10^{-01}	2.46×10^{-01}	2.96×10^{-01}	2.68×10^{-01}
Medium unbound/muscle	$P_{mu:muscle}$	2.89×10^{-01}	3.03×10^{-01}	2.11×10^{-01}	2.78×10^{-01}	3.32×10^{-01}	2.97×10^{-01}
Medium unbound/skeleton	$P_{mu:os}$	2.89×10^{-01}	3.03×10^{-01}	2.11×10^{-01}	2.78×10^{-01}	3.32×10^{-01}	2.97×10^{-01}
Medium unbound/eye	$P_{mu:eye}$	3.07×10^{-01}	3.32×10^{-01}	2.31×10^{-01}	3.00×10^{-01}	3.60×10^{-01}	3.28×10^{-01}
Medium unbound/brain	$P_{mu:brain}$	3.18×10^{-01}	3.32×10^{-01}	2.31×10^{-01}	3.06×10^{-01}	3.64×10^{-01}	3.26×10^{-01}
Medium unbound/heart	$P_{mu:heart}$	2.89×10^{-01}	3.03×10^{-01}	2.11×10^{-01}	2.78×10^{-01}	3.32×10^{-01}	2.97×10^{-01}
Medium unbound/skin	$P_{mu:skin}$	3.07×10^{-01}	3.32×10^{-01}	2.31×10^{-01}	3.00×10^{-01}	3.60×10^{-01}	3.28×10^{-01}
Medium unbound/others	$P_{mu:others}$	2.31×10^{-01}	2.35×10^{-01}	1.64×10^{-01}	2.19×10^{-01}	2.60×10^{-01}	2.29×10^{-01}
Medium unbound/lysosome	$P_{mu:lyso}$	5.10×10^{-02}	1.70×10^{-02}	1.13×10^{-02}	3.49×10^{-02}	3.10×10^{-02}	9.08×10^{-03}
Medium unbound/mitochondria	$P_{mu:mito}$	4.86×10^{-01}	7.14×10^{-01}	2.35×10^{-01}	4.83×10^{-01}	8.56×10^{-01}	7.12×10^{-01}

*Unit: dm

Estimation of metabolic clearance

MCMC simulations were used to calibrate the clearance values on the basis of kinetic concentration data. Figure 4 shows the observed concentrations as a function of the predicted ones, at final experiment time (120 hpf and 72 hpf for one valproic acid experiment only) together with their estimated uncertainty. The predicted concentrations were obtained using the best fitting (maximum posterior) clearance values. The general tendency is towards under-prediction of total medium concentrations and over-prediction of embryonic concentrations. However, overall points are reasonably aligned with the perfect fit line. The best estimate of σ is on average 2.4. Hexanoic acid and 2-methylpentanoic acid are the two least well predicted.

Figure 4. Observed concentrations versus predicted ones), in the embryo and in culture medium, for valproic acid and nine analogues.

This is the best fit obtained. The black line corresponds to perfect fit.

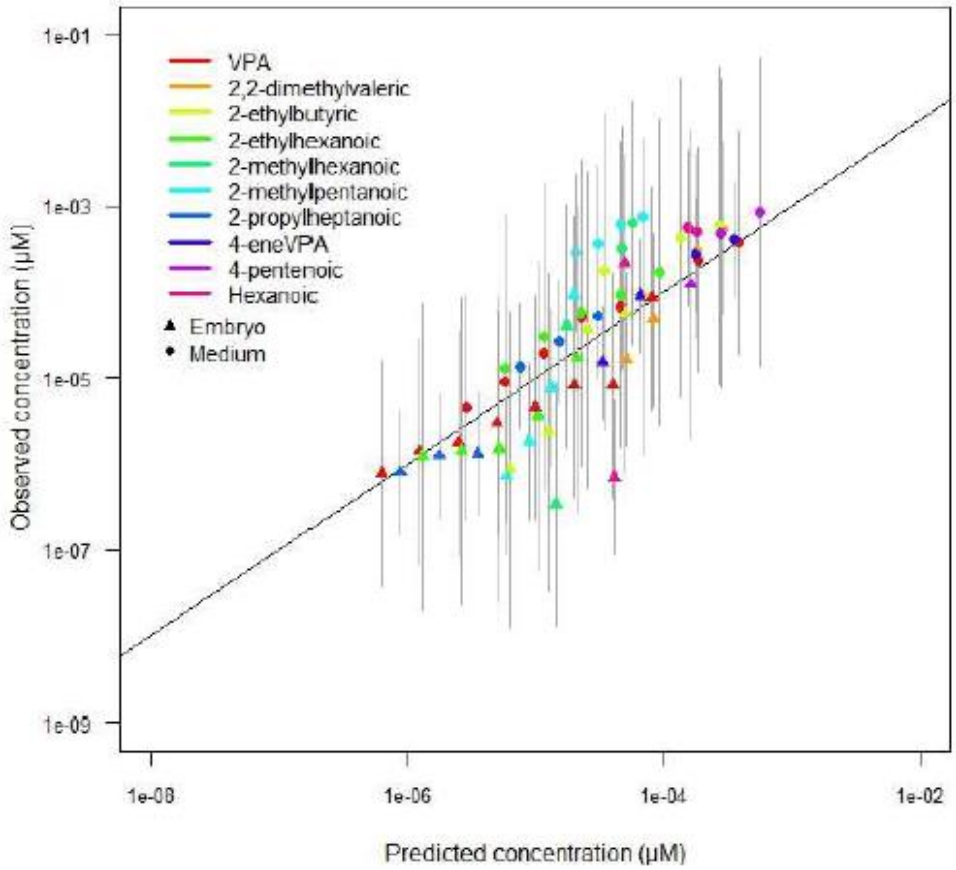

The Figures 5 and 6 present, for each chemical, the maximum posterior predicted concentrations in the embryo or in the medium, respectively, as a function of time, and the observed concentrations, following exposure to various nominal concentrations. Since the model is linear with dose, all concentrations were normalized to a nominal concentration of 1 mM to simplify the Figures (one curve only). The discontinuities seen on the concentration-time curve are due to the daily changes of culture medium. Note that the data shown in Figures 5 and 6 were used together in the calibration process. This explains partly the observed deviations of the model from the data. For exemple, for 2-methylpentanoic

acid, the observed medium concentrations remain high at 120 hpf while the observed embryo concentrations are low, pointing to significant (albeit with much uncertainty) metabolism. When estimating clearance, this conflicting evidence leads to slight over-estimation of embryo concentration by the model, and an underestimation of medium concentrations.

Figure 5. Predicted (lines) and observed (points) embryo concentrations as a function of time for VPA and nine analogues.

All concentrations were normalized to a nominal dose of 1mM. Medium was replaced every day.

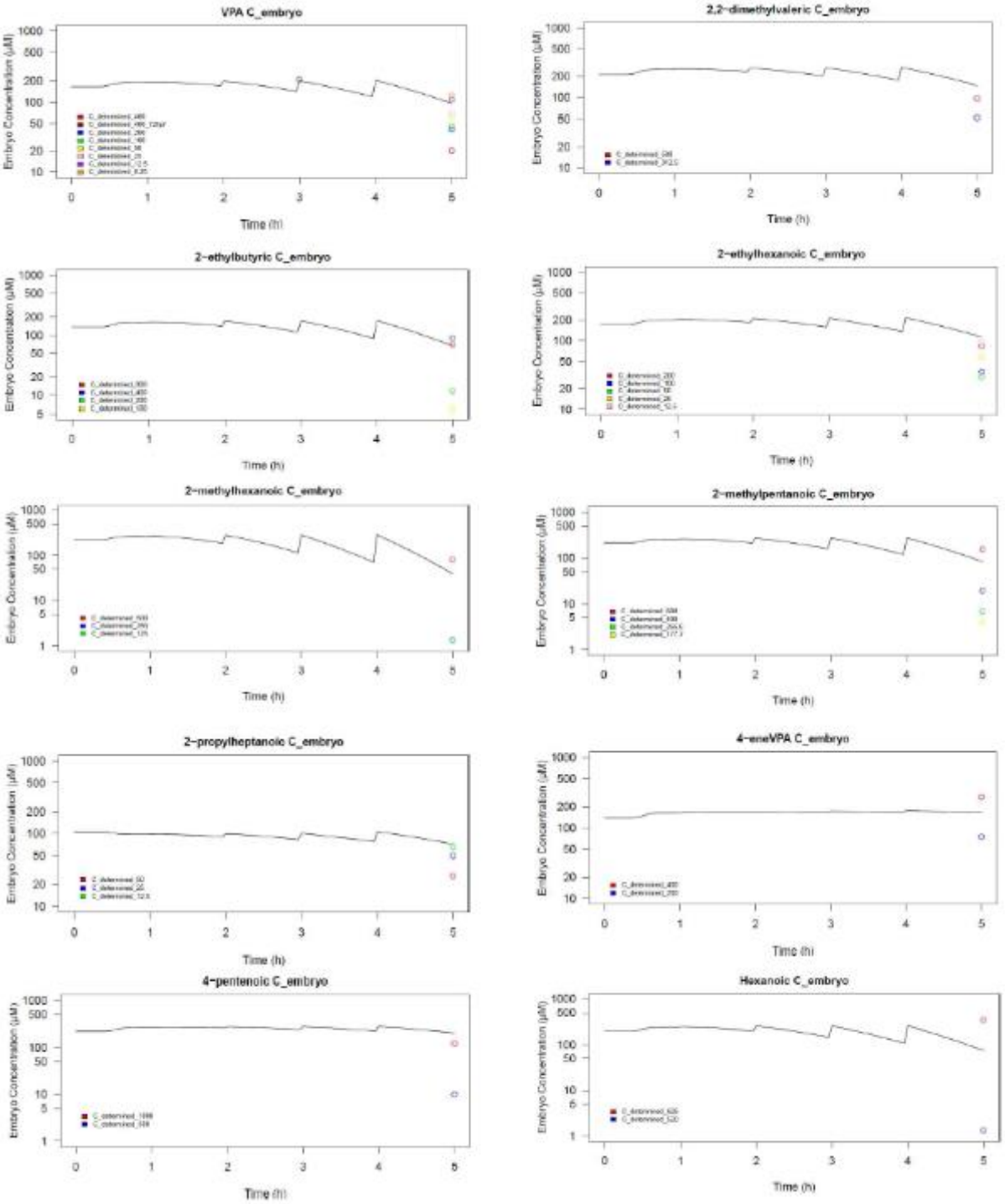

Figure 6. Predicted (lines) and observed (points) total concentrations in medium as a function of time for VPA and nine analogues.

All concentrations were normalized to a nominal dose of 1mM. Medium was replaced every day.

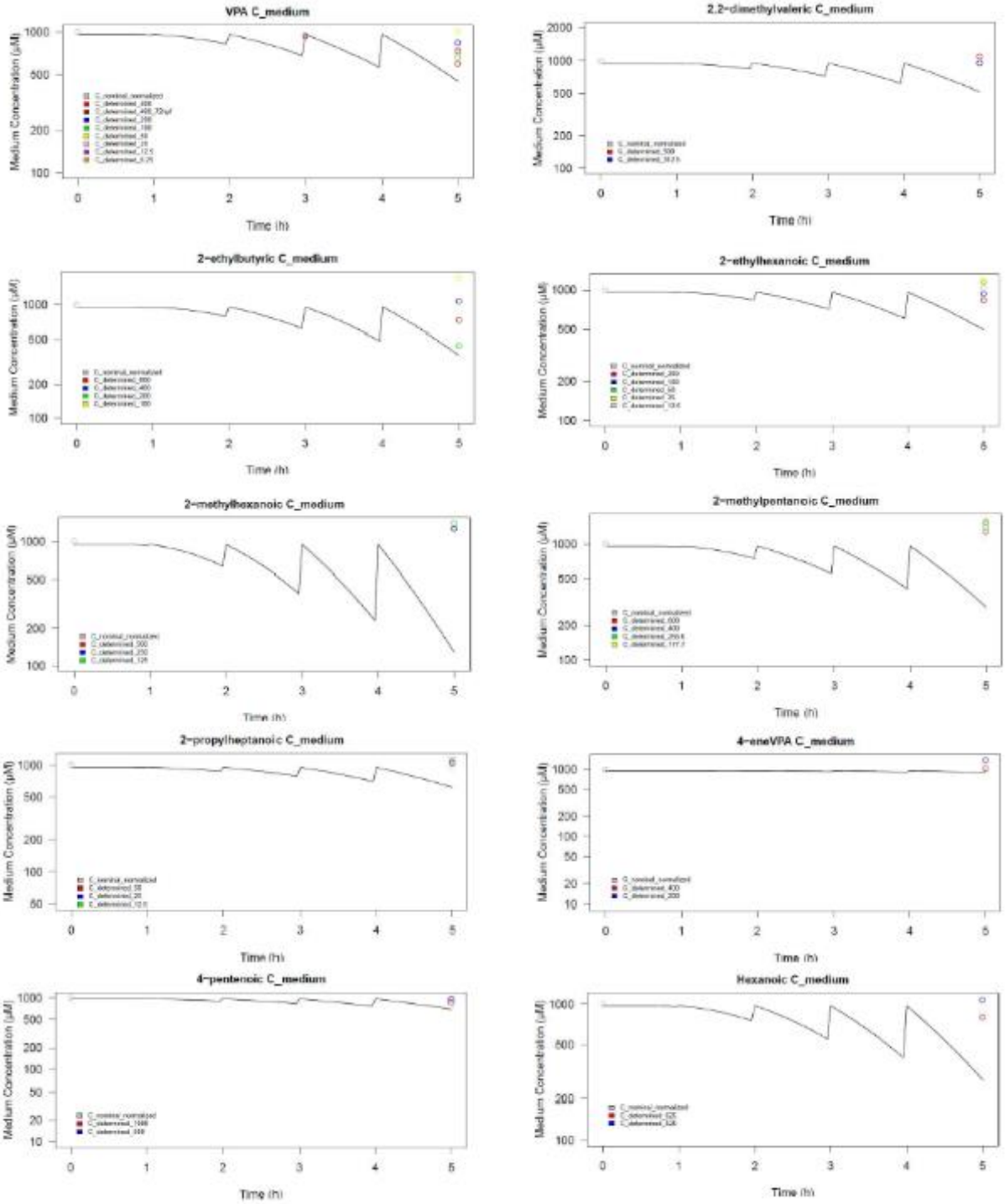

Estimation of metabolic clearance

The Table 4 summarizes the results of the MCMC calibration of metabolic clearance and uncertainty σ using concentration data for each chemical. The maximum of posterior estimates of metabolic clearance and σ values are the most likely values (best fitting volume). For every compound, the estimated metabolic clearance by the zebrafish embryo was around 10^{-10} to 10^{-11}L/min, which for an embryo volume of about 3×10^{-7} L, correspond to a half-life of about 690 minutes. (11.5 h).

4-ene-VPA is the slowest metabolized and 2-methylhexanoic acid the fastest.

The large values of σ (corresponding on average to a factor 2.4) point to large uncertainties in measurements and modelling. 2-methylhexanoic acid, 2-methylpentanoic acid and hexanoic acid in particular are affected with a factor 4 of uncertainty.

Table 4. Estimation of mean, standard deviation (SD), 95% confidence intervals (IC95%) and maximum posterior value for the metabolic clearance and residual fit uncertainty σ, for valproic acid and nine analogues.

Substance	Metabolic clearance (L/min)			σ		
	Mean ± SD	IC 95%	MP	Mean ± SD	IC 95%	MP
Valproic acid	$1.34\times10^{-10} \pm 3.32\times10^{-11}$	$[6.82\times10^{-11}; 2.01\times10^{-10}]$	1.36×10^{-10}	2.05 ± 0.317	[1.65; 2.88]	1.86
2,2- dimethylvaleric acid	$9.95\times10^{-11} \pm 5.42\times10^{-11}$	$[1.03\times10^{-11}; 2.18\times10^{-10}]$	8.53×10^{-11}	2.65 ± 0.749	[1.68; 4.58]	2.07
2-ethylbutyric acid	$2.06\times10^{-10} \pm 8.57\times10^{-11}$	$[3.60\times10^{-11}; 3.63\times10^{-10}]$	2.08×10^{-10}	3.37 ± 0.727	[2.30; 5.08]	2.91
2-ethylhexanoic acid	$1.16\times10^{-10} \pm 4.52\times10^{-11}$	$[2.92\times10^{-11}; 2.11\times10^{-10}]$	1.12×10^{-10}	2.53 ± 0.526	[1.82; 3.85]	2.16
2-methylhexanoic acid	$2.64\times10^{-10} \pm 1.00\times10^{-10}$	$[7.26\times10^{-11}; 4.64\times10^{-10}]$	2.60×10^{-10}	4.63 ± 0.820	[3.27; 6.53]	4.22
2-methylpentanoic acid	$1.58\times10^{-10} \pm 6.31\times10^{-11}$	$[2.85\times10^{-11}; 2.76\times10^{-10}]$	1.65×10^{-10}	4.41 ± 0.799	[3.08; 6.15]	4.06
2-propylheptanoic acid	$1.42\times10^{-10} \pm 8.34\times10^{-11}$	$[1.66\times10^{-11}; 3.39\times10^{-10}]$	1.24×10^{-10}	2.26 ± 0.570	[1.58; 3.71]	1.78
4-ene-valproic acid	$7.16\times10^{-11} \pm 5.92\times10^{-11}$	$[3.04\times10^{-12}; 2.24\times10^{-10}]$	1.14×10^{-11}	2.26 ± 0.672	[1.54; 4.03]	1.62
4-pentenoic acid	$7.00\times10^{-11} \pm 4.90\times10^{-11}$	$[4.43\times10^{-12}; 1.94\times10^{-10}]$	4.51×10^{-11}	2.29 ± 0.735	[1.53; 4.24]	1.51
Hexanoic acid	$1.91\times10^{-10} \pm 9.00\times10^{-11}$	$[3.05\times10^{-11}; 3.71\times10^{-10}]$	1.83×10^{-10}	4.49 ± 0.872	[3.07; 6.41]	4.10

Pharmacokinetic correction of effect concentrations

The aim of this report is to estimate internal embryo concentrations in order to calculate internal concentration to effects relationships. Relationships between internal concentrations and effects are better suited than relationship based on nominal dose for interspecies extrapolations, because their correct for pharmacokinetic differences between species or between *in vitro and in vivo*.

About use of the embryo concentrations shown on Figure 5 would be to recalculate all dose-response relationships calculated for which nominal dose replaced by concentration at 120 hpf for example. However, because of the linearity of the model as a function of dose, it is possible to simply apply, a pharmacokinetic data correction factor to adjust the effect concentrations (*EC*) computed on the basis of nominal dose.

$$Corrected\ EC = \frac{Nominal\ dose\ EC}{Pharmacokinetic\ factor} \quad (20)$$

The *Pharmacokinetic factor* (f_k) is related to nominal concentration and embryo predicted concentration obtained. It is specific for every compound.

$$Pharmacokinetic\ factor = \frac{Nominal\ concentration}{Embryo\ predicted\ concentration} \quad (21)$$

For example, for a VPA nominal concentration of 1 mM, the embryo predicted concentration is 0.112 mM. Then, the f_k is 1/0.112 = 8.9.

Figure 7 shows the concentrations causing 10% of effects, corrected or not by the *Pharmacokinetics factor*. We can observe almost the same classification between the chemicals except for the 4-ene-VPA and 2,2-dimethylvaleric acid. The EC_{10} values are lower when they are corrected by the Pharmacokinetic factor and the difference between the minimum and the maximum *EC* value is wider.

Table 5 shows the results of concentrations causing 10, 20 and 50 of effects in the embryo, uncorrected and corrected for pharmacokinetic at 120 hpf.

Figure 7. Illustration of the differences between concentration inducing10% of effects from nominal dose or corrected by the pharmacokinetic factor, for VPA and its nine analogues.

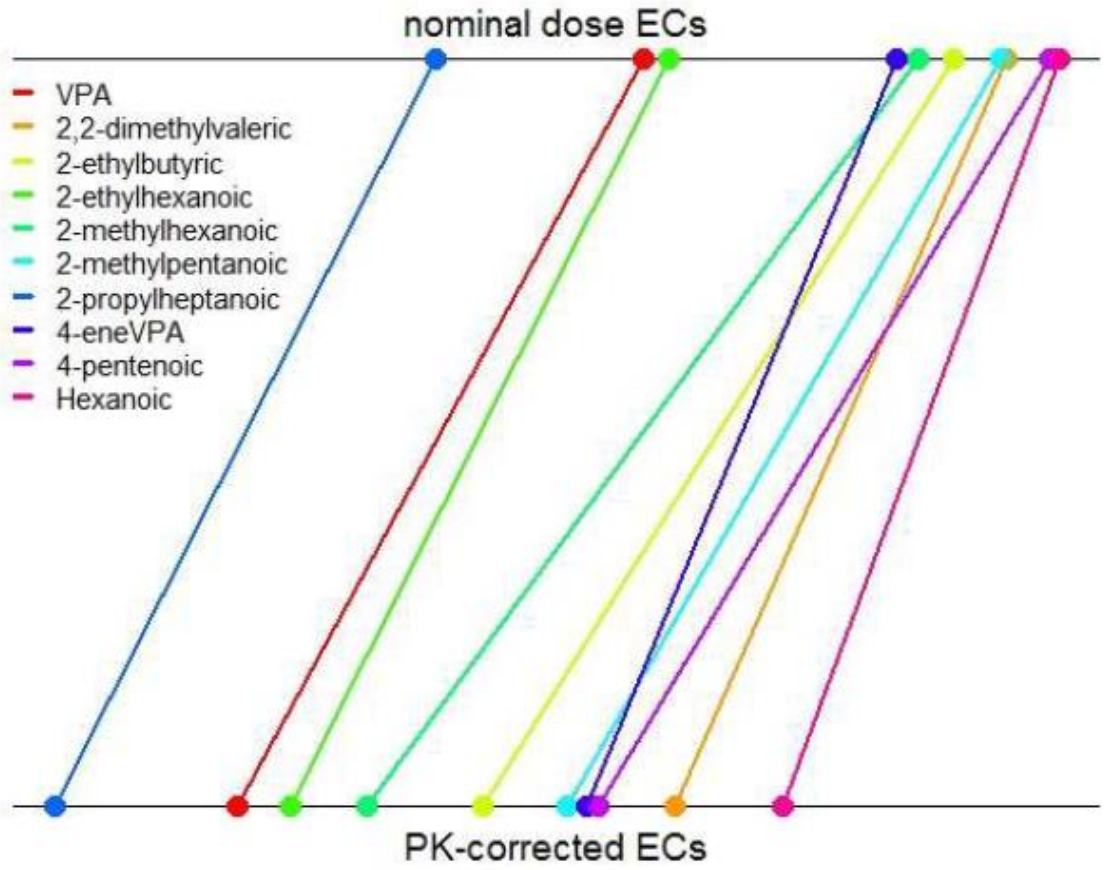

Table 5. Lethal concentrations 10, 20 and 50 in the embryo uncorrected and corrected for pharmacokinetic, in µM, for valproic acid and nine analogues 120 hpf.

Compound	Pharmacokinetic factor	EC_{10} (µM)		EC_{20} (µM)		EC_{50} (µM)	
		Nominal dose	Corrected	Nominal dose	Corrected	Nominal dose	Corrected
Valproic acid	10	53	5.11	65	6.27	96	9.26
2,2-dimethylvaleric acid	6.8	427	63.01	445	65.67	483	71.27
2-ethylbutyric acid	15	314	20.96	369	24.63	510	34.04
2-ethylhexanoic acid	8.8	61	6.91	71	8.05	103	11.79
2-methylhexanoic acid	24	258	10.67	280	11.58	333	13.78
2-methylpentanoic acid	12	412	34.12	425	35.20	482	39.92
2-propylheptanoic acid	9.0	16	1.77	17	1.88	20	2.21
4-ene-valproic acid	5.9	226	37.87	235	39.37	253	42.39
4-pentenoic acid	5.0	579	117.39	600	121.65	645	130.78
Hexanoic acid	13	548	40.66	557	41.32	575	42.66

Discussion

In this report, we describe a dynamic physiological pharmacokinetic model for zebrafish embryo. Brox *et al.* (2016) and Brinkmann *et al.* (2016) developed simple toxicokinetic models for the zebrafish embryo. However, they are not physiological, as they do differentiate tissues nor consider the rapid increase of the embryo's surface and volume.

The model is based on the VIVD steady state partition model developed by Certara® in the framework of EU-ToxRisk. Our dynamic embryo model further describes metabolism in the embryo and time evolving tissue and organ volumes. We calibrated the metabolic clearance of the zebrafish embryo for valproic acid and nine analogues using pharmacokinetic data generated for this purpose. The model can be used to base measures of effect (like EC_{50}) on internal embryo concentration rather than on nominal exposures.

The model does not consider the chorion and transport: phenomena diffusion and equilibration of concentrations are assumed to be instantaneous. This is a reasonable assumption given the small size of the embryo, but we do not have data to test it yet.

The modelling of organ growth was based on limited data on organogenesis and embryo volumes. There is room for improvement with specific measurement of embryo volumes as a function of time.

There are several limitations to this model in metabolism. The model assumes linearity. Since we have concentration data at several exposure doses we could test whether Michaelis-Menten kinetic better explain data.

We adjusted only Cl_{met}. Validation of the VIVD model is ongoing in a specific case study. However, the partition coefficients predicted by the VIVD model may not be accurate.

During simulation of repeated exposures, the accumulation in embryo was neglected, however for mass balance consideration. Indeed, medium concentration is 1000 µM corresponding to quantity 1 µmol, while embryo concentration is lower, around 100 µM, corresponding to quantity 0.1 µmol.

All the above assumptions, together with limited kinetic data (only at one time for analogues and two for VPA), translate into rather large uncertainties in predictions, in particular for 2-methylpentanoic acid ,2-methylhexanoic acid and hexanoic acid (Fig. 4).

Despite these limitations, the model predictions should be useful for risk assessment. The model is simple to use and run very quickly on a personal computer. The fact that it is linear translates into a simple pharmacokinetic correction factor at 120 hpf based on the total embryo concentration. This factor can be used to correct whole body toxicity (e.g. toxicity) *ECs* for pharmacokinetic. For specific malformations or organ toxicity, the predicted tissue/organ concentration concentrations could be used instead.

Conclusion

Our zebrafish embryo model can predict concentrations and quantities of test chemicals in different embryonic tissues, as a function of time and water or medium levels. It accounts for the physicochemical properties of the molecules but also describes metabolism and the evolving anatomy of the embryo during growth. This model can be used to relate zebrafish effects observed *in vitro* to cellular exposures and its use should improve extrapolation of *in vitro* data to human for safety assessment.

References

Bernut, Audrey, Georges Lutfalla, and Laurent Kremer. 2015. "Regard à Travers Le Danio Pour Mieux Comprendre Les Interactions Hôte/Pathogène." *Médecine/Sciences* 31 (6–7): 638–46. https://doi.org/10.1051/medsci/20153106017.

Bois, F.Y. (2009) GNU MCSim: Bayesian statistical inference for SBML-coded systems biology models. Bioinformatics 25, 1453–1454.

Brinkmann, Markus, Christian Schlechtriem, Mathias Reininghaus, Kathrin Eichbaum, Sebastian Buchinger, Georg Reifferscheid, Henner Hollert, and Thomas G. Preuss. 2016. "Cross-Species Extrapolation of Uptake and Disposition of Neutral Organic Chemicals in Fish Using a Multispecies Physiologically-Based Toxicokinetic Model Framework." *Environmental Science & Technology* 50 (4): 1914–23. https://doi.org/10.1021/acs.est.5b06158.

Brox, Stephan, Bettina Seiwert, Eberhard Küster, and Thorsten Reemtsma. 2016. "Toxicokinetics of Polar Chemicals in Zebrafish Embryo (Danio Rerio): Influence of Physicochemical Properties and of Biological Processes." *Environmental Science & Technology* 50 (18): 10264–72. https://doi.org/10.1021/acs.est.6b04325.

Ekker, Marc, and Marie-Andrée Akimento. 1991. "Le Poisson Zèbre (Danio Rerio) Un Modèle En Biologie Du Développement." *Médecine/Sciences* 7 (6): 553–60.

Feng, Jianfeng, Yongfei Gao, Min Chen, Xin Xu, Mengdi Huang, Tong Yang, Na Chen, and Lin Zhu. 2018. "Predicting Cadmium and Lead Toxicities in Zebrafish (Danio Rerio) Larvae by Using a Toxicokinetic–toxicodynamic Model That Considers the Effects of Cations." *Science of The Total Environment* 625 (June): 1584–95. https://doi.org/10.1016/j.scitotenv.2018.01.068.

Gelman, A., and D.B. Rubin. 1992. "Inference from Iterative Simulation Using Multiple Sequences (with Discussion)." *Statistical Science* 7: 457–511.

Goldsmith, J. R., and Christian Jobin. 2012. "Think Small: Zebrafish as a Model System of Human Pathology." *Journal of Biomedicine and Biotechnology* 2012: 1–12. https://doi.org/10.1155/2012/817341.

Hill, Adrian J., Hiroki Teraoka, Warren Heideman, and Richard E. Peterson. 2005. "Zebrafish as a Model Vertebrate for Investigating Chemical Toxicity." *Toxicological Sciences* 86 (1): 6–19. https://doi.org/10.1093/toxsci/kfi110.

Howe, Kerstin, Matthew D. Clark, Carlos F. Torroja, James Torrance, Camille Berthelot, Matthieu Muffato, John E. Collins, *et al.* 2013. "The Zebrafish Reference Genome Sequence and Its Relationship to the Human Genome." *Nature* 496 (7446): 498–503. https://doi.org/10.1038/nature12111.

Khazaee, Manoochehr, and Carla A. Ng. 2018. "Evaluating Parameter Availability for Physiologically Based Pharmacokinetic (PBPK) Modeling of Perfluorooctanoic Acid (PFOA) in Zebrafish." *Environmental Science: Processes & Impacts* 20 (1): 105–19. https://doi.org/10.1039/C7EM00474E.

Kimmel, Charles B., William W. Ballard, Seth R. Kimmel, Bonnie Ullmann, and Thomas F. Schilling. 1995. "Stages of Embryonic Development of the Zebrafish." *Developmental Dynamics* 203 (3): 253–310. https://doi.org/10.1002/aja.1002030302.

Kramer, Nynke I., Frans J. M. Busser, Mattheus T. T. Oosterwijk, Kristin Schirmer, Beate I. Escher, and Joop L. M. Hermens. 2010. "Development of a Partition-Controlled Dosing System for Cell Assays." *Chemical Research in Toxicology* 23 (11): 1806–14. https://doi.org/10.1021/tx1002595.

Péry, Alexandre R. R., James Devillers, Céline Brochot, Enrico Mombelli, Olivier Palluel, Benjamin Piccini, François Brion, and Rémy Beaudouin. 2014. "A Physiologically Based Toxicokinetic Model for the Zebrafish *Danio Rerio*." *Environmental Science & Technology* 48 (1): 781–90. https://doi.org/10.1021/es404301q.

Phiel, Christopher J., Fang Zhang, Eric Y. Huang, Matthew G. Guenther, Mitchell A. Lazar, and Peter S. Klein. 2001. "Histone Deacetylase Is a Direct Target of Valproic Acid, a Potent Anticonvulsant, Mood Stabilizer, and Teratogen." *Journal of Biological Chemistry* 276 (39): 36734–41. https://doi.org/10.1074/jbc.M101287200.

Quignot, N., J. Hamon, and F.Y. Bois. 2014. "Extrapolating *in vitro* Results to Predict Human Toxicity." *In In vitro Toxicology Systems*, edited by A. Bal-Price and P. Jennings, 531–50. Methods in Pharmacology and Toxicology. New-York: Springer Science.

R Development Core Team (2013). R: A language and environment for statistical computing. R Foundation for Statistical Computing, Vienna, Austria. ISBN 3-900051-07-0, URL: http://www.R-project.org.

Smith, A.F.M., and G.O. Roberts. 1993. "Bayesian Computation via the Gibbs Sampler and Related Markov Chain Monte Carlo Methods." *Journal of the Royal Statistical Society Series B* 55: 3–23.

Sztajnkrycer, Matthew D. 2002. "Valproic Acid Toxicity: Overview and Management." *Journal of Toxicology. Clinical Toxicology* 40 (6): 789–801.

3. TK-2: TK model descriptions CALUX

4. TK-3: TK model description for mEST & UKN1

Introduction to Biokinetic Modelling

Effective concentrations determined in *in vitro* toxicological assays are routinely based on a range of nominal treatment concentrations. However, the use of the nominal treatment concentration as the driving concentration for observed toxicity *in vitro* does not account for factors that reduce the free concentration within the assay and determine the true effective concentration. For cell based assay systems, this will dictate the concentration available for distribution into the cell, and subcellular compartments, and so determine the driving concentration at the target site mediating toxicity. In order to more accurately translate concentration driven toxicity from *in vitro* to *in vivo*, it is necessary to correct the nominal effect concentration, accounting for the distribution of the compound within the assay system. Factors to be considered in modelling this *in vitro* distribution include binding to the plastics used in assays, exchange at the interface between culture media and the air in the culture vessel, and binding to components that may be included in the culture media (e.g. lipids and proteins originating from foetal bovine serum, FBS); the modelling of these processes is termed biokinetics (1).

A number of biokinetic models have been published that account for some or all of the factors listed above in cell based assays. Armitage and colleagues (2) published a model framework to predict intracellular concentrations, correcting for some of the distribution factors in monolayer cell culture. This steady-state framework assumes instantaneous partitioning between media, headspace, serum-lipids, serum-proteins, dissolved organic material, and the cultured cell volume.

However, a critical assumption of the Armitage model is that the test compounds are neutral or not significantly ionised under the conditions of the *in vitro* assay. This assumption of neutrality was, to some degree, addressed in the model developed by Fischer *et al* (3) where the authors adopted the same steady-state assumption, but excluded the partitioning of compound into the headspace.

The proposed model incorporated separate partition constants for both the ionised and unionised fraction of test compound, determining the fraction ionised assuming a uniform pH=7.4 throughout the test system. This neglects the differential ionisation potential between the culture media and intracellular water resulting from their differing pH. Furthermore, the interior of the cell itself is not a uniform environment, the microenvironment of specific organelles being maintained at pH specific to their function (i.e. lysosomes (pH≈4.5), mitochondria (pH≈8), cytosol (pH≈7). Indeed, the differential ionisation of compounds between organelles and intracellular water can result in the preferential sequestration of compounds within organelles; a phenomena commonly known by the misnomer ‘ion-trapping’ (4). It is also critical to note that differences in the intrinsic permeability of the unionised/ionised form are not the only factors determining the distribution of ionised compound into cells. The potential difference maintained across the cell membrane, membrane potential (mV) can actively promote the uptake or exclusion of ionised compounds from the cell interior and can vary significantly between cell types.

Steady-state Biokinetic Model 2D Monolayer Cell Culture / CALUX

Given that compounds in this read-across are monoprotic acids, significantly ionised at physiological pH, the assumption of neutrality or uniform ionisation is not applicable. As such, an alternative model revising the relevant assumptions of the published approaches was used to predict the intracellular concentrations in 2D monolayer test systems. Based on partition coefficients between different mediums, and physical volumes, we can predict an apparent volume of distribution in the *in vitro* system. Given this volume, we can calculate the unbound medium concentrations, $C_{medium,u}$.

$$C_{medium,u} = \frac{C_{nominal} \cdot fu_{FBS,dilu} \cdot V_{medium}}{V_{medium} + k_{air} f_{ui} V_{air} + k_{cell} V_{totalcell} + k_{plastic} SA_{medium} \cdot 10^3}$$

Where $C_{nominal}$ is the nominal concentration, V_{medium} (L) is the volume of culture medium, V_{air} (L) the volume of air in the headspace above the media, and $V_{totalCell}$ (L) is the total volume of cultured cells at the time of the assay, SA_{medium} (m^2) is the surface area of plastic in direct contact with cuture medium, $fu_{FBS,dilu}$ is the fraction unbound in foetal bovine serum accounting for the dilution of FBS in culture (where FBS is not included in the culture medium $fu_{FBS,dilu}$ =1), the partition coefficients between culture medium and air, cells and plastic are k_{air}, k_{cell}, and $k_{plastic}$, respectively, and are defined below. The fraction unionised, f_{ui}, is calculated based on the Henderson Hasselbalch equation using the compound specific pKa and the compartment relevant pH.

$$f_{ui} = \frac{1}{1 + Y}$$

$$Y_{neutral} = 0$$

$$Y_{acid} = 10^{(pH - pKa)}$$

Binding to Serum Components

The predominant binding protein present in untreated foetal bovine serum (FBS) is albumin. FBS also contains lipids and free fatty acids. The lipids within FBS are diverse and not individually characterised or quantified routinely. However, the neutral lipid triacylglyceride (TAG) is routinely quantified and reported in the certificate of analysis, as is the concentration of albumin. Assuming albumin and TAG to be the most significant binding components in FBS and complete cell culture medium, we can predict the fraction unbound in FBS, fu_{FBS}.

$$fu_{FBS} = \frac{1}{1 + K_{protein} f_{protein} + \frac{P_{nl} f_{nl,FBS}}{1 + Y_{FBS}}}$$

Where $f_{protein}$ (v/v) is the fraction of FBS comprised of protein, $K_{protein}$ is the albumin:water partition coefficient, P_{nl} is the neutral lipid partition coefficient (defined below), and f_{nl} is the fraction of FBS comprised of neutral lipid. Assuming that the fraction of albumin in the FBS is representative of the total protein fraction responsible for protein binding in the FBS, this can be calculated from the mass of albumin reported in the certificate of analysis for a batch of FBS.

$$f_{protein} \approx f_{alb,FBS} = \frac{mass\ albumin \cdot PSV_{albumin}}{1000}$$

Where $PSV_{albumin}$ is the partial specific volume of albumin (0.73 mL/g (5)). The albumin to water partition coefficient, $K_{protein}$, can be determined experimentally or can be calculated based on a previously described relationship with the octanol to water partition coefficient (6).

if $logP_{ow} < 4.5$

$$logk_{albumin} = 1.08 \cdot logP_{ow} - 0.7$$

if $logP_{ow} \geq 4.5$

$$logk_{albumin} = 0.37 \cdot logP_{ow} + 2.56$$

In much the same way the volumetric fraction of neutral lipid in FBS can be calculated, using TAG as a surrogate for neutral lipid content. TAG concentration is routinely determined using an enzymatic assay and so reported as a molar concentration.

$$f_{nl,FBS} \approx f_{TAG} = \frac{[TAG] \cdot 10^{-3} \cdot MW_{TAG} \cdot PSV_{TAG}}{1000}$$

Where PSV_{TAG} is the partial specific volume of TAG (1.09 mL/g (7)) and the molecular weight of TAG is taken to be 885.453 g/mol; specifically, this corresponds to the molecular weight of trioleate, a TAG molecule comprising a glycerol backbone and three oleic acid residues.

A dilution factor, D, can then be calculated to correct fu_{FBS} for the volumetric fraction of media comprising serum, f_{serum}, and so $fu_{FBS,dilu}$ can be calculated.

$$D = \frac{1}{f_{serum}}$$

$$fu_{FBS,dilu} = \frac{fu_{FBS}}{\frac{1}{D} \cdot (1 - fu_{FBS}) + fu_{FBS}}$$

Calculation of Partition Coefficients

The partition coefficient between the culture medium and air is derived from the test compounds Henry's Law constant which may be determined experimentally or predicted using a variety of *in silico* tools. The dimensionless air medium partition coefficient is determined:

$$k_{air,u} = \frac{k_H}{RT}$$

Where K_H is the Henry's Law constant expressed in SI units (Pa m^3 mol^{-1}), R is the universal gas constant (8.314 Pa m^3 K mol^{-1}), and T is the reference temperature at which Henry's Law constant as been defined (K).

The plastic to medium partition coefficient is predicted based on the octanol to water partition coefficient using a linear relationship established by Kramer (8) and used in the model published by Comenges *et al* (9). Note that this partition-coefficient is not dimensionless and has units (m).

The partition coefficient between cells and culture medium is based on an adaption of the published approach of Rodgers and Rowland for predicting the partitioning of different compound classes between plamsa and tissues, based on composition (10, 11). We derive $K_{cell\ uu,uu}$ and $K_{iw\ uu,uu,\ organelle}$ from the steady-state Fick-Nernst-Planck equation to describe the passive permeation of electrolytes across the cell and organelle membranes, respectively, as well as the passive permeation of neutral molecules,

$$k_{cell,uu,uu} = \frac{1 + \frac{P^{unbound,ionised}}{P^{unbound,unionised}} \frac{N}{e^{N_1} - 1} Y_{ew}}{1 + \frac{P^{unbound,ionised}}{P^{unbound,unionised}} \frac{N}{e^{N_1} - 1} e^{N} Y_{iw}}$$

$$k_{IW_{organelle}^{uu,uu}} = \frac{1 + \frac{P^{unbound,ionised\ 1}}{P^{unbound,unionised}} \frac{N_1}{e^{N_1} - 1} Y_{iw}}{1 + \frac{P^{unbound,ionised\ 1}}{P^{unbound,unionised}} \frac{N_1}{e^{N_1} - 1} e^{N_1} Y_{organelle}}$$

$$N_{neutral} = 0$$

$$N_{monoacid} = -\frac{\emptyset F}{RT}$$

Where P is the permeability coefficient of either the ionised or unionised moiety. Using a ratio of the permeability coefficient between the unionised and ionised species we can describe the differential permeability of the two molecular forms. It has previously been assumed that the permeability coefficient of the ionised species is 3-4 log units lower than that of the neutral form (12). Here we assume ionised, unionised permeability coefficient ratio of 3.3 log units for the monoprotic anion. F is the Faraday constant (96484.56 C mol^{-1}) and ø is the cell membrane potential (V).

$$k_{cell,u} = \frac{C_{cell}}{C_{media_{unbound}}} = \begin{pmatrix} (1 - f_{lyso} + f_{mito})(f_{iw}(1 + Y_{iw}) + P_{nl}f_{nl} + P_{np}f_{np}) \\ +f_{lyso}(f_{iw}(1 + Y_{lyso}) + P_{nl}f_{nl} + P_{np}f_{np})K_{iw_{lyso}^{uu,uu}} \\ +f_{mito}(f_{iw}(1 + Y_{mito}) + P_{nl}f_{nl} + P_{np}f_{np})K_{iw_{mito}^{uu,uu}} \end{pmatrix} \frac{1}{1 + Y_{ew}} K_{cell,uu}$$

Incorporating $K_{cell\ uu,uu}$ and $K_{iw\ uu,uu,\ organelle}$ we adapt the original Rodgers and Rowland approach where f_{iw},f_{lyso},f_{mito},f_{nl},f_{np} denote the fractional cellular volumes of the intracellular water, lysosomes, mitochondria, neutral lipids, and neutral phospholipids, respectively. P_{nl} and P_{np} describe the partitioning of the compound between intracellular water and neutral lipids and neutral phospholipids, respectively. Where the olive oil to water ($P_{\text{vo:w}}$) and octanol to water ($P_{\text{o:w}}$) partition coefficients are used as surrogates, respectively.

This revises a fundamental assumption of the published Rodgers and Rowland approach, and previously published biokinetic models, that only unionised molecular species can passively traverse biological membranes (2, 9-11). The approach also expands on previously published biokinetic models by describing distribution into two subcellular organelle compartments (lysosome and mitochondria). Based on the approach described above, total intracellular concentrations corresponding to nominal effect concentrations determined experimentally can then be calculated.

$$C_{cell} = k_{cell,u} \cdot C_{media,dissolved,u}$$

It should be noted that while this approach can be used to model ampholytes, monoprotic and diprotic acids and bases, the equations above are described in forms with specific to neutral compounds and monoprotic acids, relevant to the compounds investigated in this read across. A description of this model has been presented previously (13), and is currently submitted for peer review.

Summary of Model Assumptions

The model described above, like those previously published (2, 3), is a steady-state approximation of multiple dynamic processes. Critically, it assumes a closed system such that the loss of test compounds within the *in vitro* system is assumed to be negligible with no metabolic clearance or instability. When that is not the case, the steady-state assumption may lead to overestimation of intracellular concentrations of the parent molecule, particularly for highly metabolized chemicals.

In line with the assumption of a closed system, the culture system is assumed to be hermetically sealed, such that the air above the culture medium is a defined volume. For volatile compounds, tested in unsealed systems, this could also result in an overprediction of intracellular compounds, since distribution into the air will act as a clearance mechanism. As part of the steady-state assumption the model assumes that the volume of cultured cells is constant with no significant increase or decrease over the course of the test assay. Finally the model assumes that all binding and partitioning processes are non-saturable, with the distribution of test compound into the cell mediated through passive diffusion. The model assumes that there are no active uptake or efflux transport processes relevant to the partitioning of the test compound within the test system.

Alternative Biokinetic Predictions / mEST & UKN1

An assumption of the biokinetic model used to predict intracellular concentrations is that cells are cultured as a 2D monolayer. Permeability into cells cultured in multi-layer, three dimensional systems may not be well described based on the approach detailed above; particularly permeability into cells that may not be in direct contact with the culture medium (i.e sandwiched between adjacent cells). Thus, we adopt a simplified approach to predict the corresponding concentration of free drug in test medium, as if the determined effective concentration was made up in complete culture medium prior to cell treatment. This predicted unbound effective concentration can then translated to an unbound plasma concentration *in vivo*; such approaches have been described previously (14).

As described above, the predominant binding components present in untreated FBS are albumin and neutral lipids. In order to predict the free concentration of test compounds in treatment medium it is necessary to account for binding to these media components. Here we assume that the binding to albumin and lipid (TAG) in complete culture (treatment) medium, are the only significant processes limiting the availability of test compound for distribution into subsequently treated cells. Thus, loss of compound due to volatility, or the binding to the plastics used in cell culture are not accounted for in this approach.

If we consider the threshold for significant volatility to be an air-water partition coefficient (K_{air} <0.03), as previously assumed by Fischer *et al*1, then the assumption that volatility has no significant impact on the freely dissolved media concentration holds for all of the compounds investigated here. Polymer-water partition coefficients have been shown to be

significantly lower than octanol-water partition coefficients (P_{ow}) (2), here used to determine the partitioning to TAG and albumin, as described below. As such, we assume here that binding to plastics used in the handling and preparation of culture medium have no significant impact on the free concentration of test compound. Finally, assuming that the maximal tested concentration does not exceed the solubility of the compound in complete culture medium, and taking the binding to protein and lipid in culture media to be linear across the tested concentration range, we can calculate an unbound fraction of test compound given the composition of the medium and the P_{ow} of the test compound.

$$fu_{media} = \frac{1}{1 + K_{alubmin} f_{alubmin} + \frac{P_{vow} f_{nl}}{1 + Y}}$$

$$Y_{neutral} = 0$$

$$Y_{monoprotic\ acid} = 10^{(pH - pKa)}$$

$$logK_{vow} = 1.115 \cdot logK_{ow} - 1.35^{4}$$

Where $f_{albumin}$ is the volumetric fraction of medium comprised of protein, $K_{albumin}$ is the albumin-water partition coefficient, K_{vow} is the olive oil-water partition coefficient (derived from P_{ow}), f_{nl} is the volumetric fraction of medium comprised of neutral lipid (TAG), and Y is the ratio of the ionised to unionised concentrations in the culture medium calculated using the Henderson-Hasselbalch equation. As above, the binding of test compound to neutral lipids is assumed to be limited to the unionised fraction of the solubilised compound in medium. The volumetric fractions of albumin and TAG in the culture medium can calculated using an analogous approach to that described above using the partial specific volumes of albumin and TAG.

$$f_{albumin} = \frac{[albumin] \cdot PSV_{albumin}}{1000}$$

$$f_{nl} \approx f_{TAG} = \frac{[TAG] \cdot PSV_{TAG}}{1000}$$

It should be noted that this relationship assumes that the neutral and the ionised fractions of compound partition equally into the hydrophobic phase and so $logK_{albumin}$ is not influenced by the ionisation state for ionisable compounds. Here, both the concentration of albumin and TAG are taken to be in units of mg/mL.

References

1. Blaauboer BJ. Biokinetic modeling and *in vitro-in vivo* extrapolations. J Toxicol Environ Health B Crit Rev. 2010;13(2-4):242-52.
2. Armitage JM, Wania F, Arnot JA. Application of mass balance models and the chemical activity concept to facilitate the use of *in vitro* toxicity data for risk assessment. Environ Sci Technol. 2014;48(16):9770-9.

3. Fischer FC, Henneberger L, Konig M, Bittermann K, Linden L, Goss KU, *et al*. Modeling Exposure in the Tox21 *in vitro* Bioassays. Chem Res Toxicol. 2017;30(5):1197-208.
4. Kazmi F, Hensley T, Pope C, Funk RS, Loewen GJ, Buckley DB, *et al*. Lysosomal sequestration (trapping) of lipophilic amine (cationic amphiphilic) drugs in immortalized human hepatocytes (Fa2N-4 cells). Drug Metab Dispos. 2013;41(4):897-905.
5. Kupke DW, Hodgins MG, Beams JW. Simultaneous determination of viscosity and density of protein solutions by magnetic suspension. Proc Natl Acad Sci U S A. 1972;69(8):2258-62.
6. Endo S, Goss KU. Serum albumin binding of structurally diverse neutral organic compounds: data and models. Chem Res Toxicol. 2011;24(12):2293-301.
7. Deckelbaum RJ, Granot E, Oschry Y, Rose L, Eisenberg S. Plasma triglyceride determines structure-composition in low and high density lipoproteins. Arteriosclerosis. 1984;4(3):225-31.
8. Kramer NI. Measuring, modelling and increasing the free concentration of test chemicals in cell assays: Utrecht University; 2010.
9. Comenges JMZ, Joossens E, Benito JVS, Worth A, Paini A. Theoretical and mathematical foundation of the Virtual Cell Based Assay - A review. Toxicol *In vitro*. 2017;45(Pt 2):209-21.
10. Rodgers T, Leahy D, Rowland M. Physiologically based pharmacokinetic modeling 1: predicting the tissue distribution of moderate-to-strong bases. J Pharm Sci. 2005;94(6):1259-76.
11. Rodgers T, Rowland M. Physiologically-based Pharmacokinetic Modeling 2: Predicting the tissue distribution of acids, very weak bases, neutrals and zwitterions. J Pharm Sci. 2007;95:1238-57.
12. Trapp S, Rosania GR, Horobin RW, Kornhuber J. Quantitative modeling of selective lysosomal targeting for drug design. Eur Biophys J. 2008;37(8):1317-28.
13. Fisher C, Jamei M, Gardner I. VIVD: A virtual *in vitro* distribution model for predicting intra- and subcellular concentrations in toxicity assays. Toxicology Letters. 2017;280:S290.
14. Gulden M, Seibert H. *In vitro-in vivo* extrapolation: estimation of human serum concentrations of chemicals equivalent to cytotoxic concentrations *in vitro*. Toxicology. 2003;189(3):211-22.

5. PBPK-1:PBPK model description for mouse

6. PBPK-1:PBPK model description for human

PBPK modelling

Physiologically based pharmacokinetic (PBPK) models for the compounds were constructed in the rat and human Simcyp Simulator (V17r1, Certara Ltd. Simcyp Division, Sheffield, UK; www.simcyp.com). The Simcyp simulator has been extensively tested and used by a consortium of industry, regulatory and academic scientists. Lists of known bugs within the code of the Simcyp simulator are maintained on our website (https://members.simcyp.com/account/softwareIssues/). The QA system used to support the production of each version of the Simcyp simulator has been described in detail (Jamei *et al*., 2013).

An aim of the read-across case study was to estimate the concentrations of the compounds in different tissues of the body specifically the foetal-placental tissue, the target organ of interest in this read-across assessment. To accomplish this a full body PBPK model was used; a schematic framework for this model is shown below. In the human simulator the ability to add further specific organs as an additional organ is available, but in the simulations for this read-across study this functionality was not required.

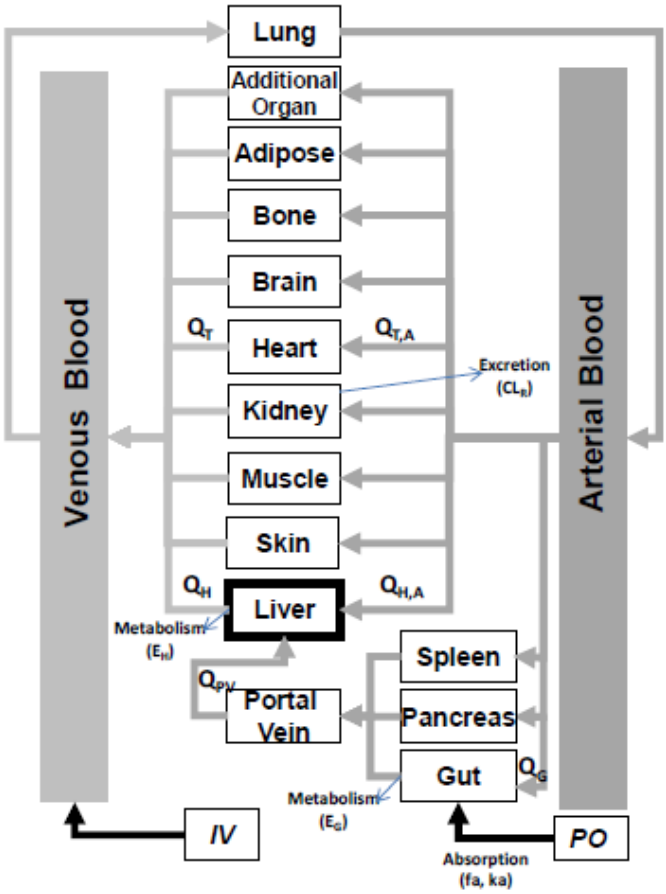

In the PBPK schematic above Q_H, Q_{HA}, Q_{PV}, Q_G, $Q_{T,A}$ and Q_T are blood flows in the total hepatic, hepatic artery, hepatic portal vein, gut and blood flows into and out of the other tissue (T) compartments, respectively; E_G and E_H are the fractions undergoing first pass metabolism in the gut and liver, respectively; CL_R is the renal clearance; fa and ka are the fraction absorbed and the first order absorption rate constant, respectively.

Distribution

In the human simulator interindividual variability in tissue distribution is accounted for through relationships between tissue volume and age, sex, weight and height (Jamei *et al*., 2009a). In both the human and rat PBPK models the *in vivo* volume of distribution at steady state (V_{ss}) is predicted using Equation 1 from Sawada *et al*. (Sawada *et al*., 1984).

$$V_{ss} = V_p + V_e \cdot E{:}P + \sum V_t \cdot K_{p,t}$$

Equation 1

Where V is the fractional body volume (L/kg) of a tissue (t), erythrocytes (e), and plasma (p), E:P is the erythrocyte: plasma drug concentration ratio and $K_{p,t}$ is the partition coefficient of drug between tissues and plasma components. Three methods are available for prediction of $K_{p,t}$. The first method was reported by Poulin and Thiel (Poulin and Theil, 2002) as corrected by Berezhkovskiy (Berezhkovskiy, 2004) (Method 1). Method 1 uses the physicochemical properties of the compounds (pKa and log P) together with *in vitro* information (B/P and fu) to predict partitioning into the tissues with the assumption that tissues and plasma are mixtures of lipids, water and proteins with a global pH of 7.4. The second method was developed by Rodgers and Rowland (Rodgers and Rowland, 2006) (Method 2). The latter splits the tissue water volume into intra- and extracellular components, with the addition of an acidic phospholipid fraction within tissues. These equations take explicit account of the extent of ionisation of a compound at the pH of the compartment concerned and have been shown to improve the prediction of tissue:plasma partition coefficients, and consequently V_{ss}, for strong bases. The Rodgers and Rowland method was further extended by the science team at Simcyp to account for ion permeability and the effect of differences in membrane potential in the different tissues on compound distribution (Method 3); however, Method 3 is currently only available in the human simulator. Method 3 also allows for the distribution of compounds into specific subcellular organelles to be modelled and forms the basis for the biokinetic model developed within the EUTOXRISK project (Fisher *et al*., 2018). These mechanistic predictions assume non-saturating conditions prevail for all binding processes, drug transport is via passive processes (i.e. no active transport), and each tissue has a well-stirred distribution limited by blood perfusion (i.e. tissues are considered as perfusion limited not permeability limited).

Performance verification for both Method 1 and Method 2 in the rat with a wide range of compounds (molecular weight of 192-1202 kDa, 19% acidic, 46% basic, 9% neutral, 27% ampholyte) is shown in the figure below. The range of *in vivo* V_{ss} for the studied compounds was 0.17-19.9 L/kg and for Method 1 and Method 2, 64% and 82% of predictions were within 2-fold of observed values, respectively.

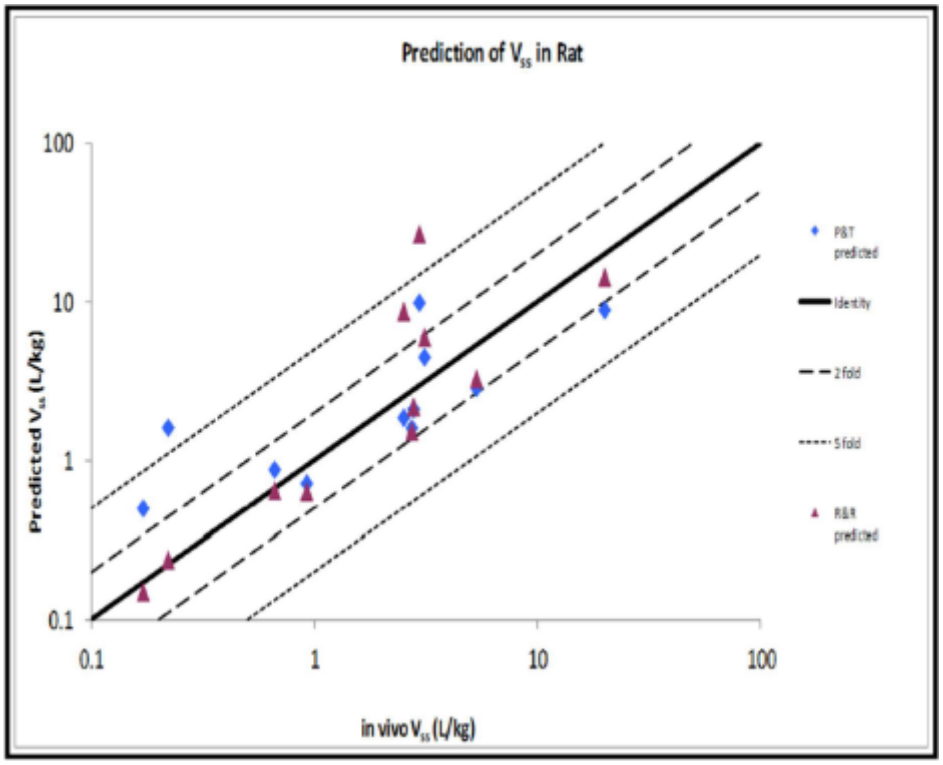

Perfusion and permeability limited distribution

Lipophilic drugs diffuse rapidly across the capillary membrane into tissue interstitial fluid such that blood flow to the tissue is the rate-limiting step in uptake. This is described as perfusion-limited distribution and is implemented in all tissues represented in the PBPK model. In addition, an option is provided within the Simcyp Simulator to allow for permeability-limited uptake, simulating both passive diffusion in parallel with active uptake and efflux in specific organs such as the liver, kidney (human only), intestine and brain. In these models the tissue is divided into compartments representing vascular, extracellular and intracellular fluid spaces - with distribution between these spaces defined as a dynamic process. The 'permeability-limited' models in the liver, brain and kidney are only available when Method 2 or 3 are selected to predict $K_{p,t}$. Given the lipophilic nature of the compounds in the read- across case study, perfusion limited models were used for all tissues in the simulations run in human in this read-across study.

Oral Absorption

For drugs in solution, several absorption models are available within the Simcyp Simulator including a first-order absorption model, a compartmental absorption transit (CAT) model (Yu and Amidon, 1998) and the advanced dissolution absorption metabolism (ADAM) model (Jamei *et al*., 2009b). Simulation of the absorption of compounds from solid dosage forms requires use of the ADAM model. The ADAM model, as implemented in the Simcyp Simulator, divides the gastro-intestinal tract (GIT) into nine anatomically defined segments from the stomach through the intestine to the colon. Drug absorption from each segment is described as a function of release from the formulation, dissolution, precipitation, luminal degradation, permeability, metabolism, transport and transit from one segment to another. It is assumed that absorption from the stomach is insignificant compared with that from the

small intestine, and that movement of liquid and solid drug through each segment of the GIT may be described by first-order kinetics. Dissolution rate from solid dosage forms is calculated from information on drug aqueous solubility and particle size using diffusion layer models (DLM) (Wang and Flanagan, 1999, 2002).

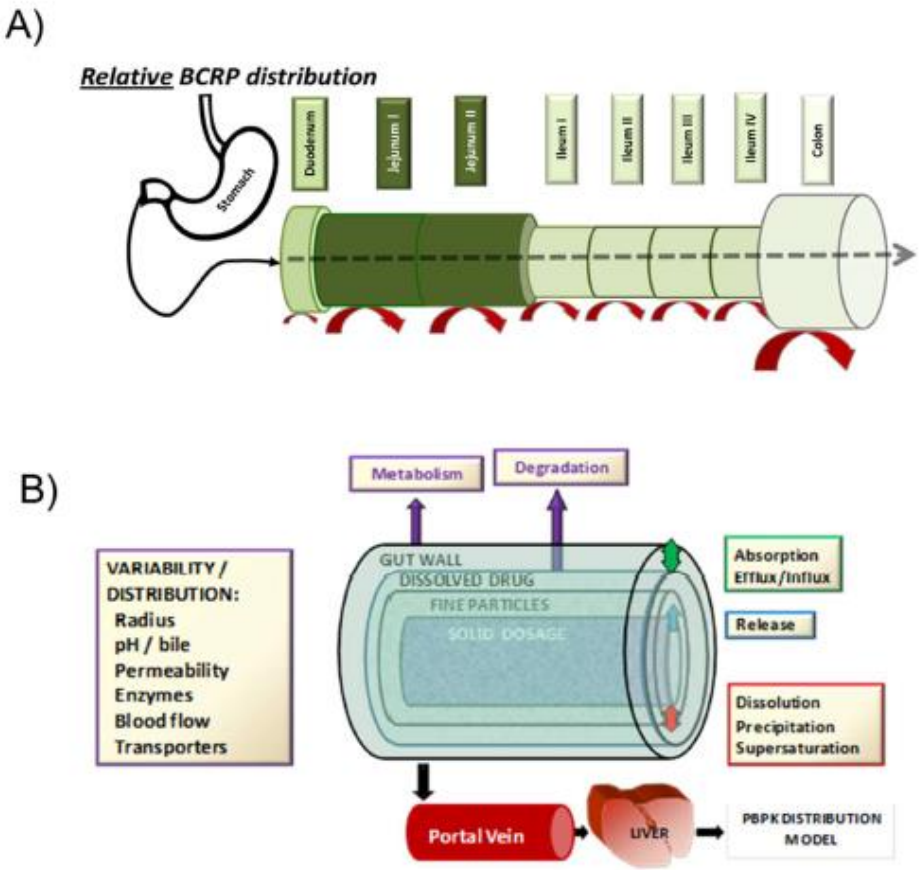

The diagrams above show the structure of the ADAM model in which the GI tract is divided into 9 sections with segregated blood flows to each section. The abundance of various enzymes and transporters in each segment varies non-monotonically along the intestine as indicated by the varying intensity of the colour for each section (BCRP distribution is indicated in A) (Harwood *et al*., 2016a; Harwood *et al*., 2016b; Harwood *et al*., 2013). B shows segments of the small intestine indicating the various processes that can be simulated (from (Darwich *et al*., 2010)).

The effective permeability in humans, $P_{eff,man}$ (jejunal), can be measured using the Loc-i-gut methodology and can be used in simulations to describe the absorptive processes in the intestine (Nilsson *et al*., 1994). For novel investigation drugs, many marketed agents, and all industrial chemicals, measured values of $P_{eff,man}$ (jejunal) are not available and therefore several methods can be used within the Simcyp Simulator to predict $P_{eff,man}$ (jejunal). These are based on data obtained with cell lines (such as Caco-2, MDCK-II or LLC-PK_1 cells)(Sun *et al*., 2002), PAMPA or from a QSPR model based upon physicochemical properties (PSA and HBD,(Winiwarter *et al*., 1998)) or by using the mechanistic permeability (MechPeff) model. The regional permeability (seven small intestine segments plus colon) for all of the methods (apart from MechPeff) is assumed to be the same by default but can be modified by the user. The regional distributions of drug metabolising

enzymes and efflux transporters such as P-gp and BCRP are also incorporated, allowing simulation of the effects of efflux transport and metabolism on drug absorption.

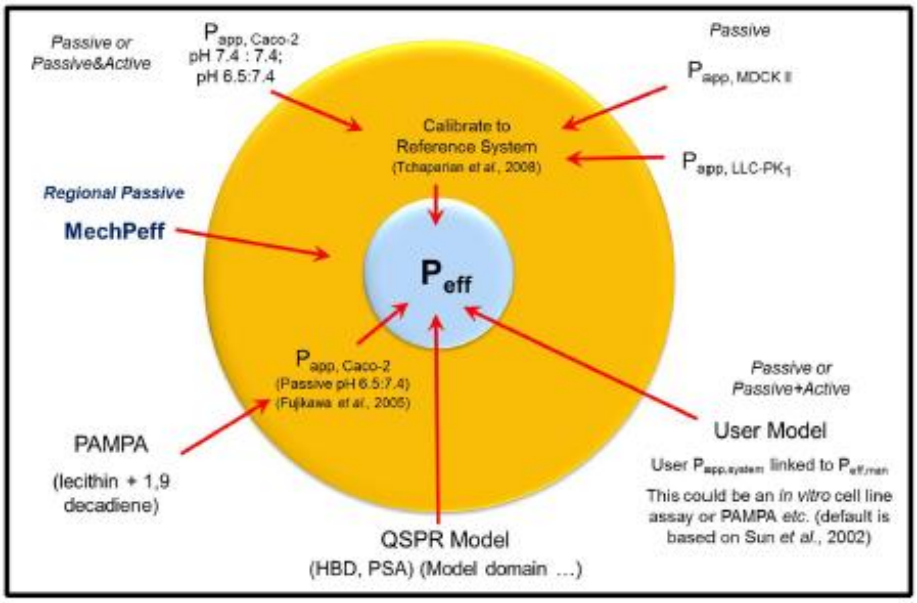

Input options to predict P_{eff} and subsequently absorption within the Simcyp Simulator are shown in the diagram above. The physicochemical based QSPR (HBD and PSA) model was used in the simulations in this study. In simulations for this read-across a simple first-order absorption model was used, while in rat simulations of VPA incorporating enterohepatic recirculation, the ADAM model was used predicting P_{eff} from HBD and PSA.

Figure 1. Prediction of fraction absorbed (fa) and first order absorption rate constant (ka; 1/h) in healthy human volunteers for the read-across source and target compounds using the hydrogen bond donor and polar surface area QSAR prediction model (circles) and the mechanistic permeability model (triangles).

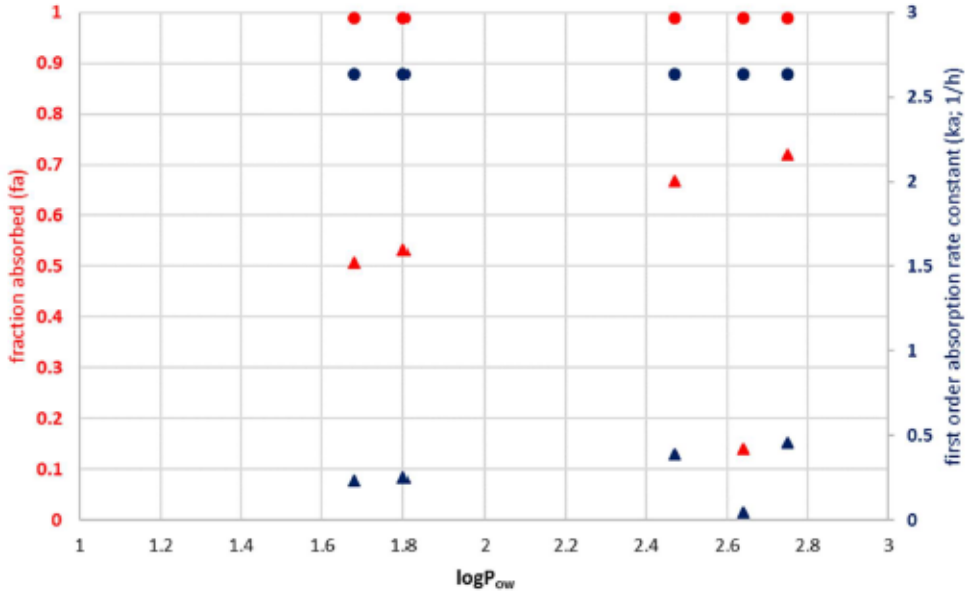

It should be noted that the QSAR (PSA and HBD) based model is not available within the Simcyp animal simulator (v17r1) and so the MechPeff model was used to predict effective permeability, and so fa and ka (1/h) in the mouse. For PBPK model simulations in humans both P_{eff} models are available, however, since data are only available to verify the predictive performance of PBPK models for VPA in humans, the QSAR (PSA and HBD) model was selected. The QSAR (PSA and HBD) model predicts the worse-case exposure scenario following an oral dose, predicting the highest fraction absorbed and most rapid absorption from the gut-lumen. Given the structural the similarity of the read-across compounds (i.e. identical number of HBDs and PSA), the model does not discriminate between compounds, predicting uniform values of fa and ka across the compound set (Figure 1).

Metabolic Clearance

Elimination of a compound can be characterized by various inputs of clearance such as intravenous or oral clearance (CL_{iv} or CL_{po}), whole organ metabolic clearance via hepatocytes (CL_{int}; µL/min/10^6 cells), liver and intestinal microsomes (CL_{int}; µL/min/mg microsomal protein) or incubation with intestinal slices (CL_{int}; µL/min/g of intestine).

Hepatic metabolic clearance

On a general basis the *in vivo* hepatic metabolic clearance is predicted using *in vitro-in vivo* extrapolation (IVIVE), as shown schematically below, followed by scaling for the specific metabolising tissue blood flow (liver in this case) and fraction of unbound drug in blood.

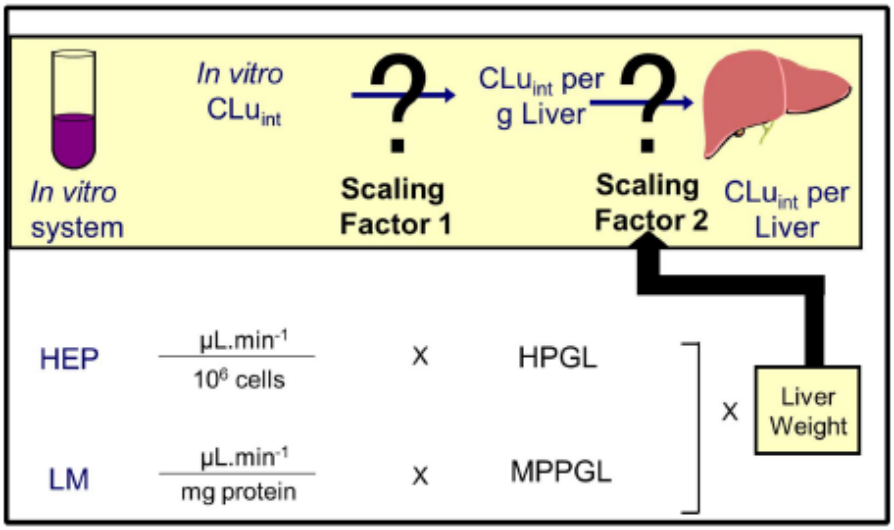

For the human simulator clearance was predicted using metabolic intrinsic clearance ($CL_{int,hep}$) data generated in human hepatocytes. *In vitro* $CL_{int,hep}$ was scaled up to the *in vivo* CL_{int} ($CL_{int,u,H}$) according to Equation 2.

$$CL_{int\ u,H} = \frac{CL_{int,hep}}{fu_{hep}} \cdot uptake \cdot HPGL \cdot LW \cdot 10^{-6} \cdot 60$$

Equation 2

Where fu_{hep} is the fraction unbound of the compound in the hepatocyte incubation, HPGL is the number of hepatocytes per gram of liver, uptake was assumed to be only be due to passive processes in these simulations (uptake =1), and 10^{-6} and 60 are to adjust units from

µl/min/10^6 cells to L/h in the whole liver. Correction for non-specific protein binding is important for IVIVE (Brown et al., 2007; McGinnity et al., 2006) and $fu_{,hep}$ was predicted as described by Kilford et al (Kilford et al., 2008), Equation 3.

$$fu_{he} = \frac{1}{1 + \frac{K_{HM}}{K_{mic}} \cdot V_R \cdot 10^{0.072 \cdot logD_{7.4}{}^2 + 0.067 \cdot logD_{7.4} - 1.126}}$$

Equation 3

Where V_R is a V_{cell}/V_{inc} ratio, where V_{cell} is the cell volume and V_{inc} the incubation volume. A K_{HM}/K_{mic} ratio of 125 was assumed (Kilford *et al*., 2008). V_R is 0.005 at the cell concentration of 10^6 cells/ml (Kilford *et al*., 2008), and was normalised for P of 1 mg/ml.

The hepatic clearance (CL_H) in humans was calculated from the whole liver scaled *in vivo* $CLint_{u,h}$ using the well stirred model Equation 4.

$$CL_{H,b} = \frac{Q_H \cdot Cl_{int_{u,h}} \cdot fu_B}{Q_H + \left(Cl_{int_{u,h}} \cdot fu_B\right)}$$

Equation 4

Where Q_H = hepatic blood flow, $CLint_{u,h}$ is the *in vivo* hepatic intrinsic clearance and fu_B = fu/(B/P). The accuracy of this *in vitro – in vivo* approach to predict human clearance from data generated in human hepatocytes; the relationship between predicted and observed human clearance for a series of 18 compounds is shown below. The predicted clearance was made using IVIVE approaches described above based on the *in vitro* intrinsic clearance generated in human hepatocyte incubations previously performed by Cyprotex. The range of LogP values for these compounds was -0.07 to 4.8, the target and all source compounds in this read-across fall within this range.

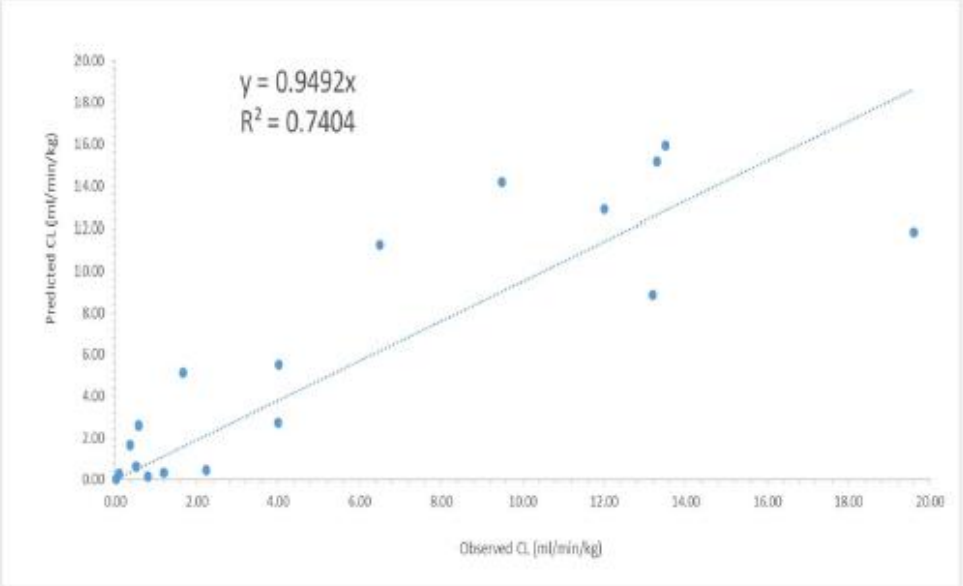

Clearance inputs in the rodent models

Equivalent *in vitro* metabolic data in mouse hepatocytes could not be generated as part of the EU-TOXRISK project. An allometrically scaling approach was used to scale the

simulated human *in vivo* clearance to the mouse, assuming the clearance of free (i.e. not bound to plasma proteins) compound scales across species based on differences in body weight (scaled with an exponent of 0.75), Equation 5.

$$CL_{species} = CL_{human} \cdot \left(\frac{BW_{species}}{BW_{human}}\right)^{0.75}$$

Equation 5

A simple allometric scaling approach was liable to result in an under-estimation of VPA exposure in rat, due to the role of EHR in rat VPA kinetics. Therefore, a reverse translation approach was adopted, back-calculating intrinsic hepatic clearance from published *in vivo* clearance (Kameya *et al*., 2009) (Equation 6- Equation 8). Simply, this calculates the whole liver clearance and then uses the reverse well-stirred liver model to determine hepatic intrinsic clearance.

$$CL_{H,b} = \frac{CL_{iv} - CL_R - CL_{add}}{BP}$$

Equation 6

$$CL_{int,u,h} = \frac{Q_H \cdot CL_{H,b}}{fu_b \cdot (Q_H - CL_{H,b})}$$

Equation 7

$$f_{u,b} = \frac{f_u}{BP}$$

Equation 8

Enterohepatic recirculation in the rat PBPK model

A rat PBPK model for VPA was constructed based on published data. Kinetic studies in rats show that enterohepatic recirculation (EHR) is a critical mechanism in the *in vivo* exposure of rats (Dickinson *et al*., 1979; Lee *et al*., 2010). In contrast to the human VPA model developed based on *in vitro* data, the rat VPA model was developed using a reverse translation approach, back-calculating hepatic intrinsic clearance based on systemic *in vivo* clearance. The rat model was also constructed incorporating EHR; in rat, glucoronidated metabolite cleared through the biliary route is deconjugated in the gut, thus back-converted to the parent compound and so available for reabsorption from the intestine. The concentration of metabolite (X) available for back-conversion is described using Equation 9.

$$\frac{dX}{dt} = f \cdot CL_{bile} \cdot uptake \cdot \frac{fu}{BP} \cdot \frac{C_{liver}}{\frac{K_{p,liver}}{BP}} - K_{bc} \cdot X$$

Equation 9

Where CL_{bile} is the biliary clearance rate, uptake is an empirical correction for active uptake into the liver (equals one in rat VPA simulations), K_{bc} is the rate constant for the back-conversion of metabolite to parent compound, and f is the fraction of biliary metabolite available for back-conversion. Back-converted metabolite was added to the duodenal compartment of the ADAM model used in rat simulations consistent with physiological bile flow into the duodenum.

Simulations with this model recovered the observed data across a dosing range from two independent studies; model inputs and simulation outputs are shown below (Table 1, Figure 2). However, insufficient data is available to model the EHR mechanism or determine its relevance for other compounds included in the read-across. Since EHR is not a relevant mechanism in humans, no further modelling was conducted in the rat.

Table 1. Valproic acid input parameters in rat full PBPK model incorporating EHR

Parameter	Value	Method / Comment	Source/Reference
MW [g/mol]	144.21		EPI-Suite (v4.1, US-EPA)
logP	2.75	experimental	EPI-Suite (v4.1, US-EPA)
Compound Type	Monoprotic acid		
pKa	4.8		ACD/Percepta (2012 release, build 2254, ACD Labs)
TPSA (Å^2)	37.3		https://pubchem.ncbi.nlm.nih.gov/compound/3121#section=Chemical-and-Physical-Properties
Hydrogen bond Donors	1		https://pubchem.ncbi.nlm.nih.gov/compound/3121#section=Chemical-and-Physical-Properties
fu	0.35	experimental	(Loscher, 1978)
B/P ratio	0.74	experimental	(Loscher, 1978)
$P_{eff,rat}$ (10^{-4} cm/s)	1.65	predicted using HBD and PSA (Simcyp v17r1)	
fu_{Gut}	1	assumed	
CL_{int} (µl/min/mg protein)	10.71	back-calculated from *in vivo* data	(Kameya *et al*., 2009)
CL_{int} Bile (metabolite) (µl/min/10^6 cells)	5.8657	back-calculated from *in vivo* data	(Singh *et al*., 1988)
K_{bc} (h^{-1})	0.08	estimated	
f	0.4	estimated	
CL_R (metabolite) (ml/min)	0.076	experimental	(Singh *et al*., 1988)

Figure 2. PBPK modelling of rat plasma concentration of VPA, for two doses applied intra venous (red- 100 mg/kg bw; blue 600 mg/kg bw).

The models with integrated enterohepatic recirculation (EHR, dashed lines) model the plasma concentrations fairly well, compared to the experimentally reported values (squares and triangles). Models without EHR (straight lines) fail to model the plasma concentration 4 h after application.

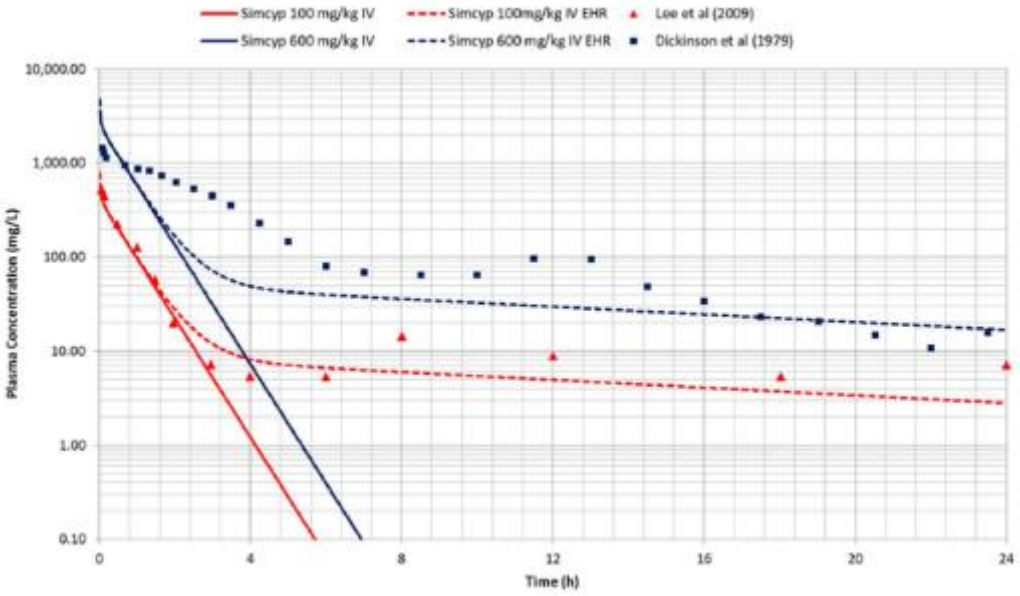

Excretion

It is possible to account for the excretion of unchanged drug in the kidney or via the biliary system in the PBPK models, but in the human and mouse models developed here hepatic metabolism was considered as the only route of clearance. Biliary clearance was only considered for the metabolites of VPA in the rat PBPK model incorporating EHR.

General description of equations for eliminating and non-eliminating organs

Each compartment within the full body PBPK model is initially described as a perfusion limited model with representative equations for an eliminating and non-eliminating organ as shown below. The equations describing the behaviour of the compound within the intestine following oral absorption are as described by Jamei *et al* (Jamei *et al*., 2009b). The basic principles for a PBPK model outlined on P19 of the WHO guidance on PBPK modelling were adhered to, namely:

1) the mixing of the chemical in the effluent blood from the tissues is instantaneous and complete;
2) blood flow is unidirectional, constant and non-pulsatile; and
3) the presence of chemicals in the blood does not alter the blood flow rate

In non-eliminating tissues the compound concentration (C) at a given time (t) is defined by Equation 10. Where Q = blood flow to the tissue, V = tissue volume, C_{ab} = arterial blood concentration, BP = blood to plasma ratio and $K_{p,t}$ is the partition coefficient of drug between tissue (t) and plasma; in the liver Equation 11 is applied.

$$\frac{dC_{tissue}}{dt} = \frac{Q_{tissue}}{V_{tissue}}\left(C_{ab} - \frac{C_{tissue}}{K_{p,t}/_{BP}}\right)$$

Equation 10

$$\frac{dC_{liver}}{dt} = \frac{1}{V_{liver}}\left((Q_{liver} - Q_{pv})C_{ab} + Q_{pv}C_{pv} - \frac{Q_{liver}C_{liver}}{K_{p,t}/_{BP}} - \frac{f_u}{BP}\cdot\frac{CLu_{int}}{K_{p,t}/_{BP}}\cdot C_{liver}\right)$$

Equation 11

Where Q_{liver} = sum of blood flow to the liver by the hepatic artery and hepatic portal vein, Q_{pv} = hepatic portal blood vein flow, C_{pv} = hepatic portal compound vein concentration, fu = fraction unbound in plasma, CLu_{int} = intrinsic clearance

Within each simulated animal or human subject the sum of the tissue blood flow rates (excluding the lung) are equal to cardiac output. In line with accepted mammalian physiology the lung receives a blood flow equal to total cardiac output. Tissue volumes and blood flow rates are within the documented range for each species considered (Jamei *et al*., 2009a; Musther *et al*., 2017).

Rodent Foetal-Placental Model

The permeability limited foetal-placental model is embedded as a physiological compartment within full PBPK model in the Simcyp Mouse and Rat Animal Simulators in V17 (Figure 3).

Figure 3. Structure of Simcyp Rodent full-PBPK model with additional Placental organ structure

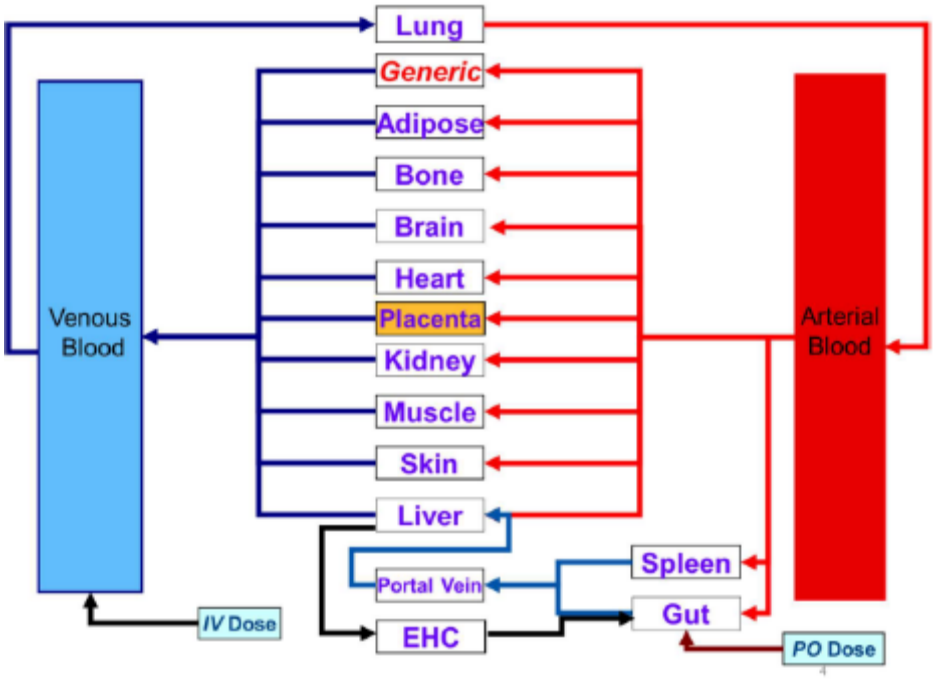

Rodent Placental Model structure

Rats and mice have a hemotrichorial and discoid type of placenta. Histologically, the placenta of rats and mice is composed of the labyrinth zone, the basal zone, the decidua and the metrial glands (Furukawa *et al*., 2014). Figure 4 shows the structure of the rodent the permeability limited foetal-placental model which consist of the maternal blood compartment, placental membrane, foetus and amniotic fluid. For simplicity of the model the 3 zones which form the placenta are considered within the "placental membrane" compartment. The foetal compartment is a composite of the total litter size. In mouse, from a total of 1246 pregnancies, litter sizes ranged from 1-17, a modal litter size is 8 foetuses (Dewar, 1968).

Figure 4. A schematic representation of the permeability limited foetal-placental PBPK model.

Solid arrows: Tissue blood flow; Dashed arrows: Clearance; Double arrows: Passive diffusion.

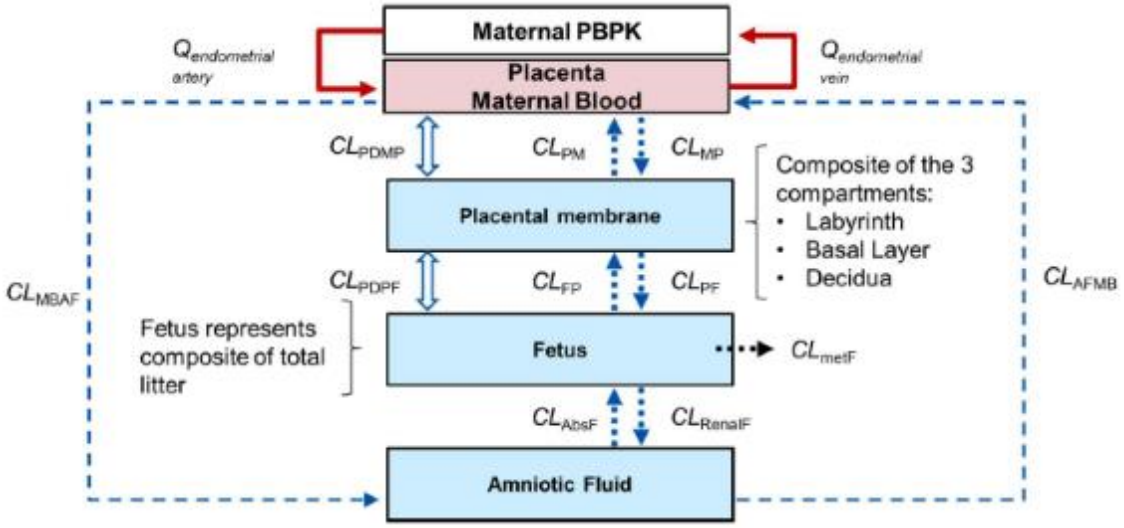

Placental model assumptions

The Foetal-placental model implemented is composed of 4 compartments, the placental maternal blood, placental membrane, foetus and amniotic fluid. Movement of compound between compartments can be considered via passive and/or active processes. Clearance can be considered in the foetal compartment. It is considered that only unbound, unionised drug is available for passive permeation, while active transport is based on unbound concentration. The following assumptions for each compartment of the foetal-placental model are detailed below:

Placenta Maternal Blood

The Placenta Maternal Blood (PMB) is assumed to consist only of blood and is considered as a well-stirred compartment in the model. The passive permeability is based on unbound unionized drug concentration while the active transport is based on unbound concentration. Drug transfer between the maternal-placenta (MP) and the placental membrane (PM) tissue is based on the related clearance and concentrations. The drug concentration in the maternal/placental compartment can be described using Equation 12.

$$V_{MB}\frac{dC_{MB}}{dt} = Q_a(C_A - C_{MB}) + CL_{PDMP}\left(fu_{PM}\cdot\frac{C_{PM}}{\beta_{PM}} - \frac{fu}{BP}\cdot\frac{C_{MB}}{\alpha_{MB}}\right) + CL_{PM}\cdot fu_{PM}\cdot C_{PM} - CL_{MP}\cdot\frac{fu}{BP}\cdot C_{MB} + CL_{AFMB} * fu_{AF}\cdot C_{AF} - CL_{MBAF} * \frac{fu}{BP}\cdot C_{MB}$$

Equation 12

Placental Membrane compartment

This is assumed to be a tissue compartment in the model. This serves as the tissue membrane that separates the maternal and foetus parts of the placenta. In rats and mice this compartment will represent the composite of 3 layers present: labyrinth, basal layer and decidua (Furukawa *et al*., 2014). The passive permeability is based on unbound unionized drug while the active transport is based on unbound concentration. This model compartment is described by Equation 13.

$$V_{PM}\frac{dC_{PM}}{dt} = CL_{MP}\cdot\frac{fu}{BP}\cdot C_{MB} - CL_{PDMP}\left(fu_{PM}\cdot\frac{C_{PM}}{\beta_{PM}} - \frac{fu}{BP}\cdot\frac{C_{MB}}{\alpha_{MB}}\right) - CL_{PF}\cdot fu_{PM}\cdot C_{PM} + CL_{PDPF}\left(fu_F\cdot\frac{C_F}{\beta_F} - fu_{PM}\cdot\frac{C_{PM}}{\beta_{PM}}\right) + CL_{FP}\cdot fu_F\cdot C_F - CL_{PF}\cdot fu_{PM}\cdot C_{PM}$$

Equation 13

Foetal Unit

The foetal unit in the rat/mouse represents a composite of the total litter size. The development of the foetus weight increases over the course of the pregnancy, however in this implementation it is assumed that there is a static foetal weight. The default implementation assumes a weight based on the administration at day 8 of mouse pregnancy. The passive permeability is based on unbound unionized drug while the active transport is based on unbound concentration. Metabolic clearance of the parent drug may be considered in the foetus. Urinary excretion of drug/metabolite is into the amniotic fluid compartment from where it may be reabsorbed by the foetus by swallowing (Equation 14).

$$V_F\frac{dC_F}{dt} = CL_{PF}\cdot fu_{PM}\cdot C_{PM} - CL_{PDPF}\left(fu_F\cdot\frac{C_F}{\beta_F} - fu_{PM}\cdot\frac{C_{PM}}{\beta_{PM}}\right) - CL_{FP}\cdot fu_F\cdot C_F - CL_{met,F}\cdot fu_F\cdot C_F - CL_{RenalF}\cdot fu_F\cdot C_F + CL_{Absf}\cdot fu_{AF}\cdot C_{AF}$$

Equation 14

Amniotic fluid compartment

The amniotic fluid unit in the rat/mouse represents a composite of the total litter volume. The amniotic fluid increases over the course of the pregnancy, however in this implementation it is assumed that there is a static amniotic fluid volume. The default system parameters for the model assumes a volume based on the administration at day 8 of mouse pregnancy. The active transport is based on unbound concentration. Urinary excretion of drug/metabolite is into the amniotic fluid compartment from where it may be reabsorbed by the foetus by swallowing (Equation 15).

$$V_{AF}\frac{dC_{AF}}{dt} = CL_{RenalF}\cdot fu_F\cdot C_F - CL_{AFMB}\cdot fu_{AF}\cdot C_{AF} + CL_{MBAF}\cdot\frac{fu}{BP}\cdot C_{MB} - CL_{AbsF}\cdot fu_{AF}\cdot C_{AF}$$

Equation 15

Table 2 shows default system parameters used in the foetal-placental model. It should be noted that these physiological parameters alter over the course of pregnancy, but are considered as static parameters in the model, i.e. do not vary with time. Values were based on available data from days 8-11 were used to best reflect the available toxicity data for valproic acid (8 days gestation). Note that these parameters should be modified based on the gestation period under study.

Table 2. Mouse System parameters used in the foetal-placental model (days 8-11)

Parameter	Unit	Value	Reference
Maternal blood volume	mL	0.04	(Raz *et al*., 2012)
Placental membrane volume	mL	2.56	(Hau and Skovgaard Jensen, 1987)
Placental membrane Relative volume of tissue wet weight (%) - EW	%	10.49	Assumed based on mouse muscle (Simcyp)
Placental membrane Relative volume of tissue wet weight (%) - IW	%	56.01	Assumed based on mouse muscle (Simcyp)
Placental membrane Relative volume of tissue wet weight (%) - NL	%	3.94	Assumed based on mouse muscle (Simcyp)
Placental membrane Relative volume of tissue wet weight (%) - NP	%	2.92	Assumed based on mouse muscle (Simcyp)
Placental membrane AP	mg/g	6.1	Assumed based on mouse muscle (Simcyp)
Placental membrane Kp_{alb}	N/A	0.064	Assumed based on mouse muscle (Simcyp)
Placental membrane Kp_{llp}	N/A	0.059	Assumed based on mouse muscle (Simcyp)
Placental membrane pH	N/A	7.4	Assumed
Foetal volume	mL	1.17	(Hau and Skovgaard Jensen, 1987)
Foetal Relative volume of tissue wet weight (%) – EW	%	10.49	Assumed based on mouse muscle (Simcyp)
Foetal Relative volume of tissue wet weight (%) - IW	%	56.01	Assumed based on mouse muscle (Simcyp)
Foetal Relative volume of tissue wet weight (%) - NL	%	3.94	Assumed based on mouse muscle (Simcyp)
Foetal Relative volume of tissue wet weight (%) -NP	%	2.92	Assumed based on mouse muscle (Simcyp)
Foetal AP	mg/g	6.1	Assumed based on mouse muscle (Simcyp)
Foetal Kp_{alb}	N/A	0.064	Assumed based on mouse muscle (Simcyp)
Foetal Kp_{llp}	N/A	0.059	Assumed based on mouse muscle (Simcyp)
Foetal pH	N/A	7.4	Assumed
Amniotic fluid volume	mL	0.19	(Cheung and Brace, 2005)
Amniotic fluid Relative volume of tissue wet weight (%) – EW	%	10.49	Assumed based on mouse muscle (Simcyp)
Amniotic fluid Relative volume of tissue wet weight (%) - IW	%	56.01	Assumed based on mouse muscle (Simcyp)
Amniotic fluid Relative volume of tissue wet weight (%) - NL	%	3.94	Assumed based on mouse muscle (Simcyp)
Amniotic fluid Relative volume of tissue wet weight (%) -NP	%	2.92	Assumed based on mouse muscle (Simcyp)
Amniotic fluid AP	mg/g	6.1	Assumed based on mouse muscle (Simcyp)
Amniotic fluid Kp_{alb}	N/A	0.064	Assumed based on mouse muscle (Simcyp)
Amniotic fluid Kp_{llp}	N/A	0.059	Assumed based on mouse muscle (Simcyp)
Amniotic Fluid pH	N/A	7.4	Assumed

Model Verification: Modelling Mouse VPA Foetal Concentrations

Valpric Acid Mouse Full-PBPK Input Parameters

Input parameters for VPA in the mouse full-PBPK model are shown in Table 3. The plasma and foetal time concentration profiles are shown in Figure 5. The foetal:maternal plasma ratios are shown in Figure 6.

Table 3. Valproic acid input mouse full PBPK parameters

Parameter	Value	References and notes
MW (g/mol)	144.2	
Compound Type	Monoprotic Acid	
pKa1	4.8	FDA Label
Log$P_{o:w}$	2.75	https://pubchem.ncbi.nlm.nih.gov/compound/valproic_acid
fu – Experimental	0.58	(Nau, 1986a)
B:P – predicted	0.74	Based on Rat value (Loscher *et al*., 1989)
Absorption Model	First Order	
fa	0.7	Fitted (Loscher and Esenwein, 1978)
ka	3	Fitted (Loscher and Esenwein, 1978)
Distribution Model	Full PBPK	
K_p Scalar	1	
V_{ss} (L/kg) – Predicted	0.455	Method 2 (Rodgers and Rowland, 2006)
CL_{IV} (mL/min)	0.28	(Loscher and Esenwein, 1978)
CL_R (L/h)	0	
Foetal-placental parameters	**Value**	**References and notes**
Placental membrane CL_{pd} (ml/min)	0.1	Fitted (Nau, 1986b)
Placental membrane fu_{ni}	0.0025	Predicted Simcyp V17
Placental membrane fu	0.892	Predicted Simcyp V17
Foetus CL_{pd} (ml/min)	0.1	Fitted (Nau, 1986b)
Foetus fu_{ni}	0.0025	Predicted Simcyp V17
Foetus fu	0.892	Predicted Simcyp V17

The disposition of VPA in both pregnant mice and embryos on day 8 of gestation following 600mg/kg oral administration of the sodium salt was modelled to replicate the study of Nau *et al*., (1986b). Concentrations in the systemic and foetus were captured using the model for the initial time points. However, the model did not recover the 4 and 6h time points (Figure 5); this is possibly due to EHR of VPA (as seen in the rat (Dickinson *et al*., 1979)), which is not accounted for in the current mouse model. Pharmacokinetic studies in non-pregnant mice show no evidence of EHR (Loscher and Esenwein, 1978), with mice showing monophasic elimination of VPA. Additionally, pregnancy related changes in the bile acid homeostasis of mice make it less likely that EHR is relevant to the PK of VPA during pregnancy (Moscovitz *et al*., 2016). While EHR would increase exposure, it will not significantly impact on the maximal plasma concentration, used as the reference point for the reverse dosimetry determining oral equivalent doses. As such, EHR has not been incorporated into the mouse PBPK models.

The Maternal to embryo ratio is shown in Figure 6. The simulated ratio (0.50) compared well to the observed data (0.4-0.6 from 10 minutes to 1 hr) Nau (1986b). Insufficient *in vivo* data are available to parameterise the permeability limited foetal-placental model for all read-across compounds. Therefore, we assume that the maternal to embryo ratio to be equal across case study compounds for the purposes of reverse dosimetry. It should be noted that in human simulations foetal-placental tissue is modelled as a perfusion-limited tissue with partition coefficients predicted using method 2 in the Simcyp simulator (v17r1), as described above.

Figure 5. Plasma and foetal concentrations following 600mg/kg dosing of Valproate sodium to 8 day gestation pregnant mice.

Green line: simulated plasma concentration, pink line: simulated foetal concentration. Circles: observed data (Nau, 1986b).

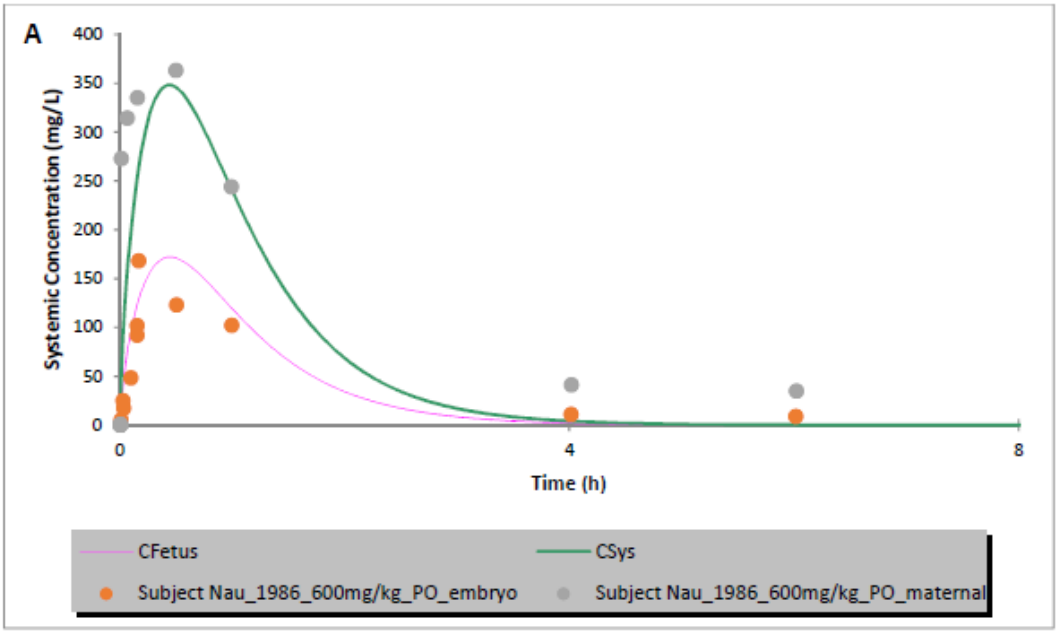

Figure 6. Foetal:maternal Plasma ratio following 600mg/kg dosing of Valproate sodium to 8 day gestation pregnant mice (Nau, 1986b).

Grey line: Based on total concentration in plasma,

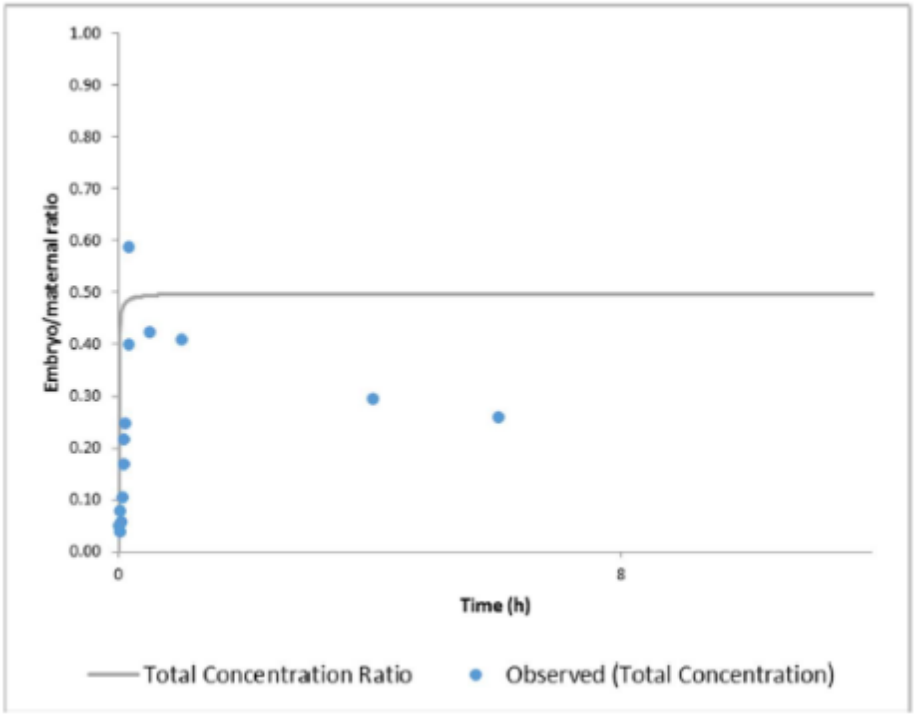

Population data

Predictions of plasma drug exposure, clearance and other parameters such as fraction metabolised by a particular pathway were made for virtual populations of healthy volunteers. Each population is generated using values and formulae describing demographic, anatomical and physiological variables. Thus, in order to assess clearance predictions in a specific population, data are required for the population variables as well as for the *in vitro* metabolism/transport of the test drug and its observed clearance in the population of interest. The parameter values within the Simcyp Simulator for creating a virtual healthy volunteer population (population, physiological parameters including liver volume and blood flows, enzyme abundances) have been described previously (Jamei *et al*., 2009a).

Physiology data used in the healthy human pregnancy population PBPK populations

A virtual population of 100 females aged 20-45 was used for the simulations, the range of physiology data used in the human pregnancy population PBPK simulations is summarised in Table 4.

Table 4. Human pregnancy population physiology data

Parameter	Mean value	Range
Age (y)	29.05	20.61 - 43.01
Weight (kg)	67.21	48.11 – 87.02
Height (cm)	162.2	151.16 – 177.77
Cardiac output (L/h)	350.73	285.71 – 443.09
Serum albumin (g/L)	43.12	34.37 – 56.06

Data for simulation of the human *in vivo* kinetics of read-across study compounds

Data and the corresponding source and/or reference used in the human compound files are shown in Table 5 - Table 9.

Table 5. Input parameter values used to simulate the kinetics of Valproic acid in human (99-66-1)

Parameter	Value	Method / Comment	Source/Reference
MW [g/mol]	144.21		EPI-Suite (v4.1, US-EPA)
logP	2.75	experimental	EPI-Suite (v4.1, US-EPA)
Compound Type	Monoprotic acid		
pKa	4.8		ACD/Percepta (2012 release, build 2254, ACD Labs)
TPSA (Å^2)	37.3		https://pubchem.ncbi.nlm.nih.gov/compound/3121#section=Chemical-and-Physical-Properties
Hydrogen bond donors	1		https://pubchem.ncbi.nlm.nih.gov/compound/3121#section=Chemical-and-Physical-Properties
fu	0.138 0.310	predicted predicted	Lhasa CORAL model
B/P ratio	0.55	assumed	
fa	0.996	predicted using HBD and PSA (Simcyp v17r1)	(Winiwarter *et al*., 2003; Winiwarter *et al*., 1998)
ka (h^{-1})	2.546	predicted (Simcyp V17r1)	
fu_{Gut}	1	assumed	
Cl_{int} (µl/min/10^6 cells)	0.219	Experimental (HµREL coculture system)	Cyprotex data (CYP1440)
Hepatocyte binding (fu_{heps})	0.954	predicted	(Kilford *et al*., 2008)

Table 6. Input parameter values used to simulate the kinetics of 2-Ethyl Butyric acid in human (88-09-5)

Parameter	Value	Method / Comment	Source/Reference
MW [g/mol]	116.16		EPI-Suite (v4.1, US-EPA)
logP	1.68	experimental	EPI-Suite (v4.1, US-EPA)
Compound Type	Monoprotic acid		
pKa	4.8		ACD/Percepta (2012 release, build 2254, ACD Labs)
TPSA (Å^2)	37.3		https://pubchem.ncbi.nlm.nih.gov/compound/6915#section=Chemical-and-Physical-Properties
Hydrogen bond donors	1		https://pubchem.ncbi.nlm.nih.gov/compound/6915#section=Chemical-and-Physical-Properties
fu	0.348 0.712	predicted predicted	Random forest (model 1) Lhasa
B/P ratio	0.55	assumed	
fa	0.996	predicted using HBD and PSA (Simcyp v17r1)	(Winiwarter *et al*., 2003; Winiwarter *et al*., 1998)
ka (h^{-1})	2.546	predicted (Simcyp V17r1)	
fu_{Gut}	1	assumed	
Cl_{int} (l/min/10^6 cells)	9.62	experimental (HµREL coculture system)	Cyprotex data (CYP1440)
Hepatocyte binding (fu_{heps})	0.955	predicted	(Kilford *et al*., 2008)

Table 7. Input parameter values used to simulate the kinetics of 2-Ethyl Hexanoic acid in human (149-57-5)

Parameter	Value	Method / Comment	Source/Reference
MW [g/mol]	144.21		EPI-Suite (v4.1, US-EPA)
logP	2.64	experimental	EPI-Suite (v4.1, US-EPA)
Compound Type	Monoprotic acid		
pKa	3.3		ACD/Percepta (2012 release, build 2254, ACD Labs)
TPSA (Å^2)	37.3		https://pubchem.ncbi.nlm.nih.gov/compound/8697#section=Chemical-and-Physical-Properties
Hydrogen bond donors	1		https://pubchem.ncbi.nlm.nih.gov/compound/8697#section=Chemical-and-Physical-Properties
fu	0.142 0.310	predicted predicted	Random forest (model 1) CORAL model
B/P ratio	0.55	assumed	
fa	0.996	predicted using HBD and PSA (Simcyp v17r1)	(Winiwarter *et al*., 2003; Winiwarter *et al*., 1998)
ka (h^{-1})	2.546	predicted (Simcyp V17r1)	
fu_{Gut}	1	assumed	
Cl_{int} (l/min/10^6 cells)	0.551	experimental (HμREL coculture system)	Cyprotex data (CYP1440)
Hepatocyte binding (fu heps)	0.950	predicted	(Kilford *et al*., 2008)

Table 8. Input parameter values used to simulate the kinetics of 2-methylhexanoic acid in human (4536-23-6)

Parameter	Value	Method / Comment	Source/Reference
MW [g/mol]	130.19		EPI-Suite (v4.1, US-EPA)
logP	2.47	experimental	EPI-Suite (v4.1, US-EPA)
Compound Type	Monoprotic acid		
pKa	4.8		ACD/Percepta (2012 release, build 2254, ACD Labs)
TPSA (Å^2)	37.3		https://pubchem.ncbi.nlm.nih.gov/compound/20653#section=Chemical-and-Physical-Properties
Hydrogen bond donors	1		https://pubchem.ncbi.nlm.nih.gov/compound/20653#section=Chemical-and-Physical-Properties
fu	0.265 0.454	predicted predicted	Random forest (model 3) Lhasa
B/P ratio	0.55	assumed	
fa	0.996	predicted using HBD and PSA (Simcyp v17r1)	(Winiwarter *et al*., 2003; Winiwarter *et al*., 1998)
ka (h^{-1})	2.546	predicted (Simcyp V17r1)	
fu_{Gut}	1	assumed	
Cl_{int} (l/min/10^6 cells)	3.95	experimental (HμREL coculture system)	Cyprotex data (CYP1440)
Hepatocyte binding (fu_{heps})	0.956	predicted	(Kilford *et al*., 2008)

Table 9. Input parameter values used to simulate the kinetics of 2-methylpentanoic acid in human (97-61-0)

Parameter	Value	Method / Comment	Source/Reference
MW [g/mol]	116.16		EPI-Suite (v4.1, US-EPA)
logP	1.8	experimental	EPI-Suite (v4.1, US-EPA)
Compound Type	Monoprotic acid		
pKa	4.8		ACD/Percepta (2012 release, build 2254, ACD Labs)
TPSA (Å^2)	37.3		https://pubchem.ncbi.nlm.nih.gov/compound/7341#section=Chemical-and-Physical-Properties
Hydrogen bond donors	1		https://pubchem.ncbi.nlm.nih.gov/compound/7341#section=Chemical-and-Physical-Properties
fu	0.265 0.454	predicted predicted	Random forest (model 1) Lhasa
B/P ratio	0.55	assumed	
fa	0.996	predicted using HBD and PSA (Simcyp v17r1)	(Winiwarter *et al.*, 2003; Winiwarter *et al.*, 1998)
ka (h^{-1})	2.546	predicted (Simcyp V17r1)	
fu_{Gut}	1	assumed	
Cl_{int} (l/min/10^6 cells)	10.2	experimental (HμREL coculture system)	Cyprotex data (CYP1440)
Hepatocyte binding (fu heps)	0.956	predicted	(Kilford *et al.*, 2008)

Physiology data used in the mouse PBPK simulations

Population variability is not accounted for in the Simcyp mouse PBPK simulator and so only population representative simulations were run; Table 10.

Table 10. Mouse population physiology data

Parameter	Mean value
Weight (g)	25
Cardiac output (ml/min)	14.010
Serum albumin (g/L)	31.240

Data for simulation of the mouse *in vivo* kinetics of read-across study compounds

Data and the corresponding source and/or reference used in the human compound files are shown in Table 11-Table 15.

Table 11. Input parameter values used to simulate the kinetics of Valproic acid in mouse (99-66-1)

Parameter	Value	Method / Comment	Source/Reference
MW [g/mol]	144.21		EPI-Suite (v4.1, US-EPA)
logP	2.75	experimental	EPI-Suite (v4.1, US-EPA)
Compound Type	Monoprotic acid		
pKa	4.8		ACD/Percepta (2012 release, build 2254, ACD Labs)
fu	0.2 0.41	scaled from human prediction	Lhasa CORAL model
B/P ratio	0.5819	assumed	
fa	0.942	predicted using $MechP_{eff}$ (Simcyp v17r1)	(Winiwarter *et al*., 2003; Winiwarter *et al*., 1998)
ka (h^{-1})	3.512	predicted (Simcyp V17r1)	
fu_{Gut}	1	assumed	
CL_{iv} (mL/min)	0.01 (min fu) 0.03 (max fu)	allometrically scaled from human prediction	Cyprotex data (CYP1440)

Table 12. Input parameter values used to simulate the kinetics of 2-Ethyl Butyric acid in mouse (88-09-5)

Parameter	Value	Method / Comment	Source/Reference
MW [g/mol]	116.16		EPI-Suite (v4.1, US-EPA)
logP	1.68	experimental	EPI-Suite (v4.1, US-EPA)
Compound Type	Monoprotic acid		
pKa	4.8		ACD/Percepta (2012 release, build 2254, ACD Labs)
fu	0.45 0.79	scaled from human prediction	Random forest (model 1) Lhasa
B/P ratio	0.5819	assumed	
fa	0.803	predicted using $MechP_{eff}$ (Simcyp v17r1)	(Winiwarter *et al*., 2003; Winiwarter *et al*., 1998)
ka (h^{-1})	1.831	predicted (Simcyp V17r1)	
fu_{Gut}	1	assumed	
CL_{iv} (mL/min)	0.79 (min fu) 1.13 (max fu)	allometrically scaled from human prediction	Cyprotex data (CYP1440)

Table 13. Input parameter values used to simulate the kinetics of 2-Ethyl Hexanoic acid in mouse (149-57-5)

Parameter	Value	Method / Comment	Source/Reference
MW [g/mol]	144.21		EPI-Suite (v4.1, US-EPA)
logP	2.64	experimental	EPI-Suite (v4.1, US-EPA)
Compound Type	Monoprotic acid		
pKa	3.3		ACD/Percepta (2012 release, build 2254, ACD Labs)
fu	0.2 0.41	scaled from human prediction	Random forest (model 1) CORAL model
B/P ratio	0.5819	assumed	
fa	0.294	predicted using $MechP_{eff}$ (Simcyp v17r1)	(Winiwarter *et al*., 2003; Winiwarter *et al*., 1998)
ka (h^{-1})	0.357	predicted (Simcyp V17r1)	
fu_{Gut}	1	assumed	
CL_{iv} (mL/min)	0.03 (min fu) 0.07 (max fu)	allometrically scaled from human prediction	Cyprotex data (CYP1440)

Table 14. Input parameter values used to simulate the kinetics of 2-methylhexanoic acid in mouse (4536-23-6)

Parameter	Value	Method / Comment	Source/Reference
MW [g/mol]	130.19		EPI-Suite (v4.1, US-EPA)
logP	2.47	predicted	EPI-Suite (v4.1, US-EPA)
Compound Type	Monoprotic acid		
pKa	4.8		ACD/Percepta (2012 release, build 2254, ACD Labs)
fu	0.36 0.56	scaled from human prediction	Random forest (model 3) Lhasa
B/P ratio	0.5819	assumed	
fa	0.918	predicted using $MechP_{eff}$ (Simcyp v17r1)	(Winiwarter *et al.*, 2003; Winiwarter *et al.*, 1998)
ka (h^{-1})	3.005	predicted (Simcyp V17r1)	
fu_{Gut}	1	assumed	
CL_{iv} (mL/min)	0.35 0.53	allometrically scaled from human prediction	

Table 15. Input parameter values used to simulate the kinetics of 2-methylpentanoic acid in mouse (97-61-0)

Parameter	Value	Method / Comment	Source/Reference
MW [g/mol]	116.16		EPI-Suite (v4.1, US-EPA)
logP	1.8	predicted	EPI-Suite (v4.1, US-EPA)
Compound Type	Monoprotic acid		
pKa	4.8		ACD/Percepta (2012 release, build 2254, ACD Labs)
fu	0.45 0.76	scaled from human prediction	Random forest (model 1) Lhasa
B/P ratio	0.5819	assumed	
fa	0.826	predicted using $MechP_{eff}$ (Simcyp v17r1)	(Winiwarter *et al.*, 2003; Winiwarter *et al.*, 1998)
ka (h^{-1})	1.983	predicted (Simcyp V17r1)	
fu_{Gut}	1	assumed	
CL_{iv} (mL/min)	0.82 (min fu) 1.13 (max fu)	allometrically scaled from human prediction	

References

Berezhkovskiy, L.M., 2004. Volume of distribution at steady state for a linear pharmacokinetic system with peripheral elimination. J Pharm Sci 93, 1628-1640.

Brown, H.S., Chadwick, A., Houston, J.B., 2007. Use of isolated hepatocyte preparations for cytochrome P450 inhibition studies: comparison with microsomes for Ki determination. Drug Metab Dispos 35, 2119-2126.

Cheung, C.Y., Brace, R.A., 2005. Amniotic fluid volume and composition in mouse pregnancy. J Soc Gynecol Investig 12, 558-562.

Darwich, A.S., Neuhoff, S., Jamei, M., Rostami-Hodjegan, A., 2010. Interplay of metabolism and transport in determining oral drug absorption and gut wall metabolism: a simulation assessment using the "Advanced Dissolution, Absorption, Metabolism (ADAM)" model. Curr Drug Metab 11, 716-729.

Dewar, A.D., 1968. Litter size and the duration of pregnancy in mice. Q J Exp Physiol Cogn Med Sci 53, 155-161.

Dickinson, R.G., Harland, R.C., Ilias, A.M., Rodgers, R.M., Kaufman, S.N., Lynn, R.K., Gerber, N., 1979. Disposition of valproic acid in the rat: dose-dependent metabolism, distribution, enterohepatic recirculation and choleretic effect. J Pharmacol Exp Ther 211, 583-595.

Fisher, C., Simeon, S., Jamei, M., Gardner, I., Bois, Y.F., 2018. VIVD: Virtual *in vitro* distribution model for the mechanistic prediction of intracellular concentrations of chemicals in *in vitro* toxicity assays. Toxicol *In vitro*.

Furukawa, S., Kuroda, Y., Sugiyama, A., 2014. A comparison of the histological structure of the placenta in experimental animals. J Toxicol Pathol 27, 11-18.

Harwood, M.D., Achour, B., Neuhoff, S., Russell, M.R., Carlson, G., Warhurst, G., Amin, R.-H., 2016a. *In vitro-In vivo* Extrapolation Scaling Factors for Intestinal P-Glycoprotein and Breast Cancer Resistance Protein: Part I: A Cross-Laboratory Comparison of Transporter-Protein Abundances and Relative Expression Factors in Human Intestine and Caco-2 Cells. Drug Metab Dispos 44, 297-307.

Harwood, M.D., Achour, B., Neuhoff, S., Russell, M.R., Carlson, G., Warhurst, G., Rostami-Hodjegan, A., 2016b. *In vitro-In vivo* Extrapolation Scaling Factors for Intestinal P-glycoprotein and Breast Cancer Resistance Protein: Part II. The Impact of Cross-Laboratory Variations of Intestinal Transporter Relative Expression Factors on Predicted Drug Disposition. Drug Metab Dispos 44, 476-480.

Harwood, M.D., Neuhoff, S., Carlson, G.L., Warhurst, G., Rostami-Hodjegan, A., 2013. Absolute abundance and function of intestinal drug transporters: a prerequisite for fully mechanistic *in vitro-in vivo* extrapolation of oral drug absorption. Biopharm Drug Dispos 34, 2-28.

Hau, J., Skovgaard Jensen, H.J., 1987. Diagnosis and monitoring of pregnancy in mice: correlations between maternal weight, Foetal and placental mass and the maternal serum levels of progesterone, pregnancy-associated murine protein-2 and alpha-fetoprotein. Lab Anim 21, 306-310.

Holmes, A.M., Creton, S., Chapman, K., 2010. Working in partnership to advance the 3Rs in toxicity testing. Toxicology 267, 14-19.

Jamei, M., Dickinson, G.L., Rostami-Hodjegan, A., 2009a. A framework for assessing inter-individual variability in pharmacokinetics using virtual human populations and integrating general knowledge of physical chemistry, biology, anatomy, physiology and genetics: A tale of 'bottom-up' vs 'top-down' recognition of covariates. Drug Metab Pharmacokinet 24, 53-75.

Jamei, M., Marciniak, S., Edwards, D., Wragg, K., Feng, K., Barnett, A., Rostami-Hodjegan, A., 2013. The simcyp population based simulator: architecture, implementation, and quality assurance. *In silico* Pharmacol 1, 9.

Jamei, M., Turner, D., Yang, J., Neuhoff, S., Polak, S., Rostami-Hodjegan, A., Tucker, G., 2009b. Population-based mechanistic prediction of oral drug absorption. AAPS J 11, 225-237.

Kameya, H., Hokama, N., Hobara, N., Ohshiro, S., Uno, T., 2009. Effects of a dopamine receptor agonist and atropine sulfate on absorption of valproic acid in rats. Biomed Res 30, 101-106.

Kilford, P.J., Gertz, M., Houston, J.B., Galetin, A., 2008. Hepatocellular binding of drugs: correction for unbound fraction in hepatocyte incubations using microsomal binding or drug lipophilicity data. Drug Metab Dispos 36, 1194-1197.

Lee, M.S., Lee, Y.-J., Chung, B.C., Jung, B.H., 2010. Simultaneous Determination of Valproic Acid and its Toxic Metabolites, 4-ene-VPA and 2,4-diene-VPA in Rat Plasma using a Gas Chromatographicmass Spectrometric Method. Journal of Pharmaceutical Investigation 40, 155-160.

Loscher, W., 1978. Serum protein binding and pharmacokinetics of valproate in man, dog, rat and mouse. J Pharmacol Exp Ther 204, 255-261.

Loscher, W., Esenwein, H., 1978. Pharmacokinetics of sodium valproate in dog and mouse. Arzneimittelforschung 28, 782-787.

Loscher, W., Fisher, J.E., Nau, H., Honack, D., 1989. Valproic acid in amygdala-kindled rats: alterations in anticonvulsant efficacy, adverse effects and drug and metabolite levels in various brain regions during chronic treatment. J Pharmacol Exp Ther 250, 1067-1078.

McGinnity, D.F., Berry, A.J., Kenny, J.R., Grime, K., Riley, R.J., 2006. Evaluation of time-dependent cytochrome P450 inhibition using cultured human hepatocytes. Drug Metab Dispos 34, 1291-1300.

Moscovitz, J.E., Kong, B., Buckley, K., Buckley, B., Guo, G.L., Aleksunes, L.M., 2016. Restoration of enterohepatic bile acid pathways in pregnant mice following short term activation of Fxr by GW4064. Toxicol Appl Pharmacol 310, 60-67.

Musther, H., Harwood, M.D., Yang, J., Turner, D.B., Rostami-Hodjegan, A., Jamei, M., 2017. The Constraints, Construction, and Verification of a Strain-Specific Physiologically Based Pharmacokinetic Rat Model. J Pharm Sci 106, 2826-2838.

Nau, H., 1986a. Species differences in pharmacokinetics and drug teratogenesis. Environ Health Perspect 70, 113-129.

Nau, H., 1986b. Valproic acid teratogenicity in mice after various administration and phenobarbitalpretreatment regimens: the parent drug and not one of the metabolites assayed is implicated as teratogen. Fundam Appl Toxicol 6, 662-668.

Nilsson, D., Fagerholm, U., Lennernas, H., 1994. The influence of net water absorption on the permeability of antipyrine and levodopa in the human jejunum. Pharm Res 11, 1540-1547.

Poulin, P., Theil, F.P., 2002. Prediction of pharmacokinetics prior to *in vivo* studies. 1. Mechanismbased prediction of volume of distribution. J Pharm Sci 91, 129-156.

Raz, T., Avni, R., Addadi, Y., Cohen, Y., Jaffa, A.J., Hemmings, B., Garbow, J.R., Neeman, M., 2012. The hemodynamic basis for positional- and inter-Foetal dependent effects in dual arterial supply of mouse pregnancies. PLoS One 7, e52273.

Rodgers, T., Rowland, M., 2006. Physiologically based pharmacokinetic modelling 2: predicting the tissue distribution of acids, very weak bases, neutrals and zwitterions. J Pharm Sci 95, 1238-1257.

Sawada, Y., Hanano, M., Sugiyama, Y., Harashima, H., Iga, T., 1984. Prediction of the volumes of distribution of basic drugs in humans based on data from animals. J Pharmacokinet Biopharm 12, 587-596.

Singh, K., Orr, J.M., Abbott, F.S., 1988. Pharmacokinetics and enterohepatic circulation of 2-n-propyl-4-pentenoic acid in the rat. Drug Metab Dispos 16, 848-852.

Sun, D., Lennernas, H., Welage, L.S., Barnett, J.L., Landowski, C.P., Foster, D., Fleisher, D., Lee, K.D., Amidon, G.L., 2002. Comparison of human duodenum and Caco-2 gene expression profiles for 12,000 gene sequences tags and correlation with permeability of 26 drugs. Pharm Res 19, 1400-1416.

Wang, J., Flanagan, D.R., 1999. General solution for diffusion-controlled dissolution of spherical particles. 1. Theory. J Pharm Sci 88, 731-738.

Wang, J., Flanagan, D.R., 2002. General solution for diffusion-controlled dissolution of spherical particles. 2. Evaluation of experimental data. J Pharm Sci 91, 534-542.

Winiwarter, S., Ax, F., Lennernas, H., Hallberg, A., Pettersson, C., Karlen, A., 2003. Hydrogen bonding descriptors in the prediction of human *in vivo* intestinal permeability. J Mol Graph Model 21, 273-287.

Winiwarter, S., Bonham, N.M., Ax, F., Hallberg, A., Lennernas, H., Karlen, A., 1998. Correlation of human jejunal permeability (*in vivo*) of drugs with experimentally and theoretically derived parameters. A multivariate data analysis approach. J Med Chem 41, 4939-4949.

Yu, L.X., Amidon, G.L., 1998. Saturable small intestinal drug absorption in humans: modeling and interpretation of cefatrizine data. Eur J Pharm Biopharm 45, 199-203.

EU-ToxRisk Case Study 2

Reporting Case Studies on Chemical Grouping (Read-Across)

Metabolism Information for Mock Submission

Note on Document History

The information contained in this document was originally assembled in respect of the case study 1 mock submission. The case study 2 mock submission is based on the same chemical class (valproic acid analogues) but for a different toxicological endpoint. Compounds for the current submission are a subset of those chosen in case study 1 and the target compound for case study 2 is **methylhexanoic acid** rather than **ethylbutyric acid**. Due to restricted time, this document has not been modified wholesale to reflect this. Rather, information relevant only to case study 1 or superfluous to case study 2 is noted in the text and/or graph/table titles. Target and analogue compounds are give in the following table:

Compound Name	CAS Number	Case Study 1 Mock Submission	Case Study 2 Mock Submission
2-Ethylbutyric Acid	88-09-5	*Target Compound*	Analogue Compound
2-Propylheptanoic Acid	31080-39-4	Analogue Compound	Analogue Compound
2-Ethylheptanoic Acid	3274-29-1	Analogue Compound	*Not included*
2-Propylhexanoic Acid	3274-28-0	Analogue Compound	*Not included*
Valproic Acid	99-66-1	Analogue Compound	Analogue Compound
2-Ethylhexanoic Acid	149-57-5	Analogue Compound	Analogue Compound
2-Ethylpentanoic Acid	20225-24-5	Analogue Compound	*Not included*
2-Methylbutyric Acid	1730-91-2	Analogue Compound	*Not included*
2-Methylpentanoic Acid	97-61-0	Analogue Compound	Analogue Compound
2-Methylhexanoic Acid	4536-23-6	Analogue Compound	*Target Compound*
Pivalic Acid	75-98-9	Analogue Compound	*Not included*

Tony Long, 30 November 2018[1]

Known Metabolism of Case Study Target and Analogues

[comments for case study 1, pivalic acid is not a case study 2 analogue]

A search of the literature has unearthed variable amounts of information on the metabolism of four out of the ten chosen analogue compounds. Sources include **PubMed, the Human Metabolome Database, PubChem, DrugBank** as well as non-specialised sources such as **Google**. Two of the ten analogue compounds (valproic acid and pivalic acid) have some representation in the **Lhasa Limited metabolism data set**. Analogue compounds with some known metabolism **are: valproic acid, 2-ethylhexanoic acid, 2-methylhexanoic acid** and **pivalic acid**.

Valproic acid

The *in vivo* and *in vitro* metabolism of valproic acid (VPA) and 4-ene VPA is extensive, well documented and reviewed1,2 for a number of animal species and human. Metabolites can be categorised as those arising from CYP-catalysed oxidation at alkyl side chains (microsomes, endoplasmic reticulum), those arising from betaoxidation pathways

[1] Contributors:
Tony Long, Ernest Murray, Catherine O'Leary-Steele and David Ponting
Lhasa Limited, Granary Wharf House, 2 Canal Wharf, Leeds LS11 5PS, West Yorkshire, UK Telephone: +44 (0)113 394 6020

(mitochondria) and those occurring as a consequence of phase II reactions of conjugation (endoplasmic reticulum and cytosol). Variability of VPA metabolism and pharmacokinetics in different disease states and co-administrations are well-studied. VPA is highly protein bound (87–95%) resulting in low clearance (6–20 ml/h/kg). Its major urinary metabolite is the valproate glucuronide accounting for 30-50% of an administered dose. beta-Oxidation is the most important oxidative biotransformation type (>40%) for VPA with CYP-based hydroxylation/dehydrogenation (15-20%) playing a secondary role. Some 50-70 different metabolites have been suggested in the literature for VPA. Some example metabolites in all three biotransformation categories are shown below.

Valproic Acid Metabolites

Metabolites from Conjugation Reactions

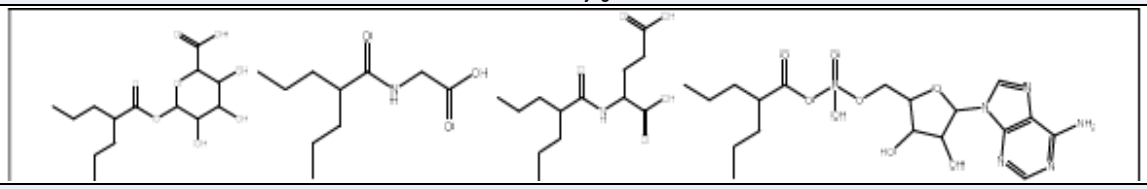

Metabolites from beta-Oxidation

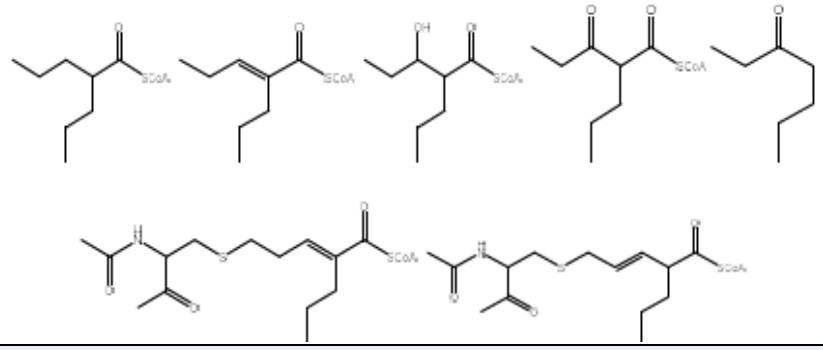

Metabolites from CYP-Catalysed Oxidation

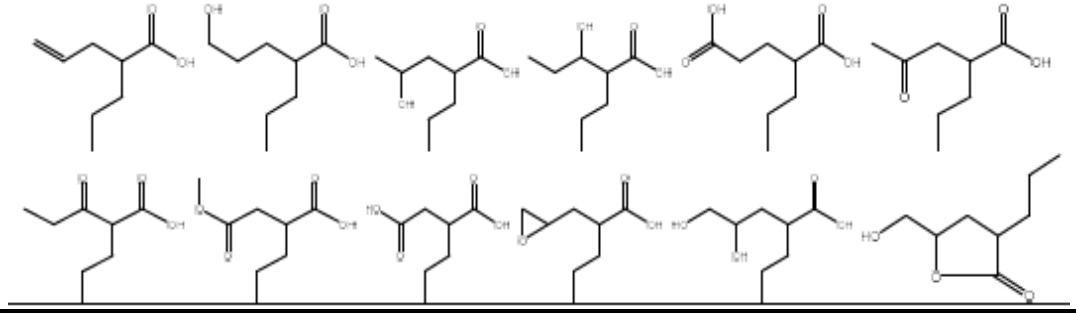

2-Ethylhexanoic acid

Along with 2-ethylhexanol, 2-ethylhexanoic acid is a metabolite of the plasticiser bis(2-ethylhexyl)phthalate and is reasonably well studied[3,4,5,6]. Data is available from both *in vitro* and *in vivo* experiments in human, rat, rabbit, mouse, monkey, guinea pig and dog. Like valproic acid (of which 2-ethylhexanoic acid is a chain isomer) metabolism is by glucuronide conjugation, beta-oxidation and CYP-mediated hydroxylation/dehydrogenation. Some example metabolites in all three biotransformation categories are shown below. Additional but uncharacterised hydroxylated metabolites and two lactones have also been reported.

2-Ethylhexanoic Acid Metabolites

Metabolites from Conjugation Reactions

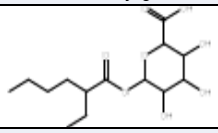

Metabolites from beta-Oxidation

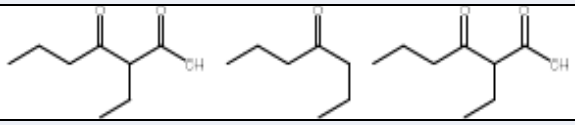

Metabolites from CYP-Catalysed Oxidation

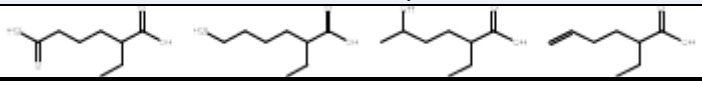

2-Methylhexanoic acid

The metabolism of 2-methylhexanoic acid has been reported to be by glucuronidation in hepatic microsomes of several species including human[7]. Glucuronidation activity toward several analogue compounds (3-methylhexanoic acid, 4-methylhexanoic acid, 5-methylhexanoic acid, 2-ethylhexanoic acid, 3-ethylhexanoic acid, 4-ethylhexanoic acid and 3-ethyloctanoic acid) increased as a function of molecular weight, but was not affected by the position of the methyl or the ethyl moiety on the hydrocarbon chain.

2-Methylhexanoic Acid and Analogues that Undergo Glucuronidation (from reference 7)

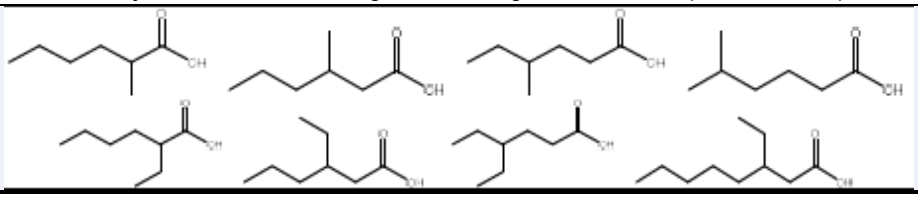

Pivalic acid [pivalic acid is not a case study 2 analogue]

Pivalic acid undergoes conjugation with glucuronic acid, glycine and carnitine in rat, dog, rabbit and monkey hepatocytes and kidney slices[8,9].

Pivalic Acid Metabolites

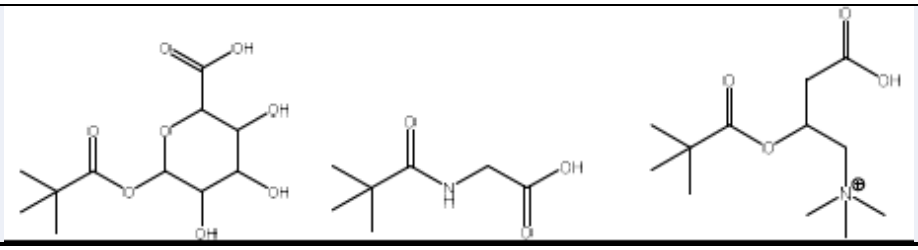

Predicted Metabolism of Case Study Target and Analogues

***Target Compound*: 2-Methylhexanoic Acid** *(CAS: 4536-23-6)*

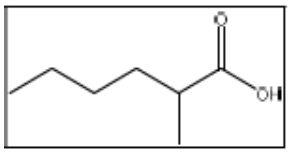

Predicted Metabolism at First Generation Only (see General Methods)

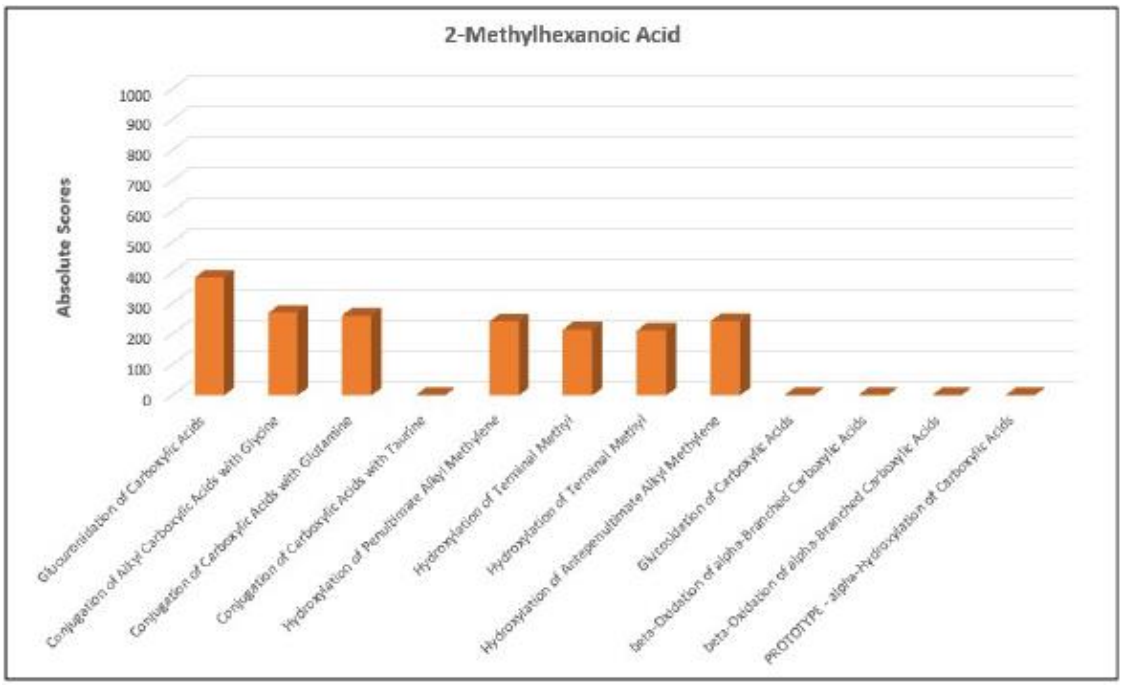

Metabolites Occurring as a Result of Biotransformations with Score > 0 (First Generation Only)

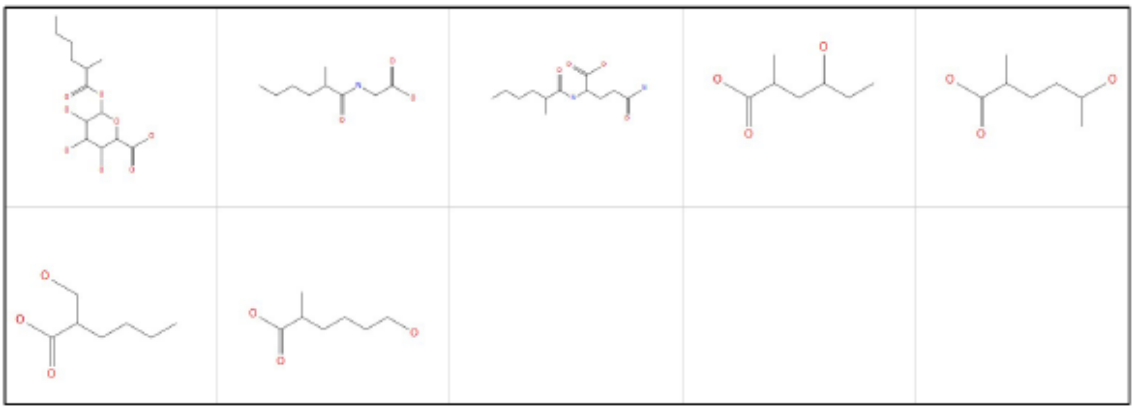

Analogue Compound 1: 2-Ethylbutyric Acid (CAS: 88-09-5)

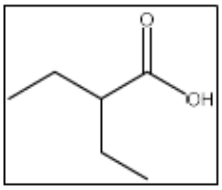

Predicted Metabolism at First Generation Only (see General Methods)

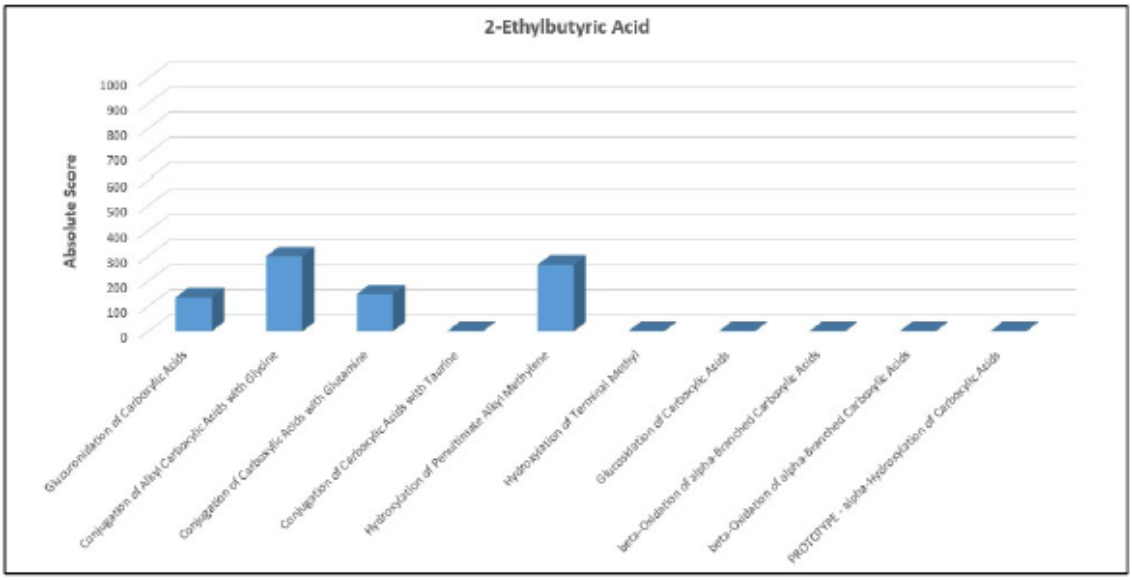

Metabolites Occurring as a Result of Biotransformations with Score > 0 (First Generation Only)

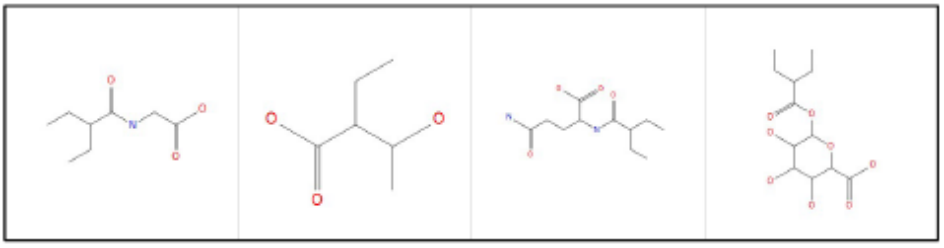

Metabolism Prediction: Comparison of Target Compound v. Analogue Compound 1 (First Generation Only)

■2-Methylhexanoic ■Acid 2-Ethylbutyric Acid (scores are not normalised)

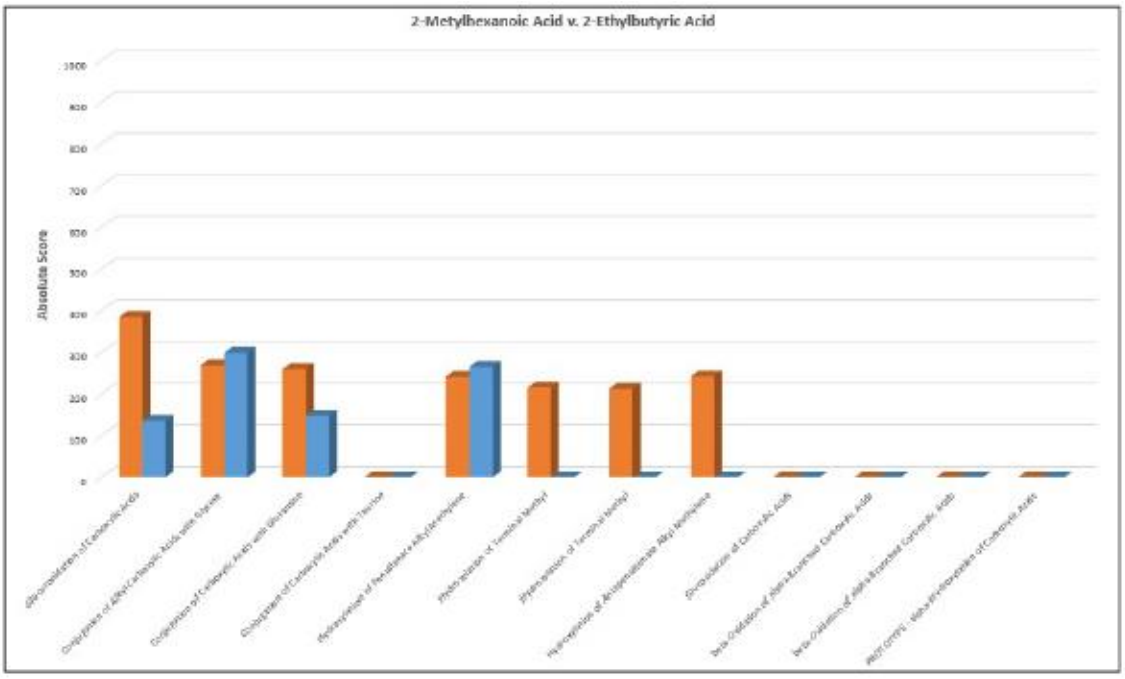

Similarity of First Generation Tree: Target Compound v. Analogue Compound 1 (See General Methods)

Biotransformation Fingerprint Method: 0.50

Concordant Metabolite Method: 0.52

Common Metabolites up to Third Generation (See General Methods)

2- Methylhexanoic Acid

No. Unique Metabolites: **295**

No. Unique Metabolites (Score > 0): **128**

2-Ethylbutyric Acid

No. Unique Metabolites: **185**

No. Unique Metabolites (Score > 0): **35**

Number of Common Metabolites (Score > 0): **0**

Common Metabolite Structures: **N/A**

Analogue Compound 2: 2-Propylheptanoic Acid (CAS: 31080-39-4)

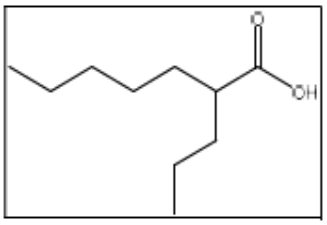

Predicted Metabolism at First Generation Only (see General Methods)

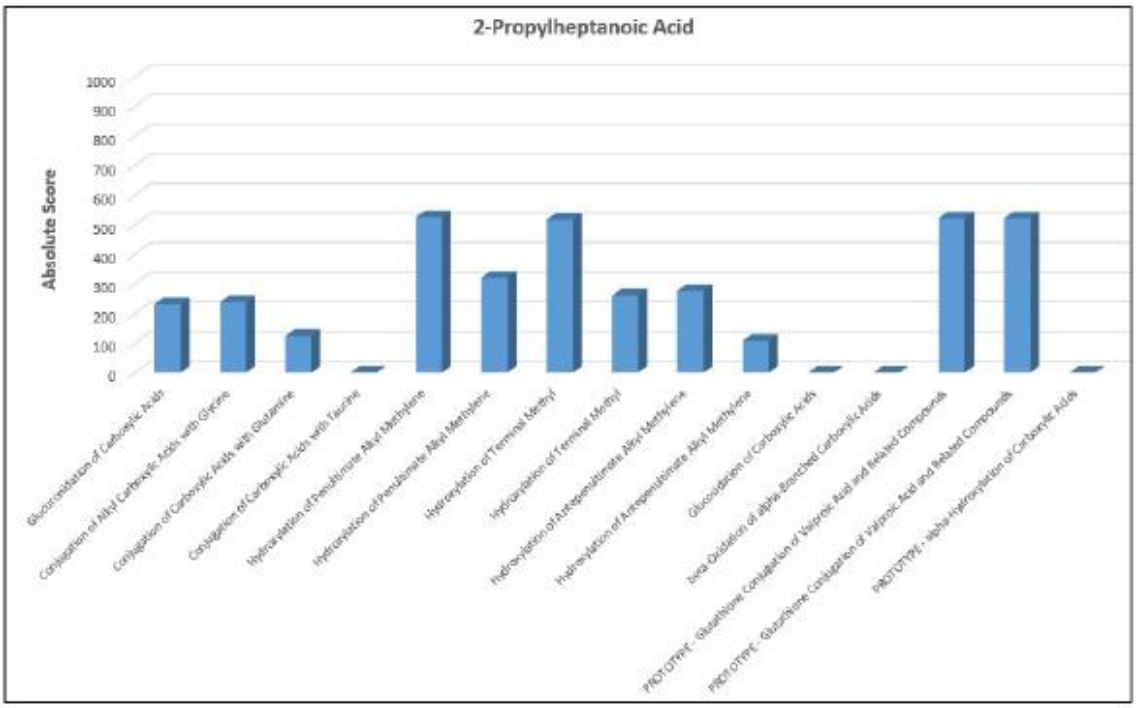

Metabolites Occurring as a Result of Biotransformations with Score > 0 (First Generation Only)

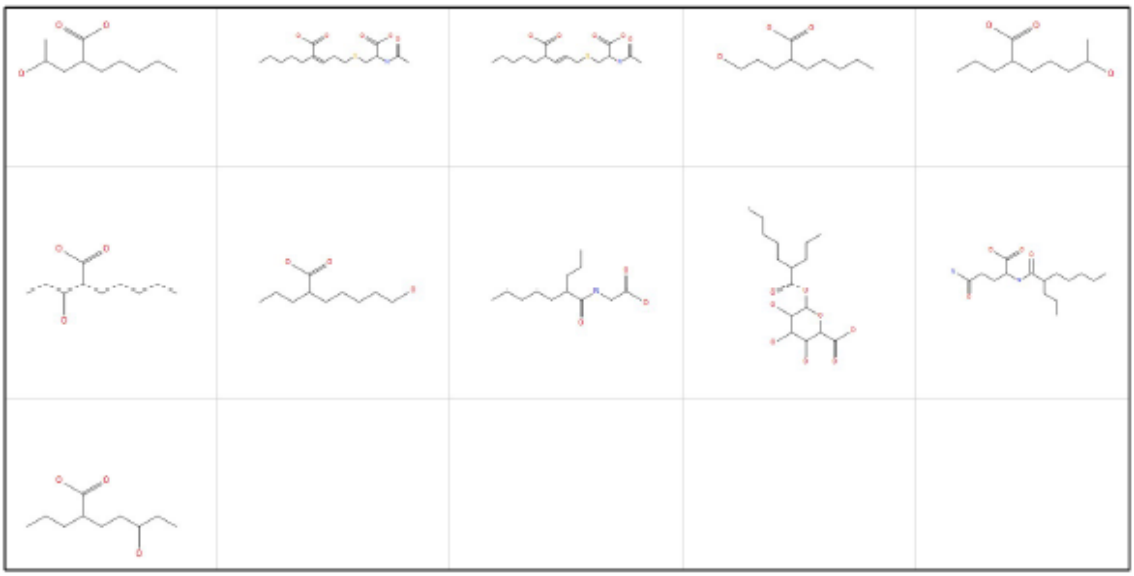

Metabolism Prediction: Comparison of Target Compound v. Analogue Compound 2 (First Generation Only)

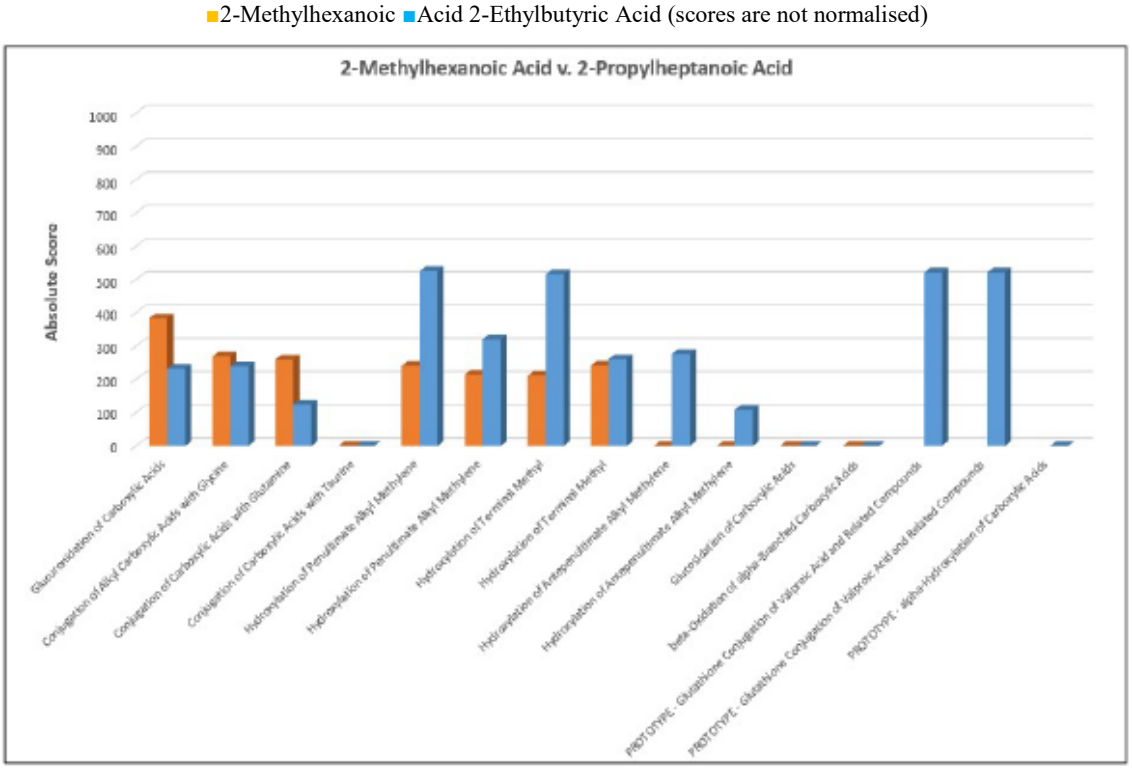

Similarity of First Generation Tree: Target Compound v. Analogue Compound 2 (See General Methods)

Biotransformation Fingerprint Method: 0.64

Concordant Metabolite Method: 0.78

Common Metabolites up to Third Generation (See General Methods)

2- Methylhexanoic Acid

No. Unique Metabolites: **295**

No. Unique Metabolites (Score > 0): **128**

2-Propylheptanoic Acid

No. Unique Metabolites: **587**

No. Unique Metabolites (Score > 0): **254**

Number of Common Metabolites (Score > 0): **0**

Common Metabolite Structures: **N/A**

Analogue Compound 3: Valproic Acid (CAS: 99-66-1)

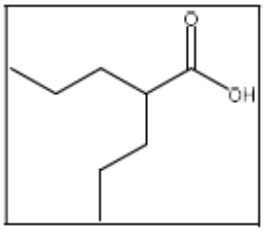

Predicted Metabolism at First Generation Only (see General Methods)

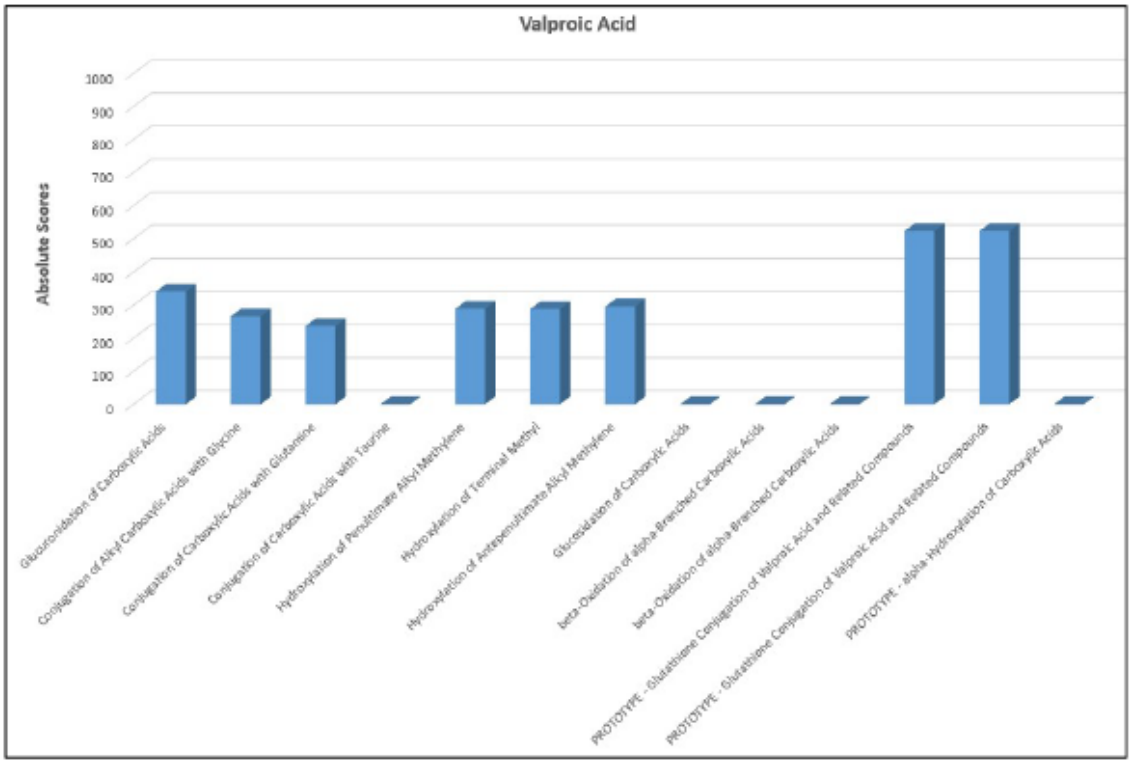

Metabolites Occurring as a Result of Biotransformations with Score > 0 (First Generation Only)

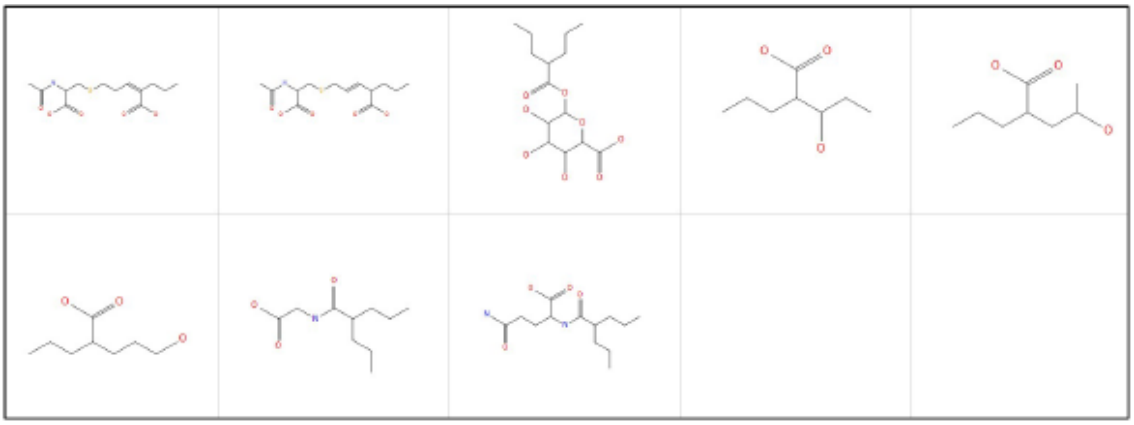

Metabolism Prediction: Comparison of Target Compound v. Analogue Compound 3 (First Generation Only)

■2-Methylhexanoic Acid ■Valproic Acid (scores are not normalised)

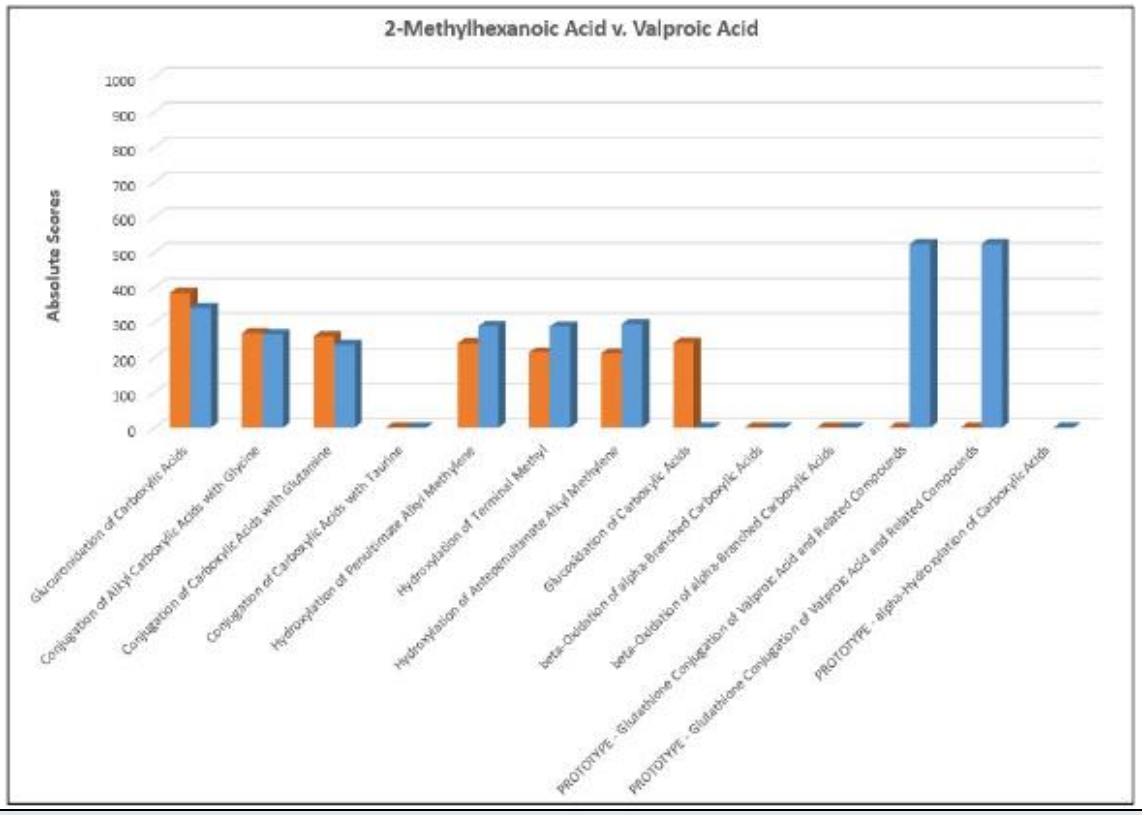

Similarity of First Generation Tree: Target Compound v. Analogue Compound 3 (See General Methods)

Biotransformation Fingerprint Method: 0.63

Concordant Metabolite Method: 0.72

Common Metabolites up to Third Generation (See General Methods)

2- Methylhexanoic Acid

No. Unique Metabolites: **295**

No. Unique Metabolites (Score > 0): **128**

Valproic Acid

No. Unique Metabolites: **337**

No. Unique Metabolites (Score > 0): **179**

Number of Common Metabolites (Score > 0): **0**

Common Metabolite Structures: **N/A**

***Analogue Compound 4*: 2-Ethylhexanoic Acid (CAS: 149-57-5)**

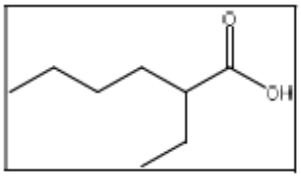

Predicted Metabolism at First Generation Only (see General Methods)

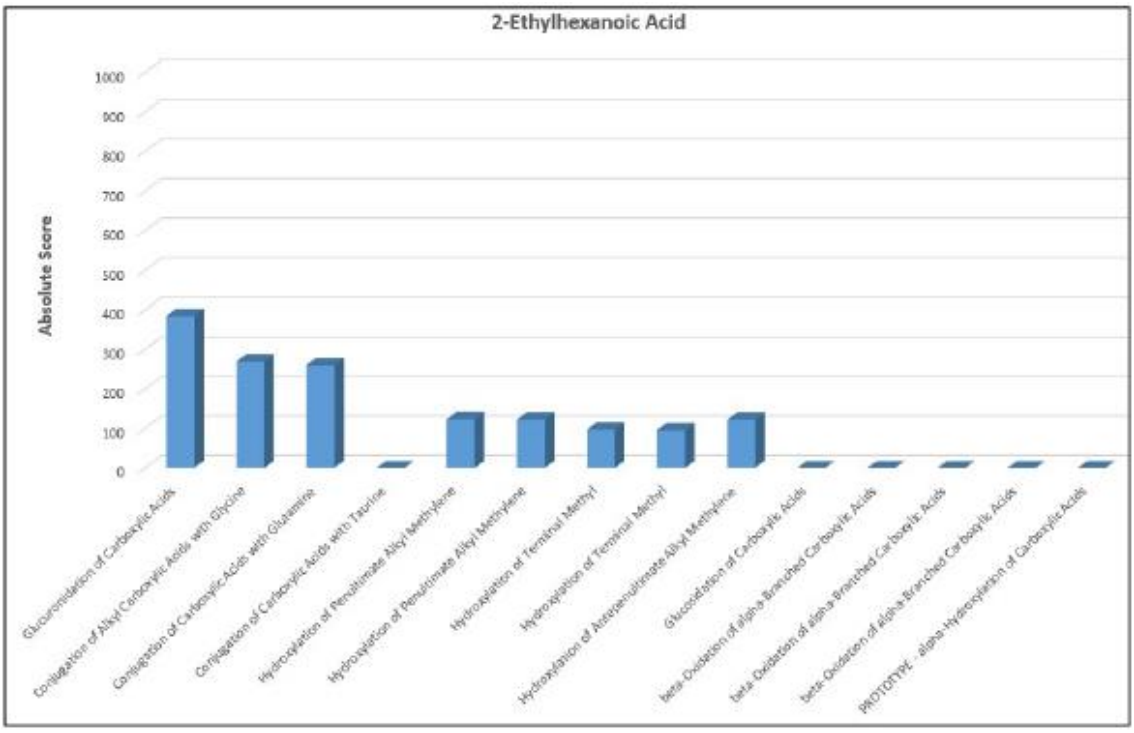

Metabolites Occurring as a Result of Biotransformations with Score > 0 (First Generation Only)

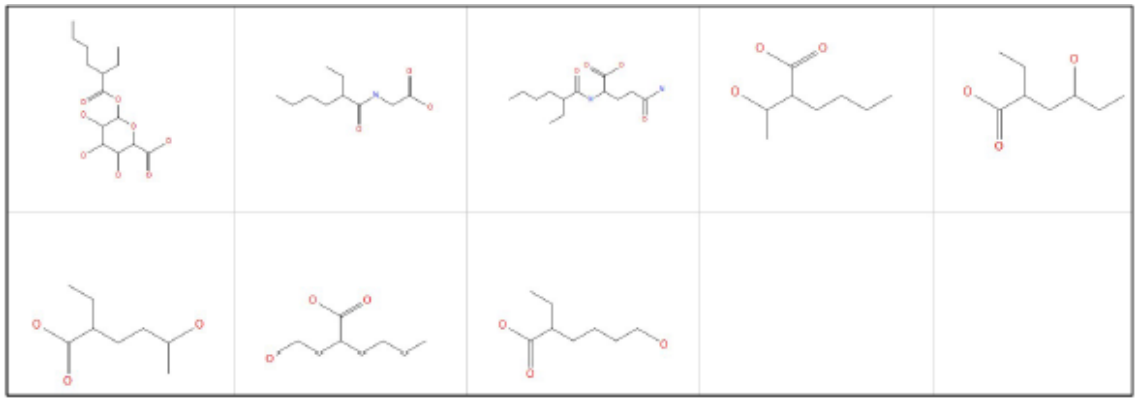

Metabolism Prediction: Comparison of Target Compound v. Analogue Compound 4 (First Generation Only)

■2-Methylhexanoic Acid ■2-Ethylhexanoic Acid (scores are not normalised)

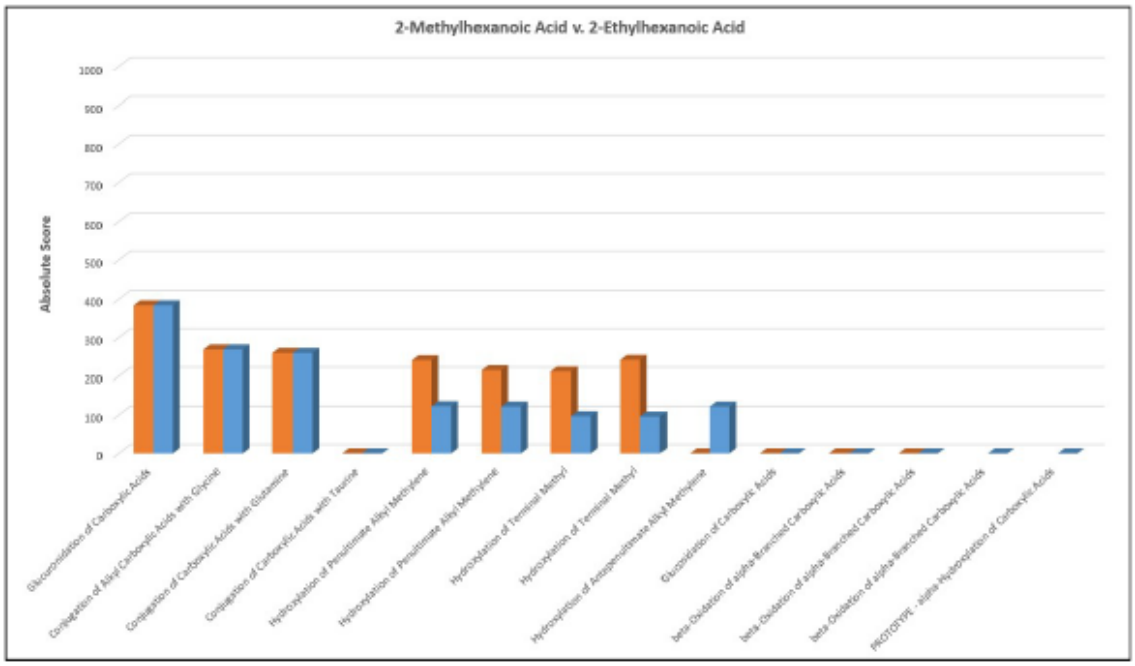

Similarity of First Generation Tree: Target Compound v. Analogue Compound 4 (See General Methods)

Biotransformation Fingerprint Method: 0.86

Concordant Metabolite Method: 0.98

Common Metabolites up to Third Generation (See General Methods)

2- Methylhexanoic Acid

No. Unique Metabolites: **295**

No. Unique Metabolites (Score > 0): **128**

2-Ethylhexanoic Acid

No. Unique Metabolites: **437**

No. Unique Metabolites (Score > 0): **233**

Number of Common Metabolites (Score > 0): **0**

Common Metabolite Structures: **N/A**

Analogue Compound 5: 2-Methylpentanoic Acid (CAS: 97-61-0)

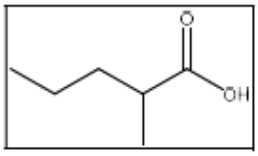

Predicted Metabolism at First Generation Only (see General Methods)

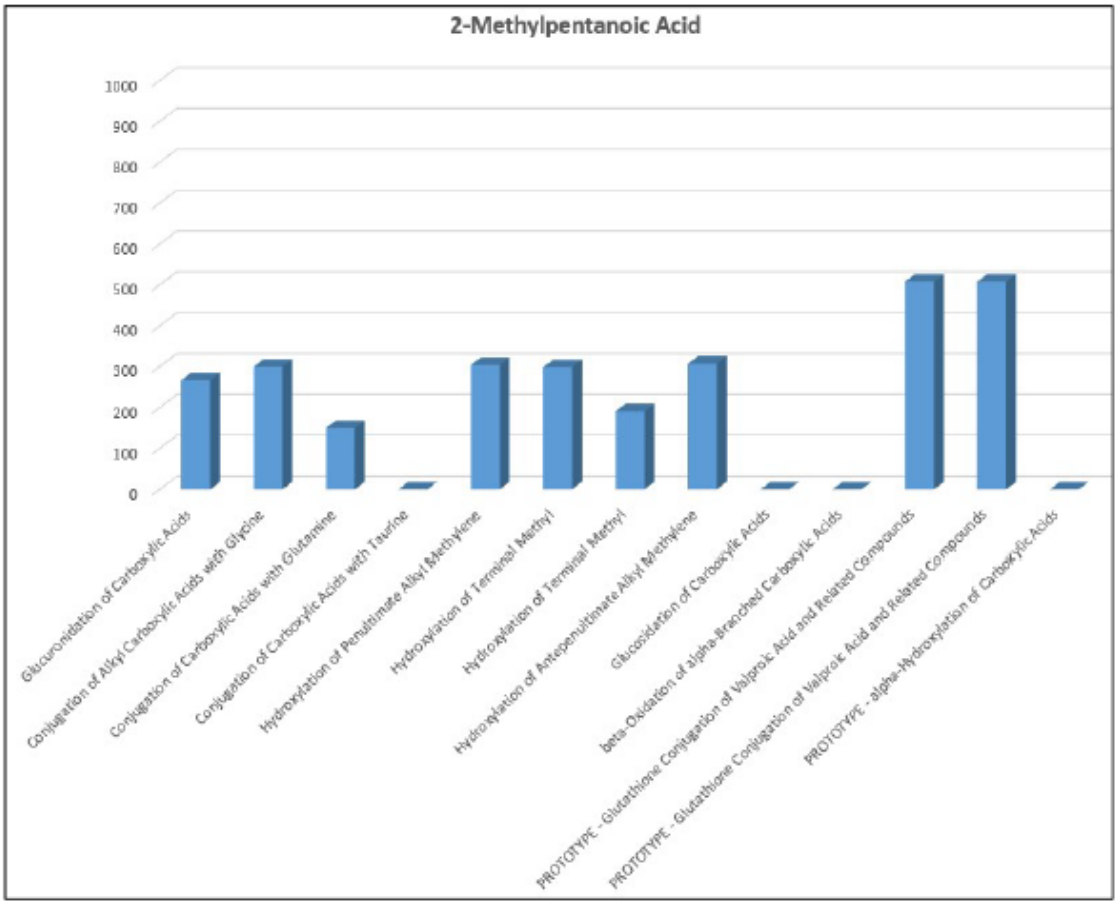

Metabolites Occurring as a Result of Biotransformations with Score > 0 (First Generation Only)

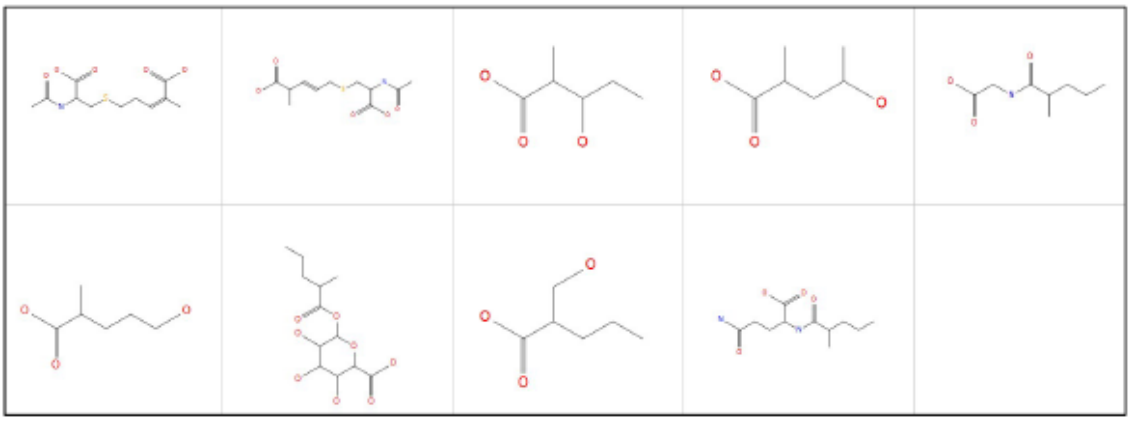

Metabolism Prediction: Comparison of Target Compound v. Analogue Compound 5 (First Generation Only)

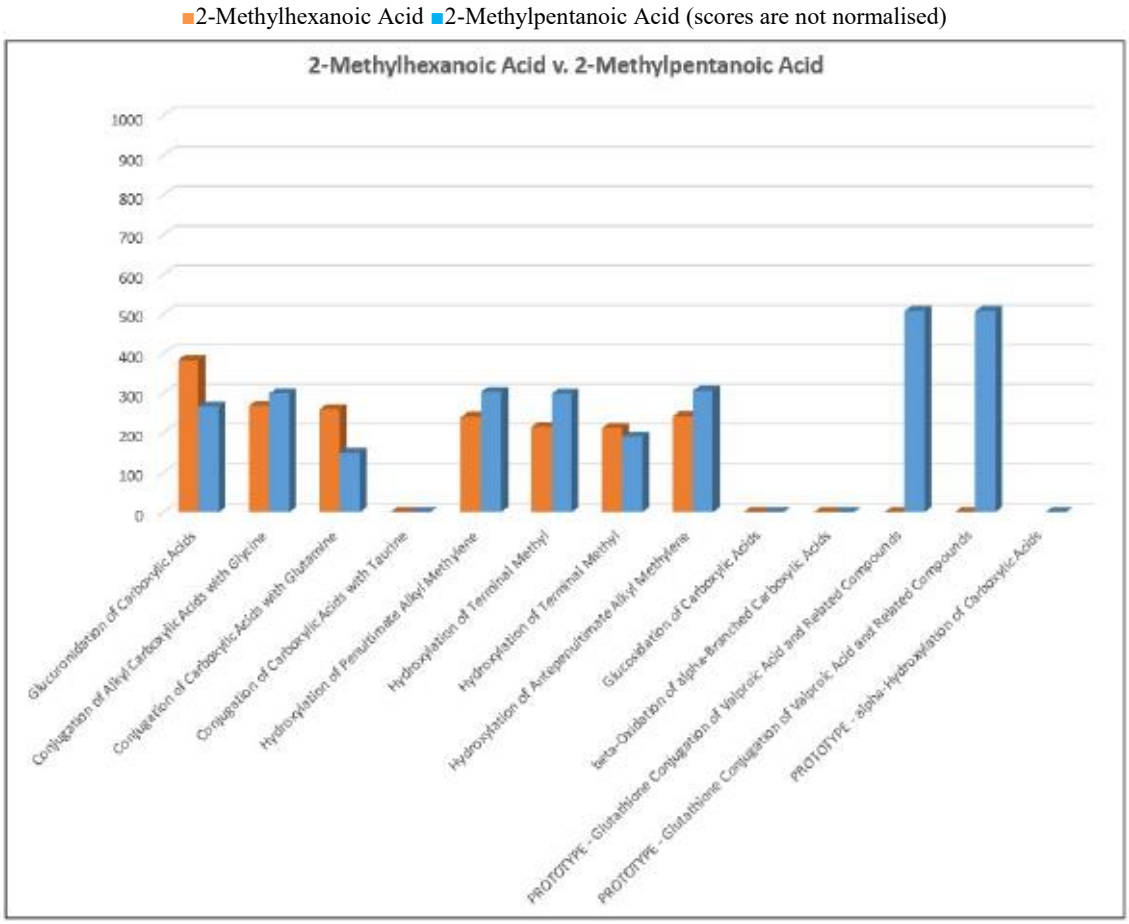

Similarity of First Generation Tree: Target Compound v. Analogue Compound 5 (See General Methods)

Biotransformation Fingerprint Method: 0.88

Concordant Metabolite Method: 0.76

Common Metabolites up to Third Generation (See General Methods)

2- Methylhexanoic Acid

No. Unique Metabolites: **295**

No. Unique Metabolites (Score > 0): **128**

2- Methylpentanoic Acid

No. Unique Metabolites: **254**

No. Unique Metabolites (Score > 0): **134**

Number of Common Metabolites (Score > 0): **0**

Common Metabolite Structures: **N/A**

General Comments on Prediction and Comparison to Published Literature

The most extensively studied and metabolically characterised analogue in this study is valproic acid itself and this has an extensive and complex metabolic profile as already discussed. Meteor Nexus is able to predict all phase II biotransformations with the exception of the adenylate (adenosine monophosphate) conjugate reported in a couple of studies. This is generally not a significant or detectable conjugate in the study of the vast majority of compounds with a carboxylic acid function. Whilst beta-oxidation is predicted for most analogues, the score assigned to the biotransformations is always zero. The reason for this is that the Meteor Nexus choice of nearest neighbour algorithm requires the metabolite structure in the data set, in the case of beta-oxidation (and in respect of the Meteor Nexus definition of this biotransformation) the final product that results after the final thiolytic cleavage and CoA deconjugation. These steps has been hinted at in the literature but never observed for valproic acid or any of its analogues. The theoretical structures and intermediates are available though for inspection in the Meteor Nexus trees. For substrates with a branched propyl chain, Meteor Nexus predicts conjugation with glutathione (biotransformation 506). Within this pathway, there are intermediates which arise as a result of sequential CYP-oxidation (terminal dehydrogenation) and beta-oxidation (internal dehydrogenation):

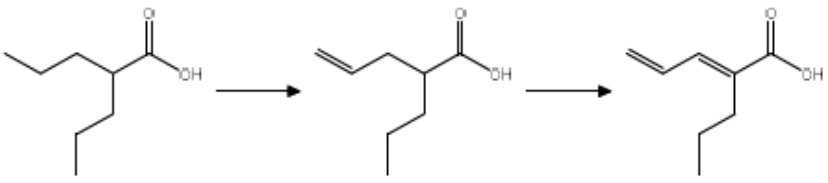

which is followed by 1,6-conjugate addition of glutathione to the 2-propyl-penta-2,4-dienoic acid. This reaction has been observed only for valproic, 4-ene- and 2,4-diene valproic acids but would in any case seem to be peculiar to propyl groups as a terminal

dehydrogenation is involved. All of the major CYP oxidations seen in the literature are predicted by Meteor Nexus including some of the non-obvious metabolites such as those resulting from lactone formation, however it is necessary to examine the larger, multi-generational trees in order to observe the predictions of these downstream metabolites. Understanding the limitation of the zero score for beta-oxidations, Meteor Nexus predicts well for this class in respect of the major and most often observed metabolites. The general (and expected) trend in prediction (and limited observation) is that the relative amount of carboaliphatic oxidation increases as the length of the alkyl chain and the side branch increases. Some degree of conjugation (by a combination of glucuronic acid, glycine, glutamine and taurine) is always predicted and these are usually the most significant contributors to clearance of these compounds *in vivo*.

Combined Graph of Biotransformation Scores for Target Compound and Analogue Compounds

[case study 1 - see notes on document history for relevance to case study 2]

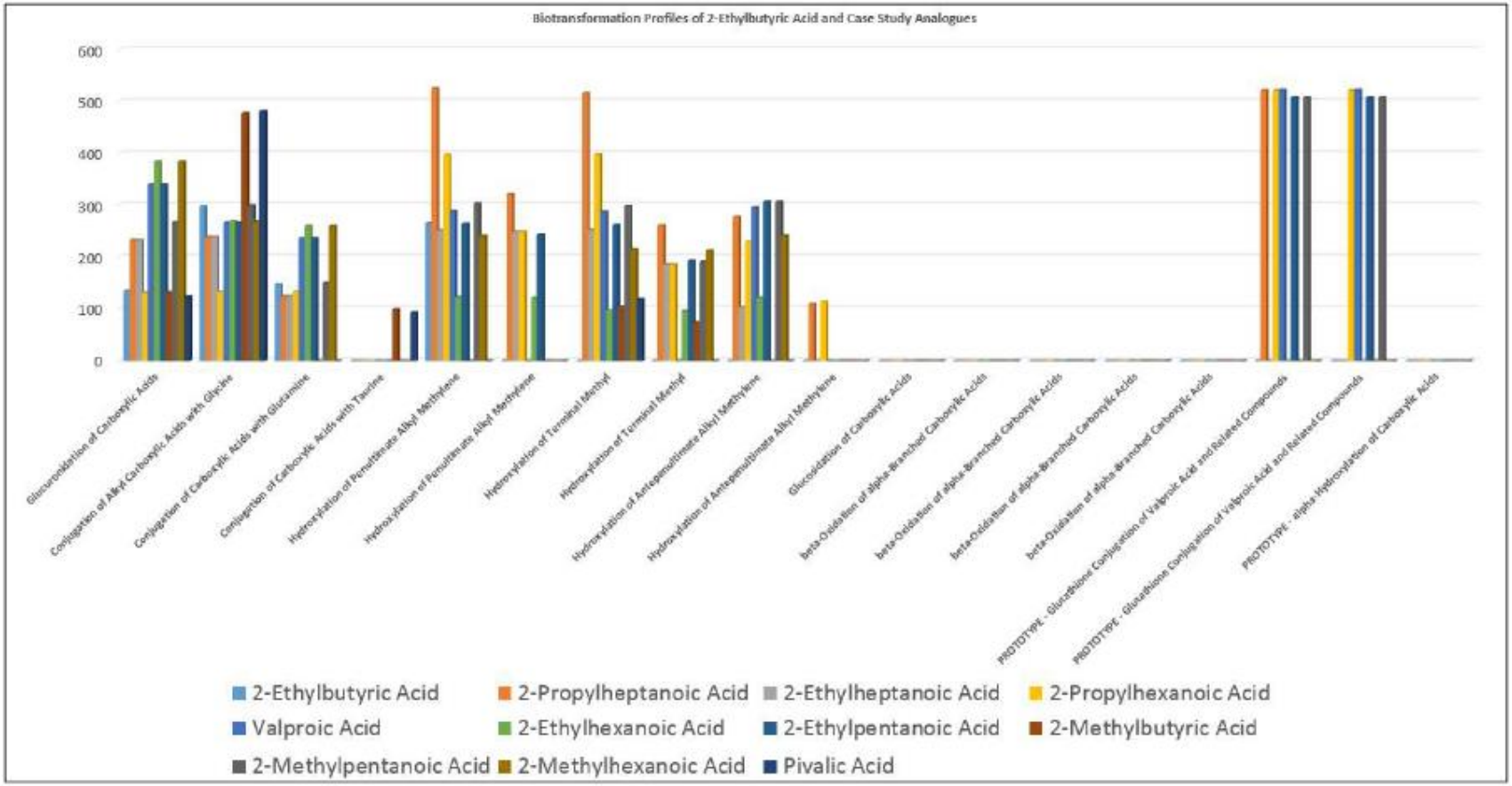

Combined Graph of Biotransformation Scores for Target Compound and Analogue Compounds (Alternative Visualisation)

[case study 1 - see notes on document history for relevance to case study 2]

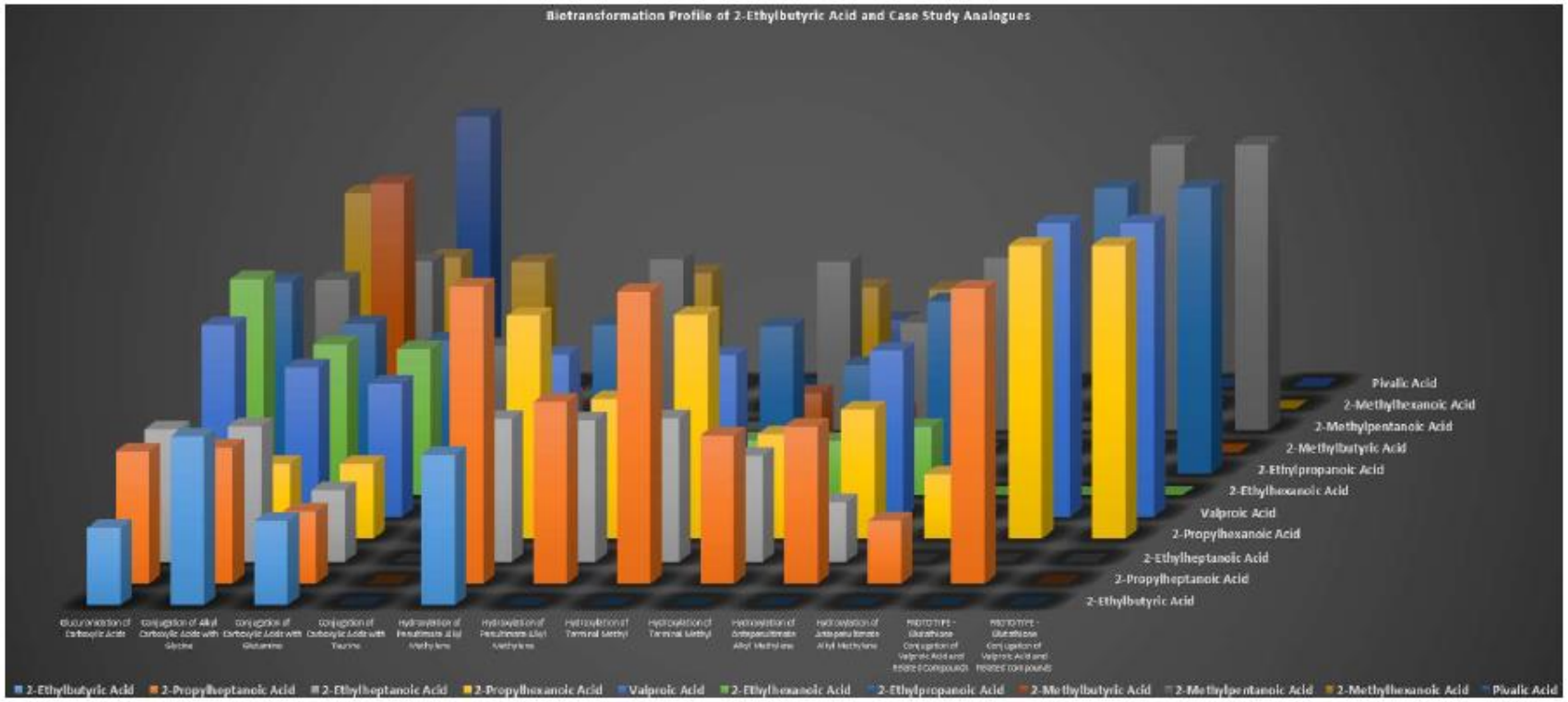

Comparison of Structural, Metabolic (Concordant Metabolite) and Biotransformation Fingerprint Similarities for Target and Analogue Compounds

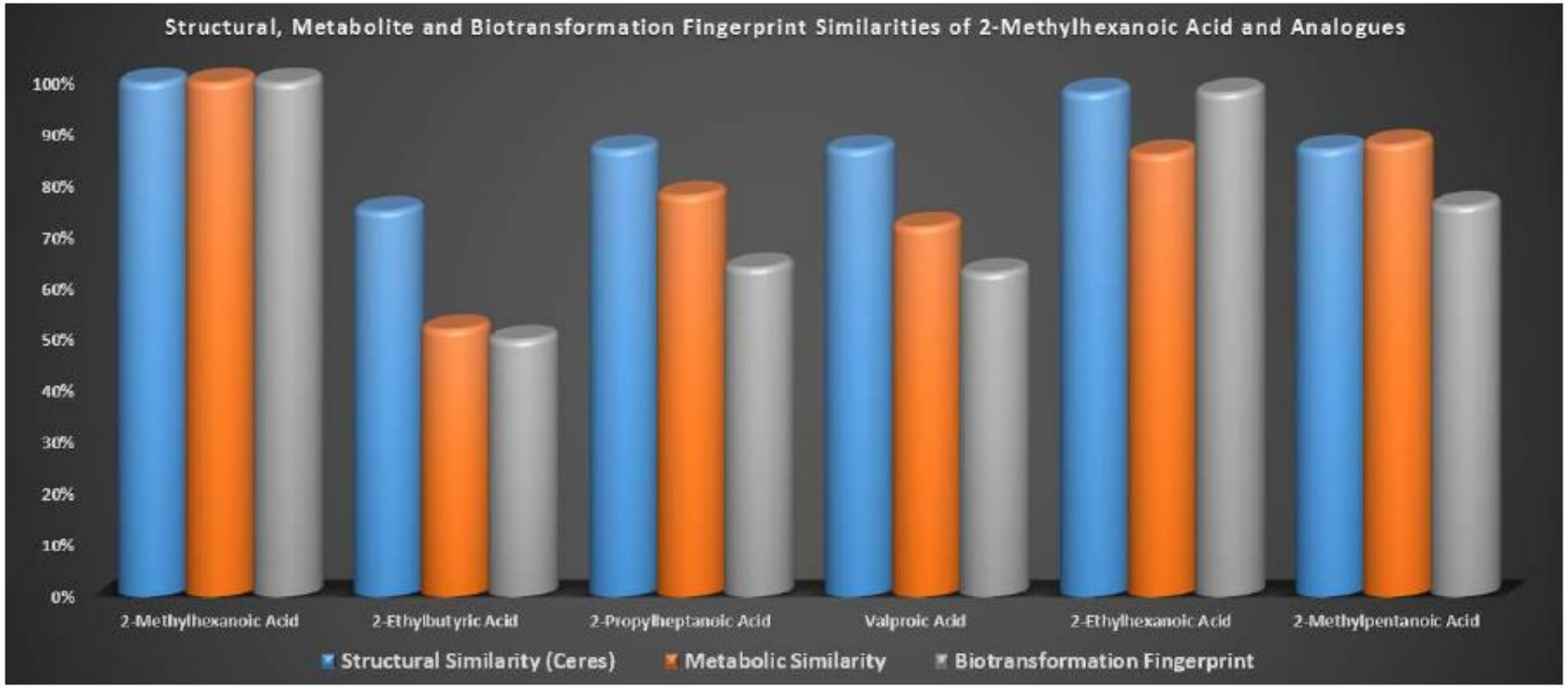

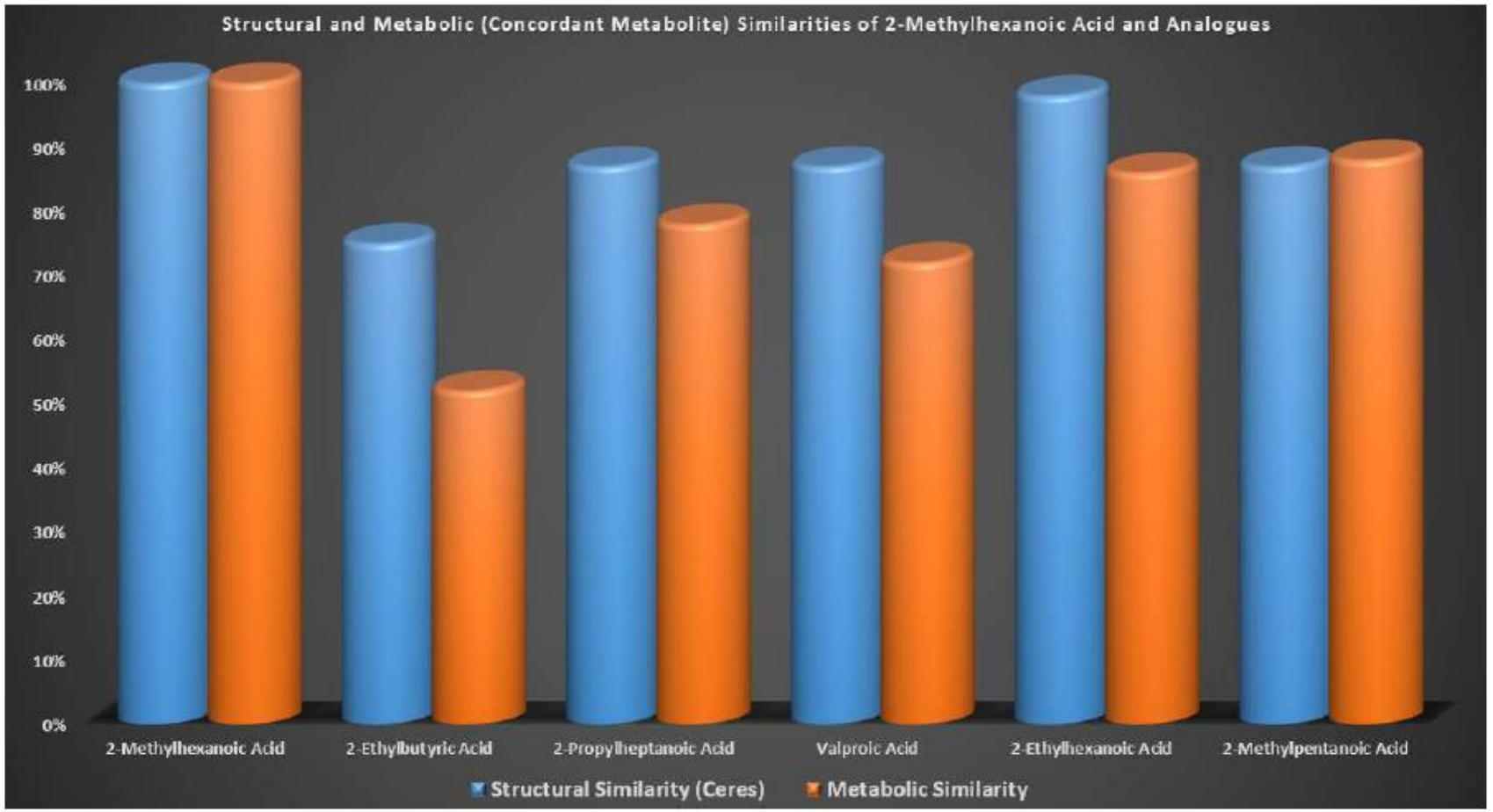
Structural and Metabolic (Concordant Metabolite) Similarities of 2-Methylhexanoic Acid and Analogues
100%
90%
80%
70%
60%
50%
40%
30%
20%
10%
0%
2-Methylhexanoic Acid
2-Ethylbutyric Acid
2-Propylheptanoic Acid
Valproic Acid
2-Ethylhexanoic Acid
2-Methylpentanoic Acid
Structural Similarity (Ceres)
Metabolic Similarity

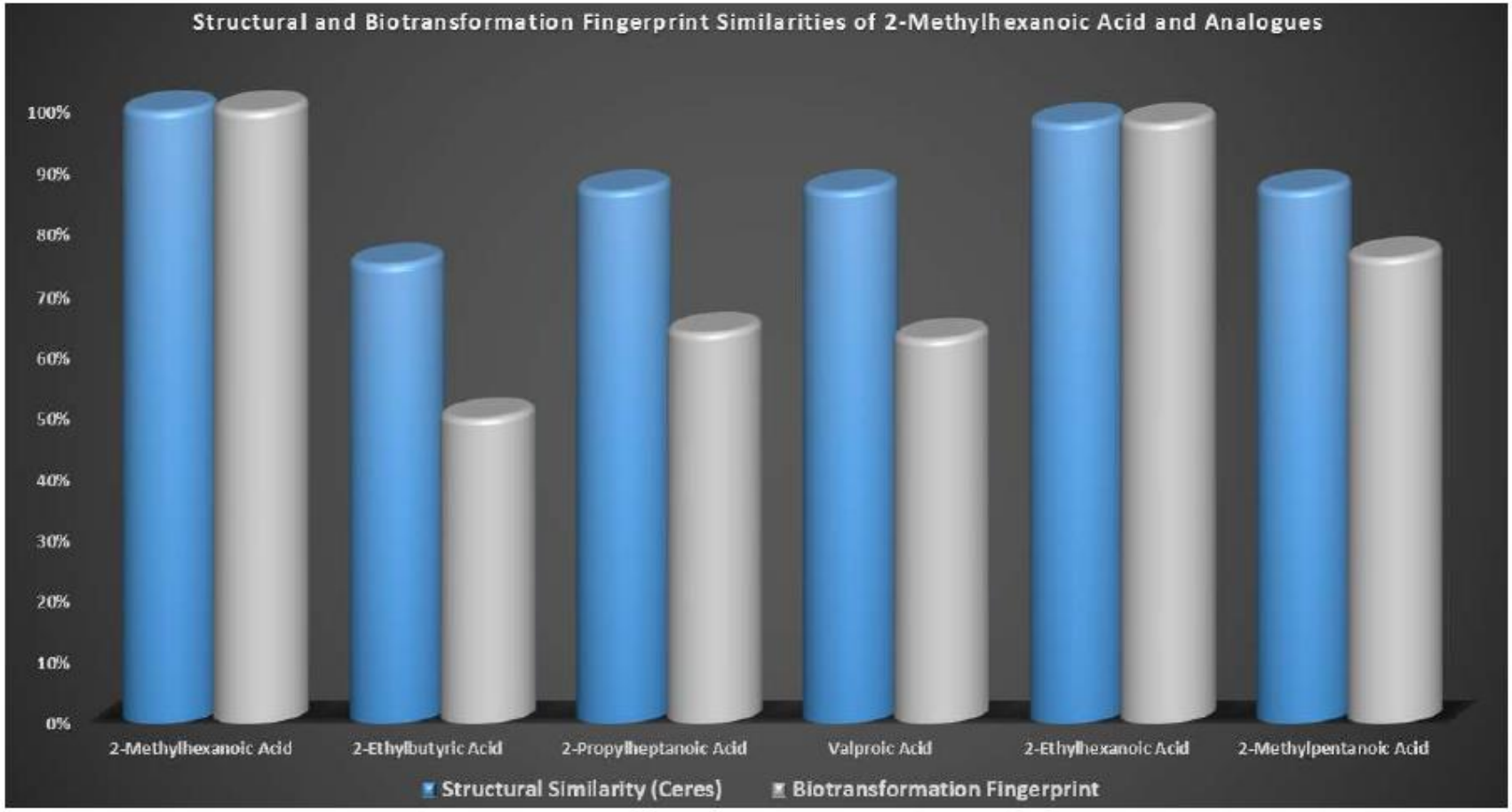
Structural and Biotransformation Fingerprint Similarities of 2-Methylhexanoic Acid and Analogues
100%
90%
80%
70%
60%
50%
40%
30%
20%
10%
0%
2-Methylhexanoic Acid
2-Ethylbutyric Acid
2-Propylheptanoic Acid
Valproic Acid
2-Ethylhexanoic Acid
2-Methylpentanoic Acid
Structural Similarity (Ceres)
Biotransformation Fingerprint

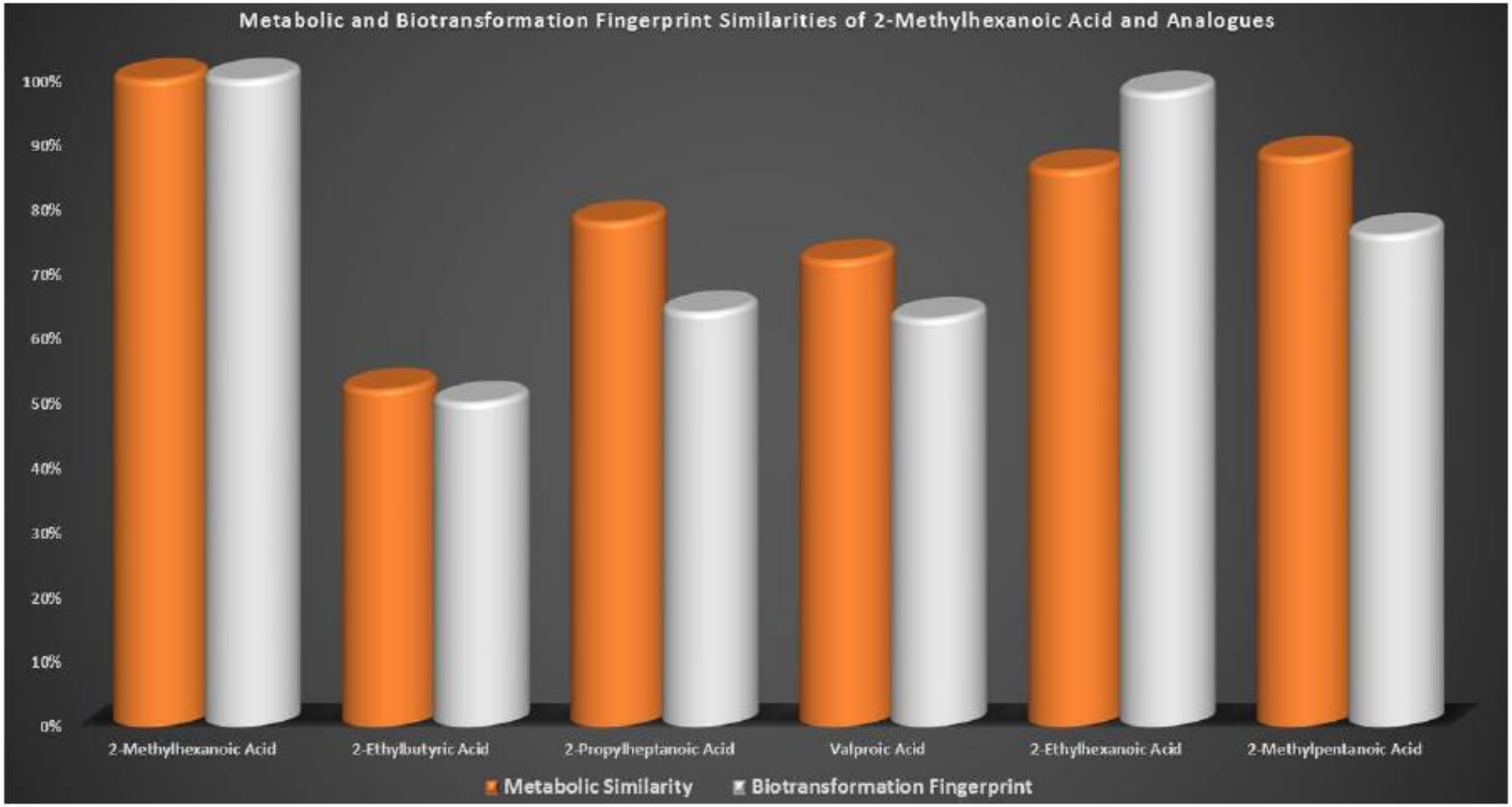
Metabolic and Biotransformation Fingerprint Similarities of 2-Methylhexanoic Acid and Analogues
100%
90%
80%
70%
60%
50%
40%
30%
20%
10%
0%
2-Methylhexanoic Acid
2-Ethylbutyric Acid
2-Propylheptanoic Acid
Valproic Acid
2-Ethylhexanoic Acid
2-Methylpentanoic Acid
Metabolic Similarity
Biotransformation Fingerprint

Biotransformation Fingerprints (Heatmap) for Target and Analogue Compounds

Tanimoto Similarity Matrix Based on Biotransformation Fingerprints for Target and Analogue Compounds

	2-Ethylbutyric Acid	2-Propylheptanoic Acid	2-Ethylheptanoic Acid	2-Propylhexanoic Acid	Valproic Acid	2-Ethylhexanoic Acid	2-Ethylpentanoic Acid	2-Methylbutyric Acid	2-Methylpentanoic Acid	2-Methylhexanoic Acid	Pivalic Acid
2-Ethylbutyric Acid	1	0.46	0.63	0.46	0.46	0.63	0.5	0.67	0.44	0.5	0.25
2-Propylheptanoic Acid	0.46	1	0.73	1	1	0.73	0.91	0.33	0.73	0.64	0.33
2-Ethylheptanoic Acid	0.63	0.73	1	0.73	0.73	1	0.8	0.44	0.78	0.87	0.44
2-Propylhexanoic Acid	0.46	1	0.73	1	1	0.73	0.9	0.33	0.73	0.64	0.33
Valproic Acid	0.46	1	0.73	1	1	0.73	0.9	0.33	0.73	0.63	0.33
2-Ethylhexanoic Acid	0.63	0.73	1	0.73	0.73	1	0.8	0.44	0.78	0.86	0.44
2-Ethylpentanoic Acid	0.5	0.91	0.8	0.9	0.9	0.8	1	0.36	0.8	0.7	0.5
2-Methylbutyric Acid	0.67	0.33	0.44	0.33	0.33	0.44	0.36	1	0.44	0.5	1
2-Methylpentanoic Acid	0.44	0.73	0.78	0.73	0.73	0.78	0.8	0.44	1	0.88	0.44
2-Methylhexanoic Acid	0.5	0.64	0.87	0.64	0.63	0.86	0.7	0.5	0.88	1	0.5
Pivalic Acid	0.25	0.33	0.44	0.33	0.33	0.44	0.5	1	0.44	0.5	1

Tanimoto Coefficient Code:

0
0.01-0.33
0.34-0.66
0.67-0.99
1

Essential Statistics* Regarding the Lhasa Limited Metabolism Dataset and Definition of Applicability Domain

Number of Unique Parent Compounds: **2739**

Number of Metabolic Biotransformations: **31897**

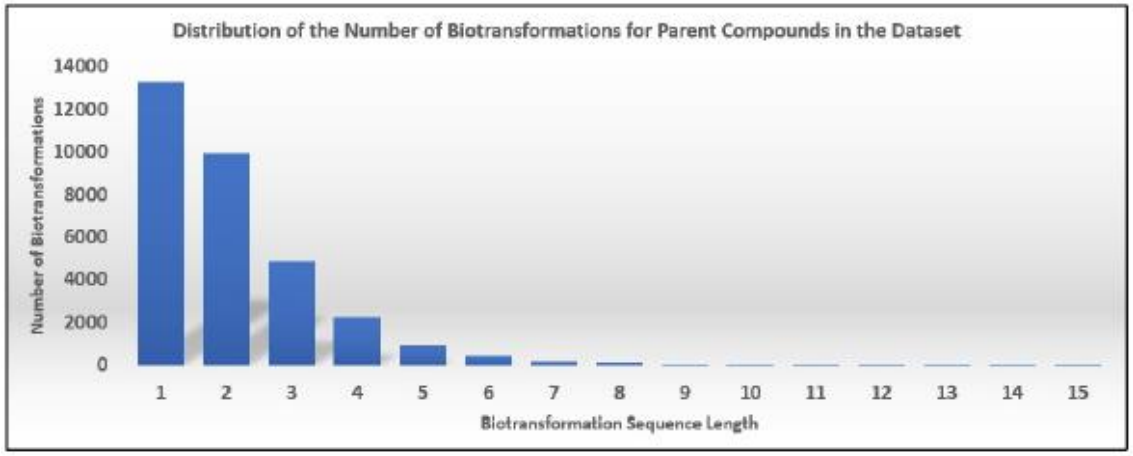

Experiment Type	Number of Experiments
In vitro	**2764**
In vivo	**2477**
Ex Vivo	**2**

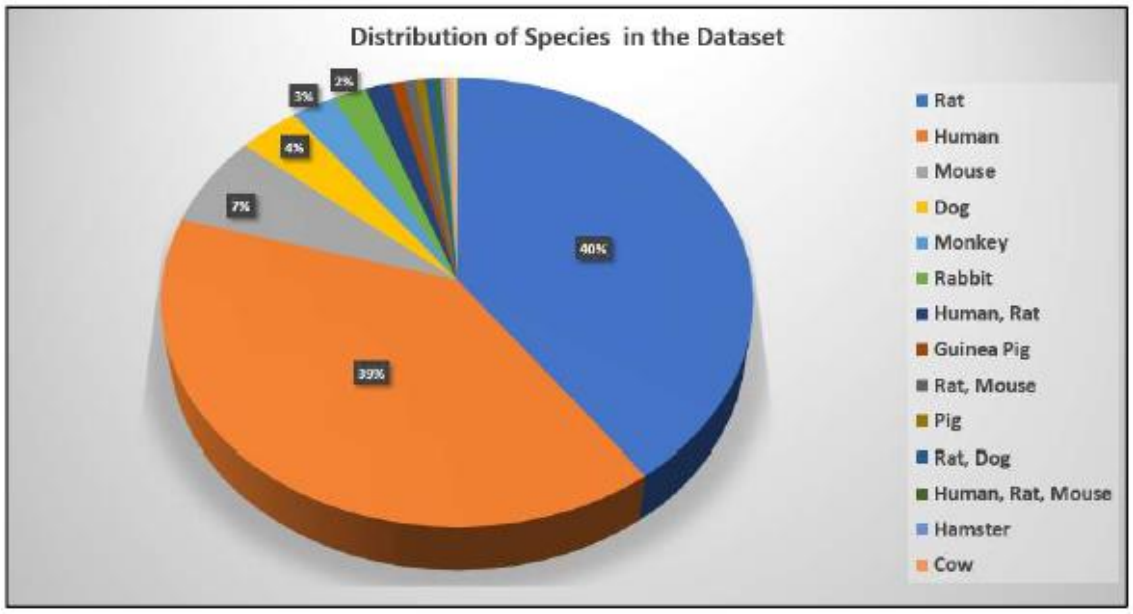

*Numbers refer to Lhasa Limited Metabolism Dataset version 2.2.0 used in this study.
Valproic acid and pivalic acid in our mock submission are part of the dataset [*pivalic acid is not an anolgue compound for case study 2*].

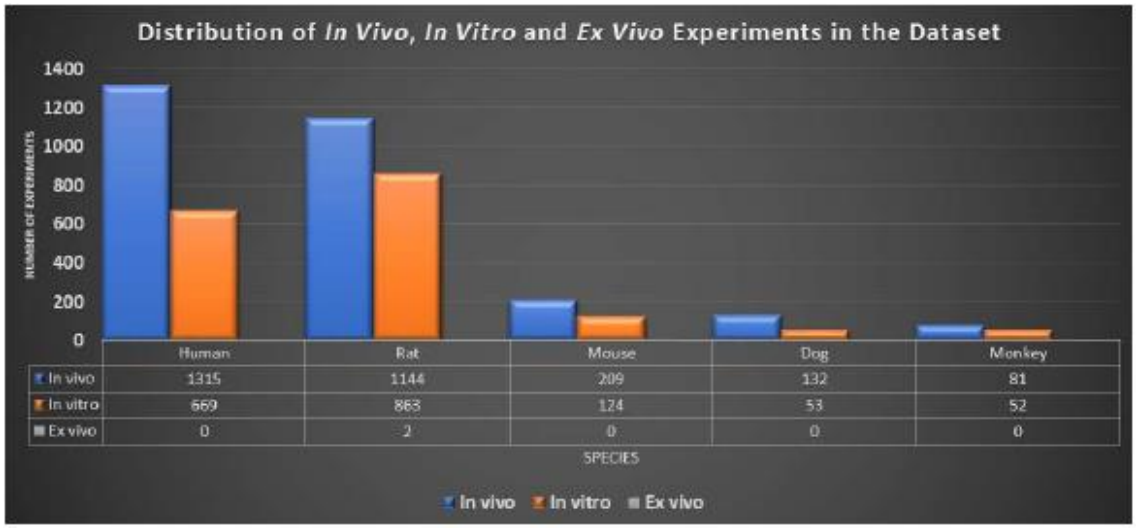

Analysis of the Applicability Domain

In this section the applicability domain is analysed. The applicability domain indicates whether or not the model/database used for the prediction of, for example, biotransformation scores cover compounds with comparable features to the predicted compounds. Applicability domains can be analysed in many different ways[20]. Here we report how well the source and target compounds are covered with regard to their structural and physico-chemical properties in the Meteor Nexus knowledge base.

Meteor Nexus is an knowledge based system. Its rules have been derived by human experts over many years from study and knowledge of the metabolic chemistry literature and as such are not built on the dataset in the same way as a QSAR or some other model is mathematically built on a training set. However, biotransformations scores, which give us a level of confidence in the occurrence of a particular biotransformation, are predicated[16] on a set of nearest neighbour parent compounds drawn from the dataset. In that respect the metabolism dataset is a viable "surrogate" training set for a definition of the applicability domain in this analysis.

Principal Component Analysis and Molecular Fingerprint Definition of the Lhasa Limited Metabolism Dataset and the Mock Submission Target and Analogue Compounds

Principal Component Analysis (PCA) is a mathematical method for dimensionality reduction that allows for multidimensional datasets to be visualized using two- or three-dimensional plots with minimal loss of information[10,11]. In this case we chose 32 structural and physicochemical properties of two datasets namely the Lhasa Limited Metabolism Dataset and the chosen case study 1 target and analogue compounds. Each compound in the dataset is represented by a 32-dimensional vector defined by the physicochemical properties calculated using RDKit and CDK nodes in KNIME.

Calculated Descriptors from RDKit and CDK
SlogP, SMR, LabuteASA, TPSA, AMW, NumLipinskiHBA, NumLipinskiHBD, NumRotatableBonds, NumHBD, NumHBA, NumAmideBonds, NumHeteroAtoms, NumHeavyAtoms, NumAtoms, NumStereocenters, NumUnspecifiedStereocenters, NumRings, NumAromaticRings, NumSaturatedRings, NumAliphaticRings, NumAromaticHeterocycles, NumSaturatedHeterocycles, NumAliphaticHeterocycles, NumAromaticCarbocycles, NumSaturatedCarbocycles, NumAliphaticCarbocycles, FractionCSP3, Atomic Polarizabilities, Bond Polarizabilities, VABC Volume Descriptor, Largest Pi Chain, Molecular Weight.

Each value was normalised using 'z-scores', meaning that each descriptor value is transformed such that the value in each column has a mean of 0.0 and a standard deviation of 1.0. Each chemical in the dataset can also be represented as a molecular fingerprint[12] using RDKit.

The first principal component calculated (PC0) accounts for as much of the variability in the original (normalised) data as possible, with each succeeding component (PC1, PC2 etc.), which are projected orthogonally to each other, accounting for as much of the remaining variability as possible. To visualise the chemical space occupied by the case study parent structures, the points calculated for the Lhasa Dataset (small blue spheres) were plotted using the values for the first two principal components (PC0 and PC1) and the case study parent compounds points were overlaid (large green spheres). This is shown in the following figure:

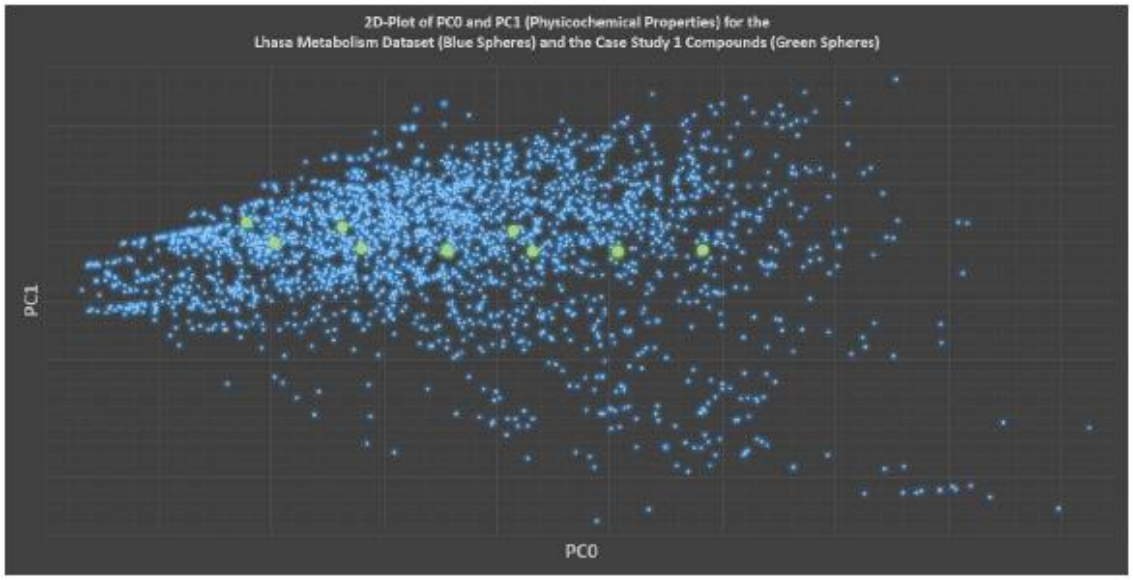

[data for case study 1 - see notes on document history for relevance to case study 2]

The figure shows that the case study compounds lie within the domain of the chemical space described by the Lhasa Metabolism Dataset as defined by these principal components.

If the data is projected using a third principal component (PC2) then the overall 3D space occupied by the case study compounds can be shown to lie within the chemical space defined by the minimum and maximum values for each axis of the three principal components as shown in the following table:

	PC0	PC1	PC2
Minimum Value of Principal Component	**-6.3509**	**-9.4763**	**-8.8195**
2,2-dimethylpropanoic acid	-3.4332	0.6506	-0.729
2-methylbutanoic acid	-2.9244	-0.0348	-0.83
2-ethylbutanoic acid	-1.728	0.5106	-0.5607
2-methylpentanoic acid	-1.3918	-0.2201	-0.5276
2-methylhexanoic acid	0.127	-0.3091	-0.1925
2-ethylpentanoic acid	0.127	-0.3091	-0.1925
Valproic acid	1.3011	0.3928	0.1298
2-ethylhexanoic acid	1.6372	-0.3379	0.163
2-ethylheptanoic acid	3.1417	-0.3265	0.5321
2-propylhexanoic acid	3.1417	-0.3265	0.5321
2-propylheptanoic acid	4.6422	-0.2871	0.9107
Maximum Value of Principal Component	**11.4787**	**5.5558**	**5.8887**

[case study 1 analogues have been greyed out]

Contribution (variance) of physicochemical descriptors to each principal component is shown in the following chart:

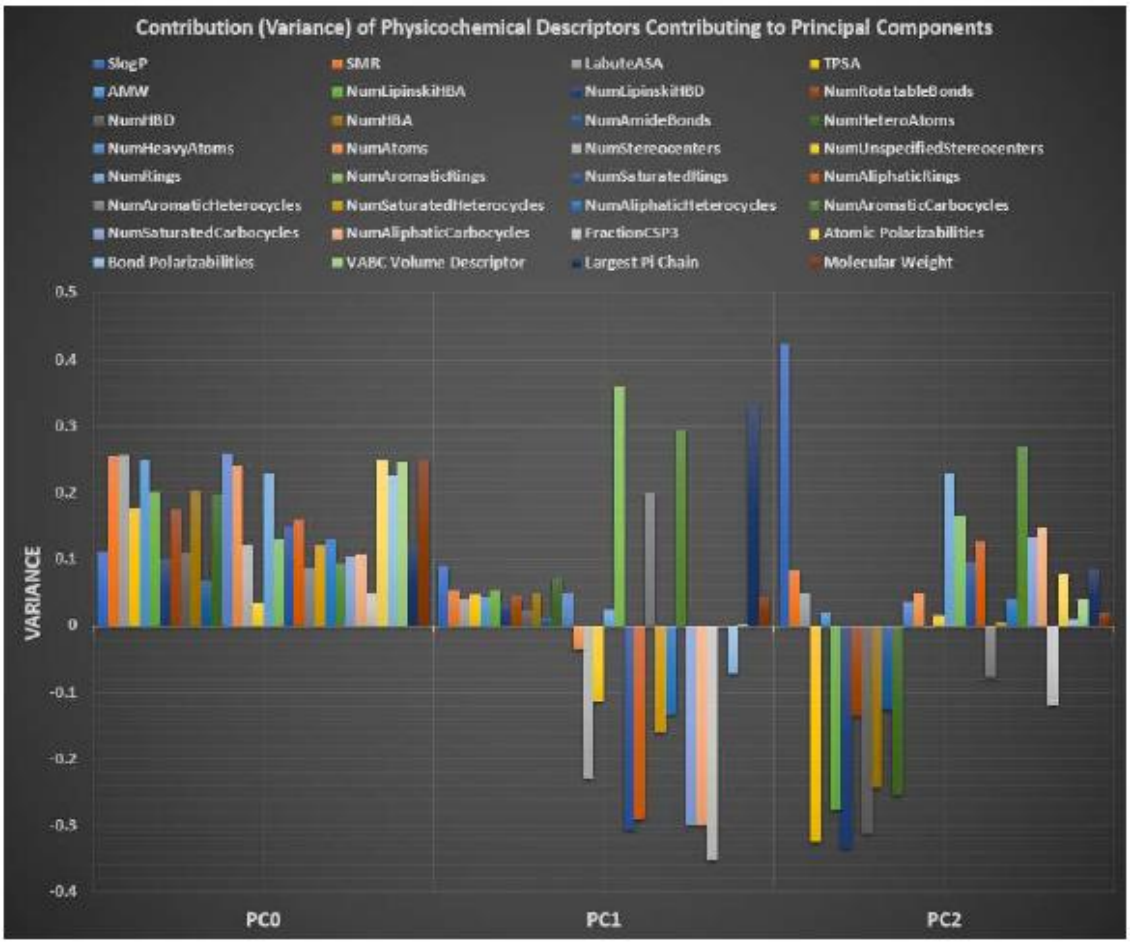

Visualisation of three principal components is best achieved interactively - in this instance a KNIME 2D/3D Scatterplot node was employed. Some representative visualisations are shown below:

Representative 3D-Visualisations Using Principal Components 0, 1 and 2 (Physicochemical Descriptors) Showing Case Study 1 Compounds (Large Purple Spheres) lying within the Chemical Space of the Lhasa Limited Metabolism Dataset (Small Red Spheres).

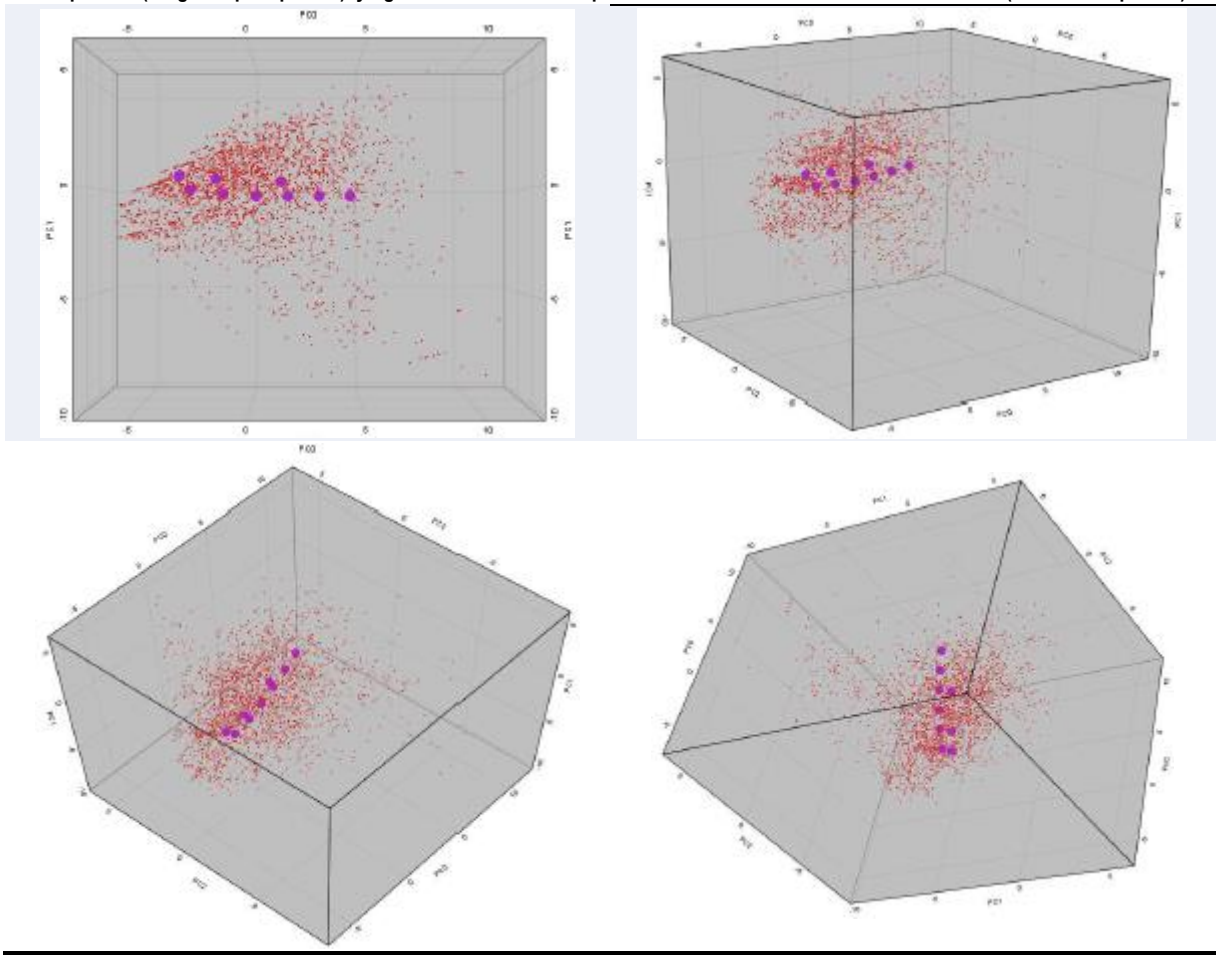

[data for case study 1 - see notes on document history for relevance to case study 2]

Note that in this table the following compounds have the same values: 2-methylhexanoic acid/2-ethylpentanoic acid and 2-ethylheptanoic acid/2-propylhexanoic acid; therefore, their points overlap in the plot giving nine points and not the expected eleven.

The Lhasa Limited metabolism dataset contains 2739 unique parent compounds. However, only a small proportion of these are used to furnish the supporting nearest neighbours in this analysis. Although most of them appear many times supporting the scores for various biotransformations, there are only 46 unique nearest neighbours (UNN) in this set. These are shown below:

Case Study Compounds in the Unique Nearest Neighbours (UNN) Set:

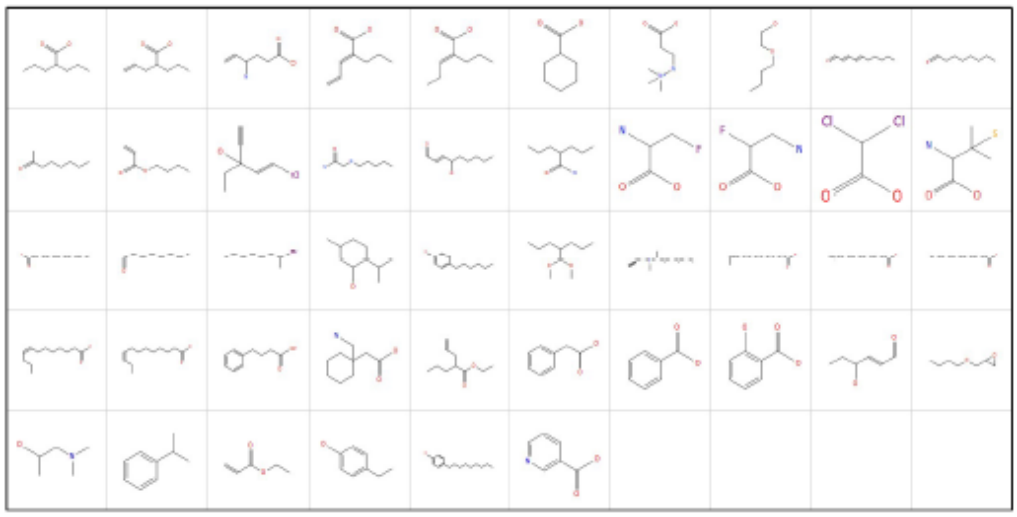

This set of compounds can be used to define a "localised" applicability domain in which the minimum and maximum values of principal components 0, 1 and 2 define a smaller area of chemical space than the whole dataset. All of the target and analogue compounds lie within this localised domain indicating that the nearest neighbours are physicochemically closer in nature to the query structures. This is to be expected as the choice of nearest neighbours within Meteor Nexus is constrained (by default) to those whose molecular weight is ±30% that of the query compound - molecular weight having some approximate covariance with other physicochemical descriptors such as LogP, total polar surface area, number of rotatable bonds and so on.

	PC0	PC1	PC2
Minimum value of Principal Component (UNN)	-6.07048	-6.6872	-5.10143
Maximum value of Principal Component (UNN)	7.234704	4.155276	3.932278
Minimum Value of Principal Component (Full Dataset)	-6.3509	-9.4763	-8.8195
Maximum Value of Principal Component (Full Dataset)	11.4787	5.5558	5.8887

Localised Applicability Domain (Purple Inner Box) Defined by the Set of 46 Unique Nearest Neighbours Compared to the Global Applicability Domain (Lilac Outer Box) Defined by the 2739 Compounds of the Lhasa Limited Metabolism Data Set. Case Study Compounds are Shown as Blue Spheres in Two-Dimensional Principal Component Space (P0 v. P1, P0 v. P2 and P1 v. P2)

[data for case study 1 - see notes on document history for relevance to case study 2]

The result of repeating the procedure of overlaying the data using the Morgan fingerprinting method is shown below:

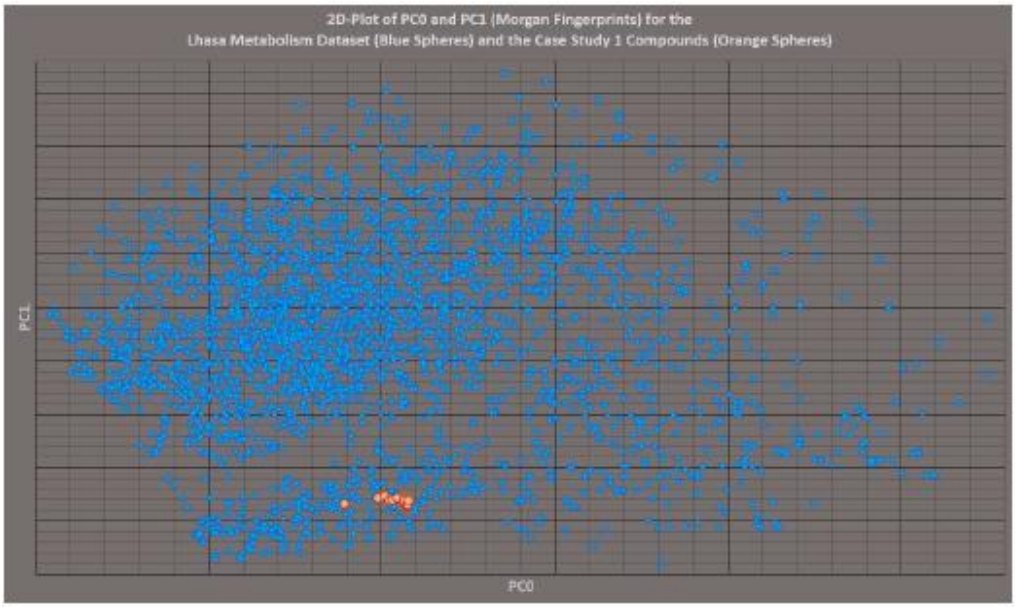

[data for case study 1 - see notes on document history for relevance to case study 2]

Applicability Domain Declaration of the Mock Submission Target and Analogues Compounds Based on Physicochemical Principal Component Analysis and Morgan Fingerprints.

The analysis of physico-chemical and structural properties indicates that all compounds are covered in the domain of the Meteor Nexus knowledge base. This is summarised in the following table:

Compound Name	CAS Number	Applicability Domain	
		Phys. Chem (PCA)	Morgan Fingerprints
2-Ethylbutyric Acid	88-09-5	In Domain	In Domain
2-Propylheptanoic Acid	31080-39-4	In Domain	In Domain
2-Ethylheptanoic Acid	3274-29-1	In Domain	In Domain
2-Propylhexanoic Acid	3274-28-0	In Domain	In Domain
Valproic Acid	99-66-1	In Domain	In Domain
2-Ethylhexanoic Acid	149-57-5	In Domain	In Domain
2-Ethylpentanoic Acid	20225-24-5	In Domain	In Domain
2-Methylbutyric Acid	1730-91-2	In Domain	In Domain
2-Methylpentanoic Acid	97-61-0	In Domain	In Domain
2-Methylhexanoic Acid	4536-23-6	In Domain	In Domain
Pivalic Acid	75-98-9	In Domain	In Domain

Quality Definition of the Lhasa Limited Metabolism Dataset

Harvesting data regarding metabolic chemistry from the literature can be extremely challenging due the uncertainties inherent in the assignment of chemical structures and reaction pathways. Some of the elements contributing to difficulty of interpretation include: incomplete chromatographic and chemical characterisation, ambiguous or unknown region and stereochemistry, length and branching of reaction sequences, incomplete or ambiguous reaction sequence characterisation, obscure or unknown chemistry, and so on. Whilst automated methods in KNIME have been developed to check certain elements such as formatting integrity, much of our work has required expert peer review. A classification

system has been developed which enables each paper to be assigned to a category depending on the degree of difficulty in its interpretation. We have defined five categories as follows: "trivial: *easy and uncontentious*" (category 1), "straightforward: *slight ambiguity*" (category 2), "moderate: *need for some expert calls*" (category 3), "challenging: *need for many expert calls*" (category 4) and "advanced: *ambiguity remaining after expert calls*" (category 5). It is not practical to peer review every submission (and is not always needed) and so attention has been primarily focussed on categories 3-5, the target percentage of submissions subject to expert peer review increasing with the difficulty of interpretation. All submissions in category 5 have been subject to peer review by at least one principal or senior project team member. A random sample (1%) of submissions from each category was subjected to a further rigorous peer review and the errors and error rates noted. By extrapolation, the residual error rate across the database could be estimated. Here we report errors is the three categories assessed: *Experimental Protocol, References, Structures and Biotransformations*.

Residual Error Rate in the Lhasa Limited Metabolism Dataset version 2.2.0

Error Category	Typical Error Issue	Error Rate
Experimental Protocol	Species/strain assignment, dose levels, assay source, assay time, total recovery, amount of unchanged drug detected.	**11.90%**
References	Typographical errors in author list or paper title.	**1.28%**
Structures and Biotransformations	Incorrect parent compound or metabolite structure, misclassified biotransformation name, misclassified metabolite type (observed, presumed, expert call).	**2.02%**

We had hoped for a residual error rate in all three categories of <5% and whilst the error rate in the *experimental protocol* category is higher than this, the information contained has no effect on the construction of the site-of-metabolism model from which nearest neighbours are chosen and upon which predicted biotransformation scores are predicated. This requires accuracy in the *structures and biotransformation* category and so we consider the residual error rate of 2% as acceptable.

Confidence Definition of References for Nearest Neighbour Examples Supporting Biotransformation Scores

This is expressed as an average across all references for each nearest neighbour example for each biotransformation for the target compound and the analogue compounds. Confidence ratings were calculated according to the method of Ponting *et al*[13]. The confidence rating is the summation of the *Chemical Characterisation Techniques Score* (0-4), the *Pathway Uncertainty Score* (0-2) and the *Metabolite Uncertainty Score* (0-2); the minimum combined score is 0 and the maximum 8. These are expressed as a percentage of the maximum. Individual rating definitions for each parameter are given in the table below:

Scheme of Assessment of Chemical Characterisation Confidence Ratings

Parameter \ Score	0	1	2	3	4
Chemical Characterisation Techniques	Insufficient	Poor	Fair	Good	Excellent
Pathway Uncertainty	Sequence assignment has high level of presumed metabolites	Sequence assignment has moderate level of presumed metabolites	Sequence assignment has low level of presumed metabolites		
Metabolite Uncertainty	Structure assignment needs high level of expert call	Structure assignment needs moderate level of expert call	Structure assignment needs low level of expert call		

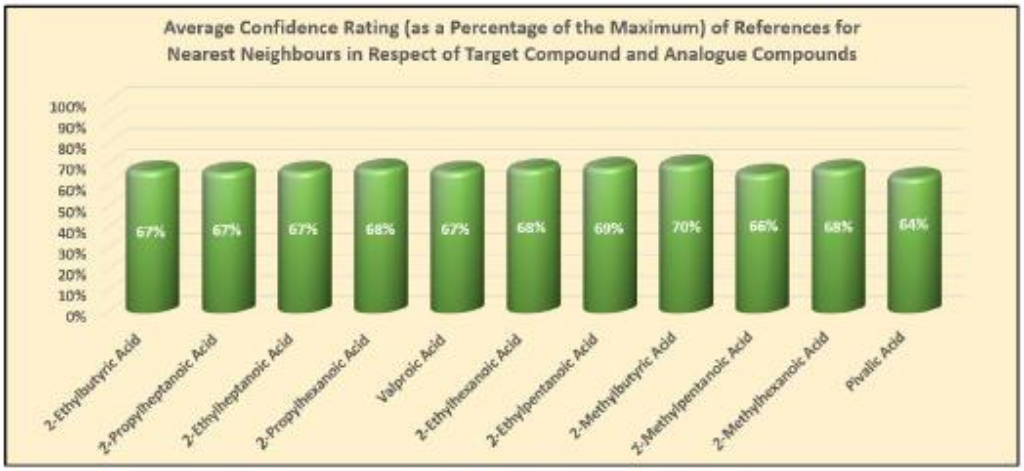

[data for case study 1 - see notes on document history for relevance to case study 2]

Individual Scores for Nearest Neighbour Examples in the Categories of: Chemical Characterisation Techniques, Pathway Uncertainty and Metabolite Uncertainty.

Comp_RefID	Techniques_verbal	Techniques_binned (0-4)	Pathway Uncertainty (0-2)	Metabolite Uncertainty (0-2)	SCORE (0-8)
Phenylbutyrate_094	excellent	4	2	2	8
Niacin_155	Poor	1	2	2	5
Phenylaceticacid_157	Insufficient	0	2	2	4
Cyclohexanecarboxylicacid_159	Poor	1	2	2	5
ButylGlycidylEther_233	Good	3	1	2	6
GSK977779_260	Good	3	2	0	5
L-menthol_415	Fair	2	2	2	6
2-Butoxyethanol_454	Poor	1	2	2	5
DCA_528	Good	3	2	2	7
R-2HMP_580	Fair	2	2	2	6
MET-88_603	Good	3	1	2	6
ButylAcrylate_859	Poor	1	1	2	4
EthylAcrylate_859	Poor	1	1	2	4
Trans-4-Hydroxy-2-hexenal_876	Good	3	2	2	7
4-Hydroxy-2-nonenal_881	Fair	2	2	2	6
ValproicAcid_920	Poor	1	1	2	4
VPA_1020	Excellent	4	2	2	8
VPA_1038	Fair	2	2	2	6
Butylphenol_1065	Poor	1	2	2	5
Ethylphenol_1065	Poor	1	2	2	5
Hexylphenol_1065	Poor	1	2	2	5
Nonylphenol_1065	Poor	1	2	2	5
2-trans-4-trans-Decadienal_1269	Good	3	2	2	7
Vigabatrin_1439	Good	3	2	2	7
10-DDNA_1492	Fair	2	2	2	6
11-DDNA_1492	Fair	2	1	2	5
8-DDNA_1492	Fair	2	2	2	6

9-DDNA_1492	Fair	2	2	2	6
LauricAcid_1492	Fair	2	2	2	6
2,4-dieneVPA_1499	Fair	2	2	2	6
Milacemide_1532	Fair	2	1	2	5
n-Butylacrylate_5008	Good	3	0	2	5
L-menthol_5037	Fair	2	1	2	5
Gabapentin_5062	Poor	1	2	2	5
2-Bromooctane_5115	Poor	1	2	2	5
2-Iodooctane_5115	Poor	1	2	2	5
2-Butoxyethanol_5116	Poor	1	2	2	5
Benzoicacid_5144	Fair	2	2	2	6
Trans-4-hydroxy-2-hexenal_5171	Fair	2	0	2	4
4-eneVPA_5181	Fair	2	1	2	5
Ethyl-4-eneVPA_5181	Fair	2	2	2	6
2-n-Propyl-4-Pentenoicacid_5210	Good	3	1	2	6
ValproicAcid_5212	Good	3	1	2	6
Fludalanine_5221	Fair	2	2	2	6
4-eneVPA_5232	Good	3	1	2	6
Penicillamine_5253	Fair	2	2	2	6
2-Propyl-2-pentenoicacid_5297	Good	3	0	2	5
PPDEA_5303	Fair	2	1	2	5
PPDIPA_5303	Fair	2	1	2	5
PPDMA_5303	Fair	2	1	2	5
Valpromide_5313	Insufficient	0	2	2	4
D-Penicillamine_5339	Poor	1	2	2	5
VPA_5386	Poor	1	2	2	5
DMAIP_5389	Fair	2	2	2	6
pAABA_5389	Fair	2	2	2	6
Doxifluridine_5409	Fair	2	0	2	4
alpha-Fluoro-beta-alanine_5409	Poor	1	2	2	5
Lauricacid_5551	Good	3	2	2	7
1-(2-chlorophenyl)propan-2-one_5614	Insufficient	0	2	2	4
1-(2-fluorophenyl)ethan-1-one_5614	Insufficient	0	2	2	4
1-(4-chlorophenyl)propan-2-one_5614	Insufficient	0	2	2	4
1-(o-tolyl)ethan-1-one_5614	Insufficient	0	2	2	4
1-(p-tolyl)propan-2-one_5614	Insufficient	0	2	2	4
1-phenylpropan-2-one_5614	Insufficient	0	2	2	4
acetophenone_5614	Insufficient	0	2	2	4
octan-2-one_5614	Insufficient	0	2	2	4
Octanal_5616	Insufficient	0	0	2	2
Ethchlorvynol_5624	Fair	2	1	2	5
SalicylicAcid_5638	Poor	1	2	2	5
SalicyluricAcid_5638	Poor	1	2	2	5
4-Nonylphenol-a_5786	Good	3	1	1	5
4-Nonylphenol-b_5786	Good	3	2	0	5
4-eneVPA_6173	Fair	2	1	2	5
4-eneVPA_6183	Good	3	1	2	6
2F-4-eneVPA_7066	Excellent	4	0	2	6

General Methods

Descriptions of Meteor and its reasoning (scoring) methods[14,15,16,17] as well as discussions of some use cases[18,19] have been published previously.

Program Versions

Nexus v.2.2.0 (Build 52 , Nov 2017)

Meteor Nexus v.3.1.0

Knowledge Base: Meteor KB 2018 1.0.0

Lhasa Limited Metabolism Data 2.2.0

Predicted Metabolism at First Generation Only

Process Constraints

Lhasa default except:

Max. Depth: 1

Score Threshold: 100

Inactive Biotransformations: 428

Report

Biotransformation Names, Biotransformation Numbers, and Absolute Scores for the target compound and each analogue compound were exported as a tsv file which was opened in Microsoft Excel for the purposes of creating a bar chart for ease of visualisation. For visual comparison of scores for analogue compound to target compound, the bar chart for the analogue compound was pasted onto a copy of that for the target compound.

Post Processing Filters

Score: >0 (tolerance ±0.0)

Report

Metabolite structures resulting from biotransformations having a score of >0 were exported as an sdf file which was conveniently visualised using Power MV, ChemFileBrowser or KNIME. Metabolic trees (mx files) were also saved for the target compound and each analogue compound.

Similarity of First Generation Only Trees: Target Compound v. Analogue Compound

CONCORDANT METABOLITE METHOD

In this general method (presented at the General Assembly Meeting, Egmond aan Zee, September 2017), structural similarities of concordant (predicted) metabolites for closely related analogues are assessed based on the dichotomous data Tanimoto method using extended circular fingerprints as the choice of molecular descriptors. Concordant metabolites are defined here as those arising via the same biotransformation occurring at comparable positions with the target analogues. The similarity of the entire metabolic tree (in our investigations to date, only the first generation of metabolites have been considered) can then be assessed based on the continuous data Tanimoto method using the computed similarities (a number between zero and one) for each concordant pair.

Process Constraints

Lhasa default except:

Max. Depth: 1

Score Threshold: 100

Inactive Biotransformations: 428

Post Processing Filters

Score: >0 (tolerance ±0.0)

Report

Metabolite structures resulting from biotransformations having a score of >0 were exported as an sdf file as described above.

Comparing the Metabolic Trees

Step 1

For both target and analogue compounds, metabolites arising from the same biotransformations (concordant metabolites) were matched by eye. As an example, concordant metabolites for the target (2-ethylbutyric acid) and analogue compound 4 (valproic acid) are shown in the following table. It can be seen that there are four concordant metabolite pairs (M1, M2, M3 and M5). Valproic acid metabolites M6, M7, M11 and M12 do not have counterparts in the 2-ethylbutyric acid metabolic tree:

Target Structure/Metabolite	Name (CAS no.)	Analogue Structure/Metabolite	Name (CAS no.)	Biotransformation
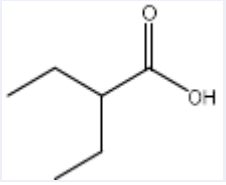	**88-09-5** 2-Ethylbuytric Acid	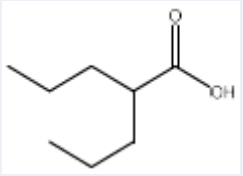	**75-98-9** Valproic Acid	N/A
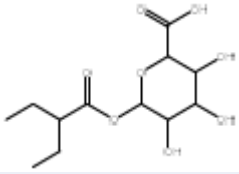	M1	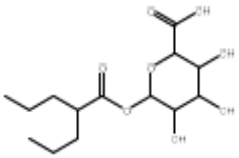	M1	Glucuronidation of Carboxylic Acids
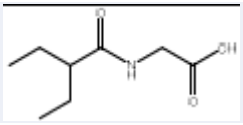	M2	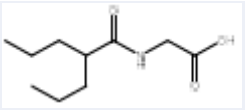	M2	Conjugation of Alkyl Carboxylic Acids with Glycine
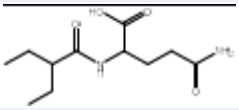	M3	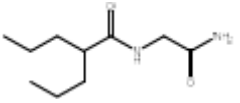	M3	Conjugation of Carboxylic Acids with Glutamine
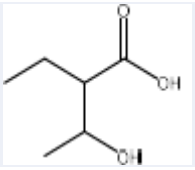	M5	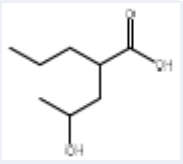	M5	Hydroxylation of Penultimate Alkyl Methylene
		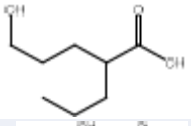	M6	Hydroxylation of Terminal Methyl
		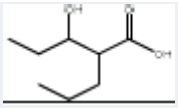	M7	Hydroxylation of Antepenultimate Alkyl Methylene
		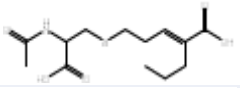	M11	PROTOTYPE – Glutathione Conjugation of Valproic Acid and Related Compounds
		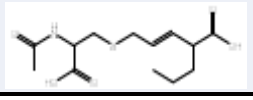	M12	PROTOTYPE – Glutathione Conjugation of Valproic Acid and Related Compounds

Step 2

An [i,j] matrix of metabolite structural similarities was computed for both target and analogue compounds. This was achieved using a simple KNIME workflow in which the sdf files of query structure and unique first generation metabolites (resulting from biotransformations having a score of >0) were input into Lhasa's Tanimoto structural similarity node, wherein each structure in one sdf file is compared to each structure in the

other. The [i,j] matrix of metabolite structural similarities is shown for 2-ethylbutyric acid and valproic acid, below:

	99-66-1	M11	M12	M1	M7	M5	M6	M2	M3
88-09-5	0.83	0.16	0.18	0.11	0.66	0.62	0.70	0.27	0.22
M2	0.27	0.34	0.33	0.14	0.25	0.24	0.26	**0.91**	0.60
M5	0.67	0.16	0.17	0.14	0.85	**0.64**	0.58	0.24	0.21
M3	0.26	0.38	0.37	0.18	0.24	0.24	0.27	0.64	**0.98**
M1	0.13	0.20	0.20	**0.98**	0.16	0.17	0.15	0.15	0.18

Only the similarity values of concordant metabolites are of interest for the next step and these are highlighted in red in the above table (M1-M1, M2-M2, M3-M3 and M5-M5).

Step 3

An overall similarity assessment of the two metabolic trees can be generated by using the structural similarity values from the [i,j] matrix and feeding these into the version of Tanimoto equation that uses continuous rather than binary data. This equation is shown below:

$$\text{Tanimoto Similarity} = \frac{\sum_{j=1}^{n} x_jA.x_jB}{\sum_{j=1}^{n}(x_jA)^2 + \sum_{j=1}^{n}(x_jB)^2 - \sum_{j=1}^{n} x_jA.x_jB}$$

An example calculation follows. In the equation, ***xjA*** can be interpreted as: *x* is the *jth* value of object **A** and similar for x_jB. The compound showing the higher number of predicted metabolites was assigned as compound A. In this example, valproic acid has 8 predicted metabolites and 2-ethylbutyric acid 4. Valproic acid is assigned as compound A and 2-ethylbutyric acid as B. In order to assign the values of x_jA each metabolite is compared to itself and that value is, of course, always 1.

So:

$$\sum_{j=1}^{n} x_jA = 8$$

and

$$\sum_{j=1}^{n} (x_jA)^2 = 8$$

The values of x_jB are taken directly from the structural Tanimoto [i,j] matrix, and so:

$$\sum_{j=1}^{n} x_jA.x_jB = (1 \times 0.98) + (1 \times 0.98) + (1 \times 0.91) + (1 \times 0.64) + (1 \times 0) + (1 \times 0) + (1 \times 0) + (1 \times 0) = \mathbf{3.51}$$

and

$$\sum_{j=1}^{n} (x_jB)^2 = (0.98)^2 + (0.98)^2 + (0.91)^2 + (0.64)^2 = \mathbf{3.16}$$

The main equation then simplifies to:

$$Similarity = \frac{3.51}{8 + 3.16 - 3.51} = \mathbf{0.46}$$

Calculations were executed in Microsoft Excel using simple formulae but the method is amenable to automation.

BIOTRANSFORMATION FINGERPRINT METHOD

We have defined the biotransformation fingerprint for a compound as a binary vector in which the occurrence of a given biotransformation is labelled as 1 and lack of occurrence of a given biotransformation is labelled as 0. In order to compare two molecules using the Tanimoto coefficient for binary data we need the fingerprints for the two molecules plus a third binary vector in which the occurrence of a given biotransformation in both molecules is recorded. In this analysis the occurrence of a biotransformation is defined as a biotransformation predicted with a score of >0.

Process Constraints

Lhasa default except:

Max. Depth: 1

Score Threshold: 100

Inactive Biotransformations: 428

Post Processing Filters

Score: >0 (tolerance ±0.0)

Example Calculation - Comparison of 2-Ethyl Butyric Acid to Valproic Acid

Biotransformation Name	A	B	AB
Glucuronidation of Carboxylic Acids	1	1	1
Conjugation of Alkyl Carboxylic Acids with Glycine	1	1	1
Conjugation of Carboxylic Acids with Glutamine	1	1	1
Conjugation of Carboxylic Acids with Taurine	0	0	0
Hydroxylation of Penultimate Alkyl Methylene	1	1	1
Hydroxylation of Penultimate Alkyl Methylene	1	1	1
Hydroxylation of Terminal Methyl	0	1	0
Hydroxylation of Terminal Methyl	0	1	0
Hydroxylation of Antepenultimate Alkyl Methylene	0	1	0
Hydroxylation of Antepenultimate Alkyl Methylene	0	1	0
PROTOTYPE - Glutathione Conjugation of Valproic Acid and Related Compounds	0	1	0
PROTOTYPE - Glutathione Conjugation of Valproic Acid and Related Compounds	0	1	0
Totals:	**5**	**11**	**5**

Where:

A = Biotransformations occurring for 2-ethylbutyric acid

B = Biotransformations occurring for valproic acid

AB = Biotransformations occurring for both 2-ethylbutyric acid and valproic acid

Applying the Tanimoto equation for binary data:

$$\boldsymbol{Similarity = \frac{AB}{(A + B) - AB} = \frac{5}{(5 + 11) - 5} = 0.46}$$

Coefficients were calculated between the target compound and all analogue compounds. These are conveniently visualised as a bar chart (comparing, for example, to the structural Tanimoto similarities). All analogues were also compared to each other and, together with the target compound, this is conveniently represented by a Tanimoto fingerprint matrix or heatmap.

Note on Assignment of Biotransformations for Both Methods:

For symmetric compounds like valproic acid, application of some biotransformations will generate only one metabolite (e.g. hydroxylation of terminal methyl) whilst those that are dissymmetric (like 2-propylheptanoic acid) will generate two metabolites for the same reaction, because the biotransformation operates twice – once on each different branch. For the purpose of generating the fingerprint, symmetric analogues like VPA are treated as if dissymmetric, that is, the biotransformation is scored twice. This is reasonable treatment – both carbon atoms in each propyl side-chain will react, it is just that the metabolites (ignoring any substrate/metabolite enantioselectivity) are identical. This makes for a "fairer" comparison. If both compounds to be compared are symmetric (e.g. 2-ethylbutyric and valproic) then one comparison is enough although for the fingerprint method we have scored twice to maintain parity across the analogue set. If both compounds are disymmetric then a four-fold comparison would be needed (1a:1b, 1a:2b, 2a:1b and 2b:2b) at least for the concordant metabolite method. As the target in this study is symmetrical this has not been needed, but this is a general feature of symmetry handling that needs to be considered as we automate the methods going forward.

Common Metabolites up to Third Generation

Process Constraints

Lhasa default except:

Max. Depth: 3

Score Threshold: 100

Inactive Biotransformations: 428

Post Processing Filters

Hide Duplicates AND Score: >0 (tolerance ±0.0)

Report

Numbers of both unique metabolites and unique metabolites resulting from biotransformations having a score of >0 were recorded. For the target compound and each analogue compound unique metabolites resulting from biotransformations having a score of >0 were exported as an sdf file. For the target compound, the sdf file included a data field containing the molecular formulae for the target compound itself and its suggested metabolites. These molecular formulae were processed into a text file (*target MF text file*) using Microsoft Excel.

Detection of Common Metabolites

For each analogue compound a further post processing filter was added to the metabolic tree using AND logic. This was the “formula matches” filter and the input for this was the *target MX text file* (described above). On activation of the filters, the metabolic tree for the analogue now contained: unique metabolites resulting from biotransformations having a score of >0 and having a molecular formula identical to one found in the metabolic tree for the target compound. In most case the analogue compound metabolic tree collapsed to display zero nodes (indicated that there were no predicted metabolites in common between target compound and analogue compound). In cases where nodes passed this final filter, manual inspection of the target compound metabolic tree was need to establish that metabolites with identical formulae in respect of target and analogue trees were structural isomers and not, in fact, identical.

References

1. Silva MFB, Aires CCP, Luis PBM, Ruiter JPN, Ijlst L, Duran M, Wanders RJA, and Tavares de Almeida I. **Valproic Acid Metabolism and its Effects on Mitochondrial Fatty Acid Oxidation: A Review**. *Journal of Inherited Metabolic Disease* (2008), 31, 205-216.
2. Ghodke-Puranik Y, Thorn CF, Lamba JK, Leeder JS, Song W, Birnbaum AK, Altman RB and Klein TE. **Valproic Acid Pathway: Pharmacokinetics and Pharmacodynamics**. *Pharmacogenetics and Genomics* (2013), 23, 236-241.
3. English JC, Deisinger PJ and Guest D. **Metabolism of 2-Ethylhexanoic Acid Administered Orally or Dermally to the Female Fischer 344 Rat**. *Xenobiotica* (1998), 28, 699-714.
4. Pennanen S, Auriola S, Manninen A and Komulainen H. **Identification of the Main Metabolites of 2-Ethylhexanoic Acid in Rat Urine Using Gas Chromatography-Mass Spectrometry**. *Journal of Chromatography B: Biomedical Sciences and Applications* (1991), 568, 125-134.
5. Pennanen S, Kojo A, Pasanen M, Liesivuori J, Juvonen RO and Komulainen H. **CYP Enzymes Catalyze the Formation of a Terminal Olefin from 2-Ethylhexanoic Acid in Rat and Human Liver**. *Human and Experimental Toxicology* (1996), 15, 435-442.
6. Walker V and Mills GA. **Urine 4-Heptanone: a beta-Oxidation Product of 2-Ethylhexanoic Acid from Plasticisers**. *Clinica Chimica Acta* (2001), 306, 51-61.
7. Hamdoune M, Duclos S, Mounie J, Santona L, Lhuguenot JC, Magdalou J and Goudonnet H. ***In vitro* Glucuronidation of Peroxisomal Proliferators: 2-Ethylhexanoic Acid Enantiomers and Their Structural Analogs**. *Toxicology and Applied Pharmacology* (1995), 131, 235-243.
8. Kanazu T and Yamaguchi T. **Comparison of *in vitro* Carnitine and Glycine Conjugation with Branched-Side Chain and Cyclic Side Chain Carboxylic Acids in Rats**. *Drug Metabolism and Disposition* (1997), 25, 149-153.
9. Kanazu T and Yamaguchi T. **Substrate Specificity for Carnitine and Glycine Conjugation of Branched Side-Chain and Cyclic Side-Chain Carboxylic Acids in Various Experimental Animals.** *Xenobiotica* (2009), 39, 335-344.
10. Xue L and Bajorath J. **Molecular Descriptors for Effective Classification of Biologically Active Compounds Based on Principal Component Analysis Identified by a Genetic Algorithm.** *Journal of Chemical Information and Computer Sciences* (2000), 40, 801-809.
11. Xue L and Bajorath J. **Accurate Partitioning of Compounds Belonging to Diverse Activity Classes**. *Journal of Chemical Information and Computer Sciences* (2002), 42, 757-764.
12. Rogers D and Hahn **M. Extended-Connectivity Fingerprints.** *Journal of Chemical Information and Modeling* (2010), 50, 742-754.
13. Ponting DJ, Murray E and Long A. **Quantifying Confidence in the Reporting of Metabolic Biotransformations**. *Drug Discovery Today* (2017), 22, 970-975.
14. Marchant CA, Briggs KA and Long A. ***In silico* Tools for Sharing Data and Knowledge on Toxicity and Metabolism: Derek for Windows, Meteor, and Vitic**. *Toxicology Mechanisms and Methods*, (2008), 18, 177-187.
15. https://www.lhasalimited.org/products/meteor-nexus.htm
16. Marchant CA, Rosser EM and Vessey JD. **A k-Nearest Neighbours Approach Using Metabolism-Related Fingerprints to Improve *in silico* Metabolite Ranking**. *Molecular Informatics*., (2017), 36.

17. Judson PN, Long A, Murray E and Patel M. **Assessing Confidence in Predictions Using Veracity and Utility – A Case Study on the Prediction of Mammalian Metabolism by Meteor Nexus**. *Molecular Informatics*, (2015), 34, 284-291.

18. Long A, Fielding K, McSweeney N, Payne MP and Smoraczewska E. **Expert Systems: The Use of Expert Systems in Drug Design – Toxicity and Metabolism**. (2012) *in Drug Design Strategies: Quantitative Approaches*, Livingstone DJ and Davis A (editors), Royal Society of Chemistry - Drug Discovery Series, pp. 279-344, ISBN: 978-1-84973-166-9.

19. Long A and Murray A. **Prediction of Xenobiotic Metabolism**. (2018) *in Applied Chemoinformatics: Achievements and Future Opportunities*, Gasteiger J and Engels T (editors), Wiley-VCH (2018), ISBN: 978-3-527-34201-3.

20. Hanser T, Barber C, Marchaland JF and Werner S. **Applicability Domain: Towards a More Formal Definition.** *SAR and QSAR in Environmental Research* (2016), 27, 893-909.

Target and Analogues	Structural Similarity (Ceres)	Metabolic Similarity	Biotransformation Fingerprint
2-Methylhexanoic Acid	100%	100%	100%
2-Ethylbutyric Acid	75%	52%	50%
2-Propylheptanoic Acid	87%	78%	64%
Valproic Acid	87%	72%	63%
2-Ethylhexanoic Acid	98%	86%	98%
2-Methylpentanoic Acid	87%	88%	76%

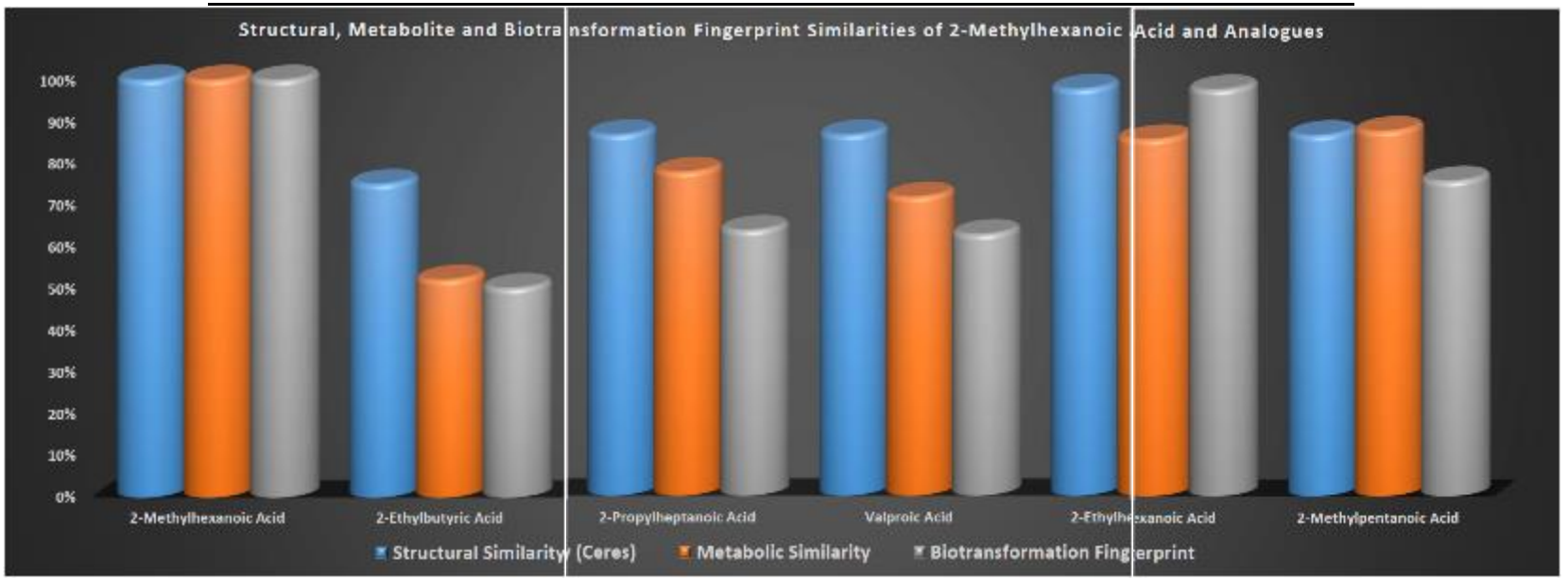

Target and Analogues	Structural Similarity (Ceres)	Metabolic Similarity
2-Methylhexanoic Acid	100%	100%
2-Ethylbutyric Acid	75%	52%
2-Propylheptanoic Acid	87%	78%
Valproic Acid	87%	72%
2-Ethylhexanoic Acid	98%	86%
2-Methylpentanoic Acid	87%	88%

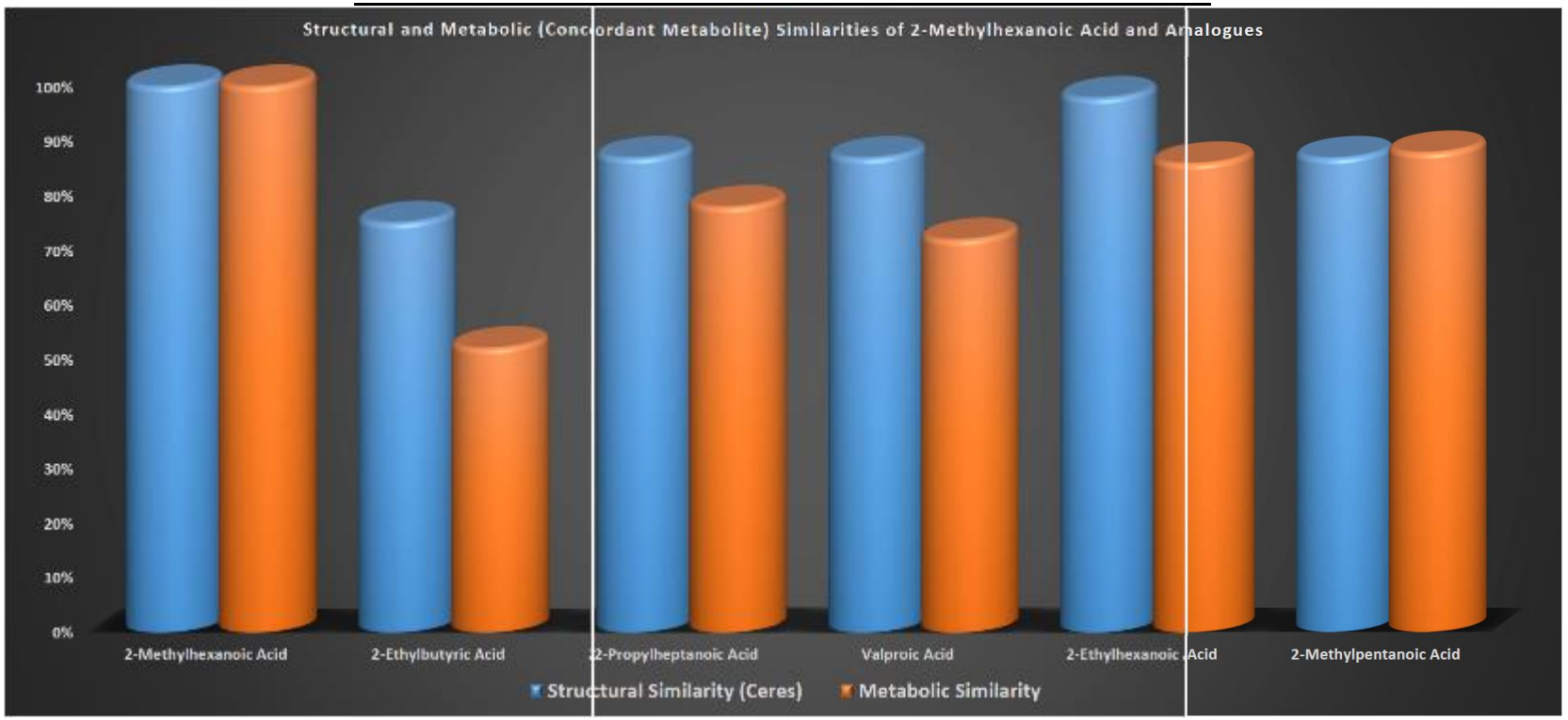

Target and Analogues	Structural Similarity (Ceres)	Biotransformation Fingerprint
2-Methylhexanoic Acid	100%	100%
2-Ethylbutyric Acid	75%	50%
2-Propylheptanoic Acid	87%	64%
Valproic Acid	87%	63%
2-Ethylhexanoic Acid	98%	98%
2-Methylpentanoic Acid	87%	76%

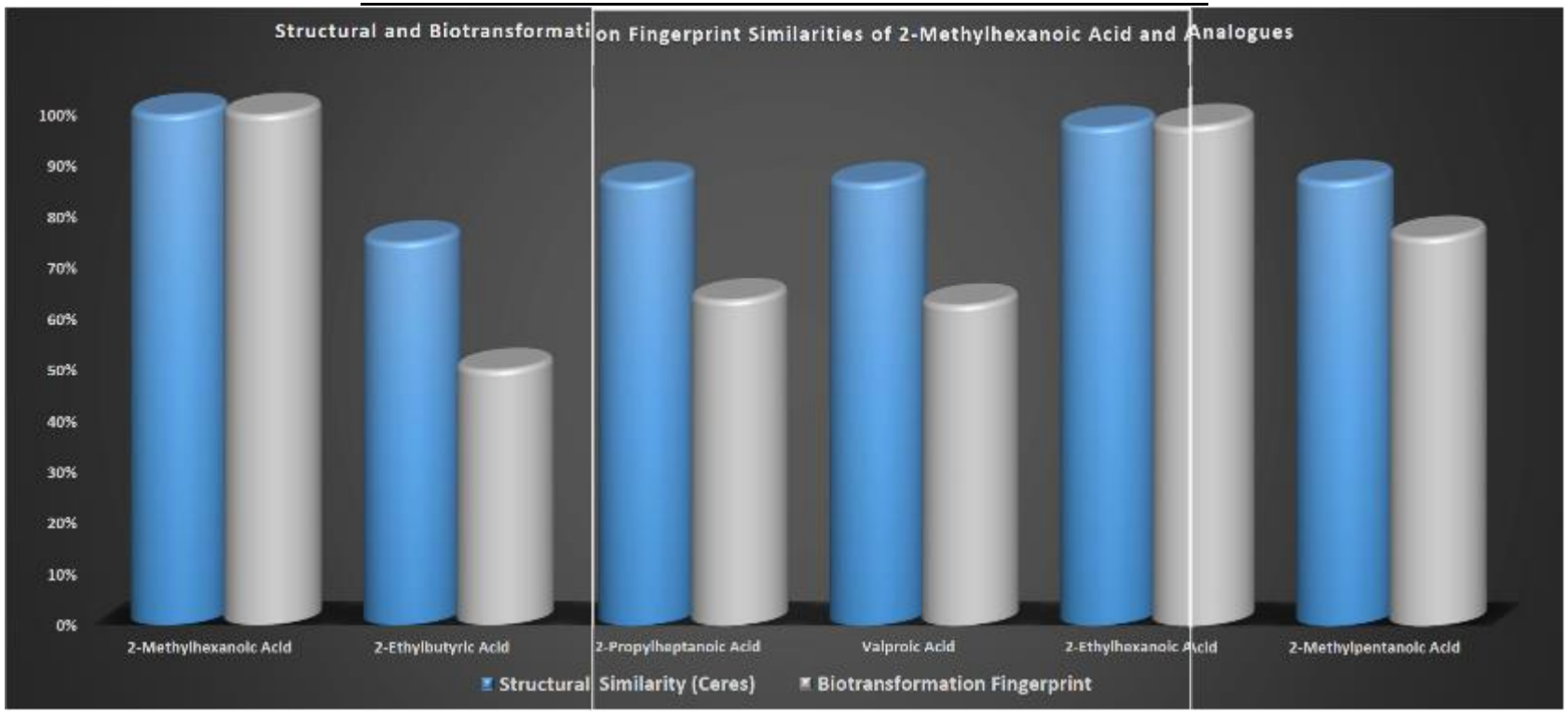

Target and Analogues	Metabolic Similarity	Biotransformation Fingerprint
2-Methylhexanoic Acid	100%	100%
2-Ethylbutyric Acid	52%	50%
2-Propylheptanoic Acid	78%	64%
Valproic Acid	72%	63%
2-Ethylhexanoic Acid	86%	98%
2-Methylpentanoic Acid	88%	76%

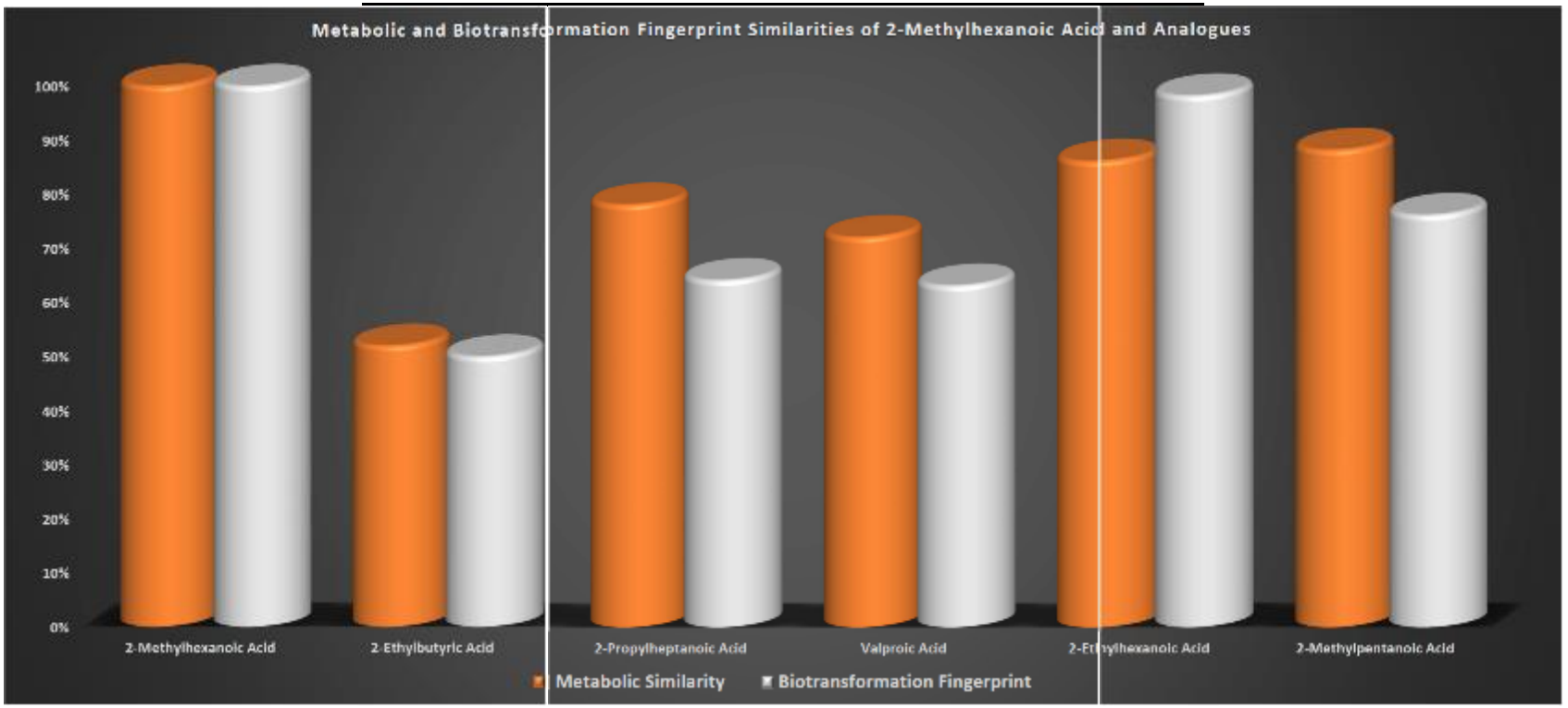

7. Class-1: Dempster-Schafer Classification model description

Dempster-Shafer theory for combining evidence and estimating uncertainty

Introduction

In vitro and *silico* methods play an important part in assessing the safety of chemical. In order to make unbiased decisions on incomplete data from a number of different sources, e g. assay outcomes or predictions from *in silico* models, the reliability and uncertainty of the various sources need to be taken into account.

By far the most common method used for combining evidence from multiple source is the consensus approach; e.g., if two sources predict outcome A and one source predict outcome B, then outcome A is reported as the consensus prediction. The consensus method is easy to apply but, naively, assumes that all models are equally reliable. Also, the uncertainty of each source is not taken into account. In order to account for these limitations Dempster-Shafer theory (DST) [1-2], is used for providing an unbiased decision based on the quality and reliability of the sources.

Method

DST is an extension of generalized Bayesian statistical inference in which evidence can be associated with multiple events.

The following example is used to illustrate the general theory and algorithms of DST:

Binary case (*Y*) with an "event" being Toxic (*T*) or non-Toxic (*N*) is investigated:

In a traditional probability approach - the probabilities are additive: p(*Y*) ≡ p(*T* or *N*) = p(*T*) + p(*N*)

DST provides a mechanism to take uncertainty due into account and replaces traditional probability functions with *belief* and *plausibility* functions.

Thus the set of outcomes of Y is P(Y) = {{y1},{y2},{y1,y2},∅}

where ∅ denotes the empty set.

In this way, *belief* and *plausibility* can be viewed as lower and upper bounds, respectively, of the probability for the outcome.

DST uses *probability mass functions* (m):

$0 \leqslant m(f_i) \leqslant 1$

$m(\emptyset) = 0$

$\Sigma m(f_i) = 1$

Having a binary variable Y={y1,y2}, (T or N) the probability masses can be assigned to:

{y1} and {y2} and to {y1,y2}:

$\Sigma m(f_i) = 1 = m(\{y1\}) + m(\{y2\}) + m(\{y1,y2\})$

The probability masses m({y1}) and m({y2}) is the proportion of the overall belief with respect to outcomes y_1 and y_2, respectively, and m({y1,y2}) is the proportion of the overall belief not committed to y_1 but also not ascribed to y_2 as well as not committed to y_2 but also not ascribed to y1. Thus m({y1,y2}) quantifies the level of uncertainty in the system under investigation.

Belief (Bel) and plausibility (Pls) is defined for the 2 outcomes T and N as:

Bel({T}) = m({T}) Bel({N}) = m({N}

Pls({T}) = m({T}) + m({T,N}) Pls({N}) = m({N}) + m({T,N})

Assay 1 predicts 70% probability for toxicity of the investigated compound.

From experience (validation), the reliability of the assay is estimated to 60%.

This gives the following masses, beliefs and plausibilities:

m({T}) = p(T) * rel(T) = (0.70)*(0.60) = 0.42

40% chance (100 -60) that the test result is unreliable ->

basic probability mass associated with uncertainty: **m({T,N})** = 0.40

Sum of masses must be one: **m({N})** = 1 - 0.42 - 0.40 = 0.18

Beliefs and plausibilities are then calculated to be:

Bel(T) = 0.42 Pls(T) = 0.42 + 0.40 = 0.82

Bel(N) = 0.18 Pls(N) = 0.18 + 0.40 = 0.58

If 2 sources are combined then the probability masses are:

q(fk) = m1(fi)*m2(fj)

q(∅) = m1(∅)*m2(∅)

q(Y) = m1(Y)*m2(Y)

By using Dempster's combination rule and assigning all conflicts (to assays give different results) to the null set, normalizing by dividing by 1-q(∅) to insure mD(∅)=0 as required, to joint basic probability mass mD is mD(Y)=q(Y)/(1-q(∅)). The same normalization is performed for q(fk).

For two assays, 1 and 2 the following DST scheme is then constructed:

Assay 1 predicts 70% probability for toxicity
From experience (validation) - estimation of reliability = 60%

Assay 2 predicts 60% probability for toxicity
From experience (validation) - estimation of reliability = 80%

For combining the sources:

Applying the Dempster combination rule

$q(\{T\}) = m1(\{T\})*m2(\{T\}) + m1(\{T\})*m2(\{T,N\}) + m1(\{T,N\})*m2(\{T\})$

$q(\{N\}) = m1(\{N\})*m2(\{N\}) + m1(\{N\})*m2(\{T,N\}) + m1(\{T,N\})*m2(\{N\})$

$q(Y) \equiv q(\{T,N\}) = m1(\{T,N\})*m2(\{T,N\})$

$q(\emptyset) = m1(\{T\})*m2(\{N\}) + m1(\{N\})*m2(\{T\})$

This, in turn, gives the following outcome from the DST analysis.

	Assay1 **70 %** probability for toxicity **30 %** probability for non-toxicity Reliability 60 %	**Assay2** **60 %** probability for toxicity **40 %** probability for non-toxicity Reliability 80 %
	$m1(\{T\}) = 42\ \%$, $m1(\{N\}) = 18\ \%$, $m1(\{T,N\}) = 40\ \%$	$m2(\{T\}) = 48\ \%$, $m1(\{N\}) = 32\ \%$, $m1(\{T,N\}) = 20\ \%$
Bel ({T}) =	42 %	48 %
Pls ({T}) =	40 + 42 = 82 %	48 + 20 = 62 %
Bel ({N}) =	18 %	32 %
Pls ({N}) =	18 + 40 = 58 %	32 + 20 = 52 %

$q(\{T\}) = m1(\{T\})*m2(\{T\}) + m1(\{T\})*m2(\{T,N\}) + m1(\{T,N\})*m2(\{T\})$ (= 0.48)
$q(\{N\}) = m1(\{N\})*m2(\{N\}) + m1(\{N\})*m2(\{T,N\}) + m1(\{T,N\})*m2(\{N\})$ (= 0.22)
$q(Y) \equiv q(\{T,N\}) = m1(\{T,N\})*m2(\{T,N\})$ (= 0.08)
$q(\emptyset) = m1(\{T\})*m2(\{N\}) + m1(\{N\})*m2(\{T\})$ (= 0.22)

Dempster combination rule [$mD(Y)=q(Y)/(1-q(\emptyset))$]

$q(\{T\}) = 0.48/(1-0.22) = 0.615$
$q(\{N\}) = 0.22/(1-0.22) = 0.282$
$q(\{T,N\}) = 0.08/(1-0.22) = 0.103$

Bel ({T}) =	61.5 %
Pls ({T}) =	61.5 + 10.3 = 71.8 %
Bel ({N}) =	28.2 %
Pls ({N}) =	28.2 + 10.3 = 38.5 %

The results are that the belief for being toxic and non-toxic is 61.5 % and 28.2 %, respectively, with an uncertainty of 10.3 %. Since the plausibility for the compound being non-toxic is 38.5, well below 50 %, as well as the belief and plausibility for being toxic is above 50% the compound would be considered as toxic.

Software

The DST software applied in this study was developed in the EU-ADR project (ICT-215847) and implemented in Java.

To facilitate easier usage of the software several utility programs for data input and analysis were developed using Python.

A leave-out-out cross-validation was performed in order to calculate the positive (PPV) and negative prediction (NPV) value, respectively, for the assays based on the source compounds.

PPV = TP/(TP + FP)

NPV = TN/(TN + FN)

TP, FP are compounds predicted as true and false positives, respectively.

TN, FN are compounds predicted as true and false negatives, respectively.

References

1. G. Shafer, A Mathematical Theory Of Evidence, Princeton University Press (1976)

2. A.P. Dempster, Upper and lower probabilities induced by a multivalued mapping, Ann. Math. Stat., 38 (2) (1967), pp. 325-339

8. Class-2: Bayesian Automatic Classification model description

Automatic Classification

In addition to expert judgment on the meaning of the individual test results, an automatic classification method was used to decide, considering all the evidence, in which category the target compound is likely to fall. The predicted *in vivo* NTD was discretized in 5 levels (missing data, negative, mildly positive, positive, strongly positive. Only MPA and MHA had Missing *in vivo* data (in fact MHA has *in vivo* data, but they were blinded to the analysis to check how MHA would be predicted). A Bayesian consensus approach was developed. The method can be summarized as follows:

- a prediction model was fitted to individual test data on training chemicals (source chemicals for which both *in vitro*-derived effect measures and *in vivo* data were available); A Bayesian framework and Bayesian numerical calibration algorithms (MCMC sampling) were used, under normality assumption for the *in vivo* data likelihood, given the *in vitro* predictors (those key-event measurements were continuous variables);
- the poorly predictive tests were removed from consideration on the basis of posterior predictive checking of their classification accuracy (on the training set of chemicals only, we had too few chemicals to do a formal validation);
- use the remaining (sufficiently predictive) tests were used to build a set of predictions for the test chemical (MHA or MPA).

Results for MHA classification

A/ On the basis of in vitro measurements

Once trained, the classifier assigns MHA to category negative (which is the correct classification according to the *in vivo* data available in fact) with probability 90% of the case and strongly positive with probability 10%. Figure X1 shows the assignment of MHA by the best classifiers. The strongly positive assignments come from only two tests which responded strongly to MHA.

Figure X1. Results of automatic classification of MHA (red crossed circle) given its response in the various assays relevant to the underlying AOP.

The black dots mark the positions of the source chemicals used for training the classifier.

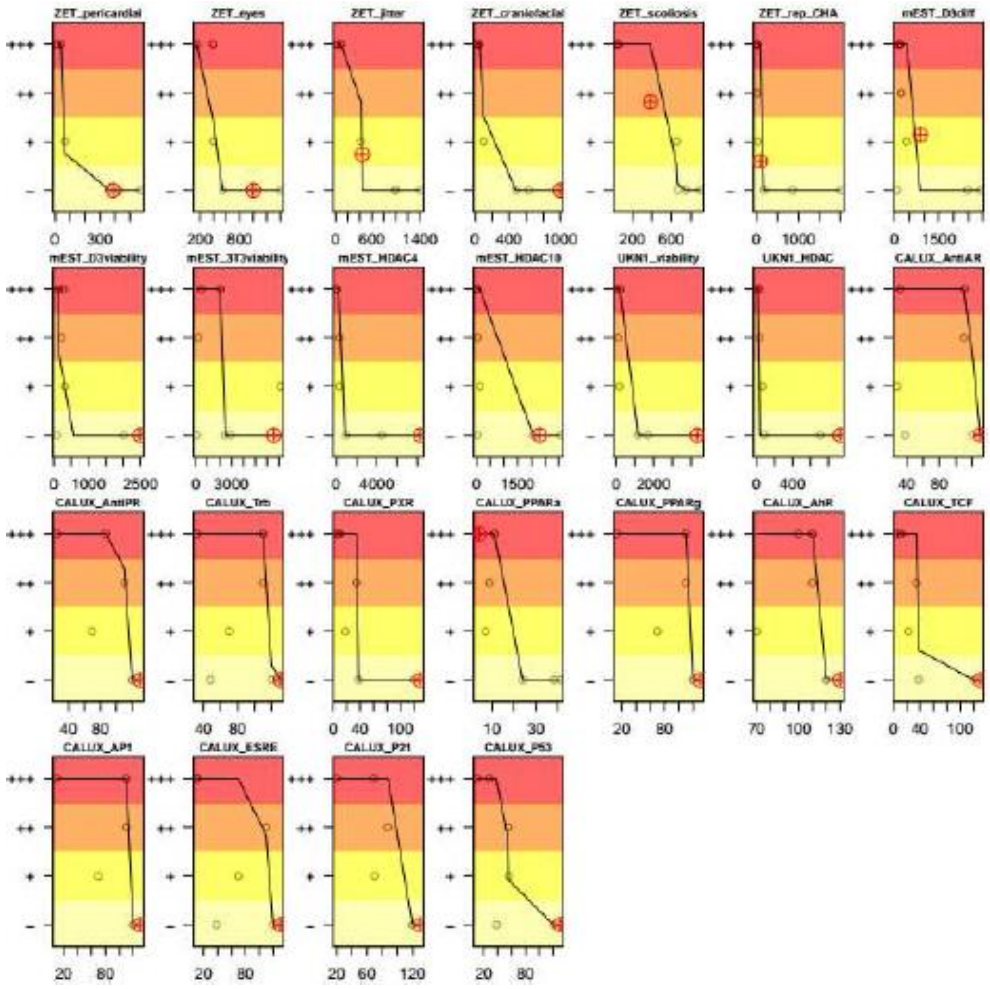

If only the best tests and relevant to neurodevelopmental toxicity are used (ZET_pericardial, ZET_eyes, ZET_jitter, UKN1_viability), the classifier assigns MHA to category negative with probability 93% of the case and strongly positive with probability 7%. See Figure X1 for the assignment of MHA by those classifiers. The strongly positive assignments come from only two tests which responded strongly to MHA.

If only the best tests and relevant to neurodevelopmental and developmental toxicity are used (All five ZET read outs, ZET reporter for cranio-facial deformation, mEST cell viability at day 3, UKN1 cell viability and all 14 CALUX assays), the classifier assigns MHA to category negative with probability 90% of the case and strongly positive with probability 10%. See Figure X1 for the assignment of MHA by those classifiers.

B/ On the basis of in vitro measurements corrected for mouse pharmacokinetics

Once trained on this specific data, the classifier assigns MHA to category negative with probability 27%, mildly positive with probability 43%, positive with probability 26%, and strongly positive with probability 3%. Figure X2 shows the assignment of MHA by the

best classifiers. The low number of training chemicals (only three) is probably responsible for the uncertainty in the predictions. The pharmacokinetic correction also seems to increase the predicted toxicity (although MHA appears negative *in vivo*, in fact).

Figure X2: Results of automatic classification of MHA (red crossed circle) given its response in the various assays relevant to the underlying AOP, after pharmacokinetic correction for the mouse.

The black dots mark the positions of the source chemicals used for training the classifier.

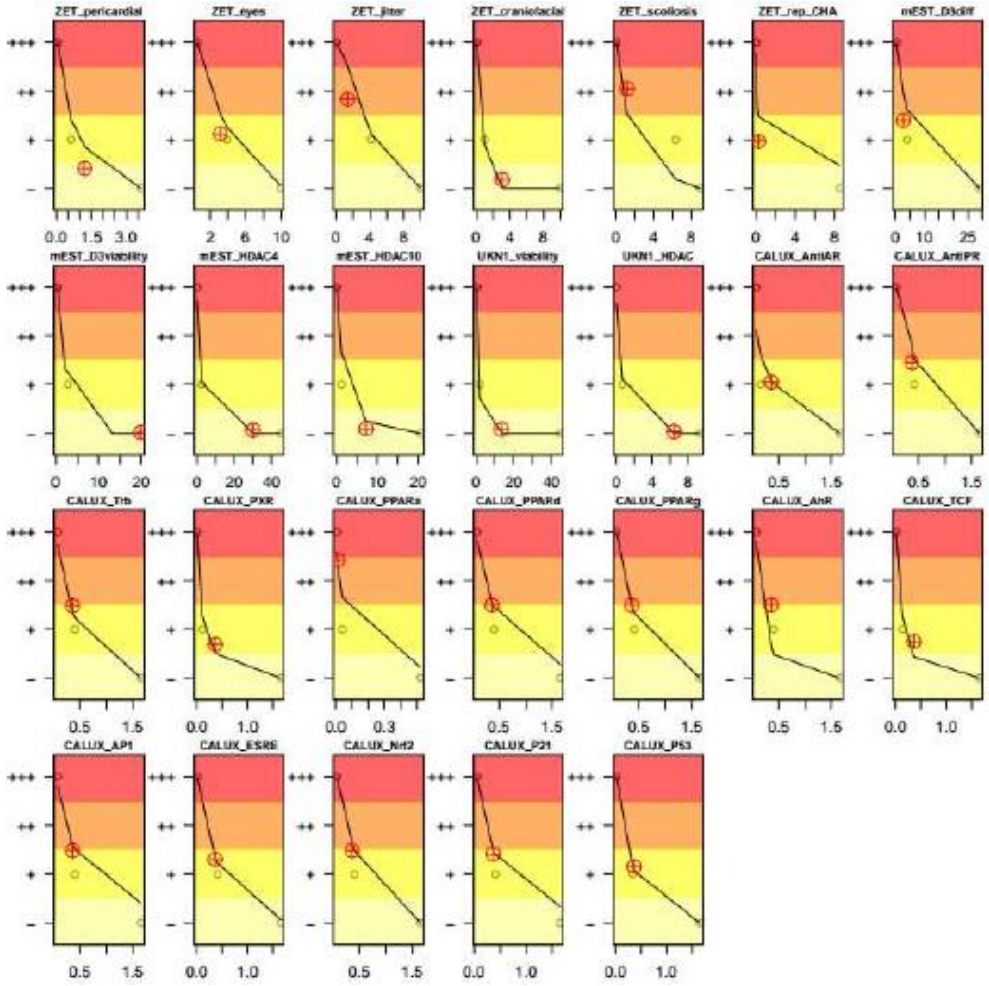

If only the best tests and relevant to neurodevelopmental toxicity are used (ZET_pericardial, ZET_eyes, ZET_jitter, UKN1_viability), the classifier assigns MHA to category negative with probability 39%, mildly positive with probability 37%, positive with probability 22%, and strongly positive with probability 1%. See Figure X2 for the assignment of MHA by those classifiers.

If only the best tests and relevant to neurodevelopmental and developmental toxicity are used (All five ZET read outs, ZET reporter for cranio-facial deformation, mEST cell viability at day 3, UKN1 cell viability and all 14 CALUX assays), the classifier assigns MHA to category negative with probability 20%, mildly positive with probability 44%, positive with probability 30%, and strongly positive with probability 4%. See Figure X2 for the assignment of MHA by those classifiers.

C/ On the basis of in vitro measurements corrected for human pharmacokinetics

Once trained on this specific data, fewer tests appear predictive, and the classifier assigns MHA to category negative with probability 46%, mildly positive with probability 40%, positive with probability 12%, and strongly positive with probability 2%. Figure X3 shows the assignment of MHA by the best classifiers. The low number of training chemicals (only three) is probably responsible for the uncertainty in the predictions. The pharmacokinetic correction also seems to increase the predicted toxicity.

Figure X3: Results of automatic classification of MHA (red crossed circle) given its response in the various assays relevant to the underlying AOP, after pharmacokinetic correction for the mouse.

The black dots mark the positions of the source chemicals used for training the classifier.

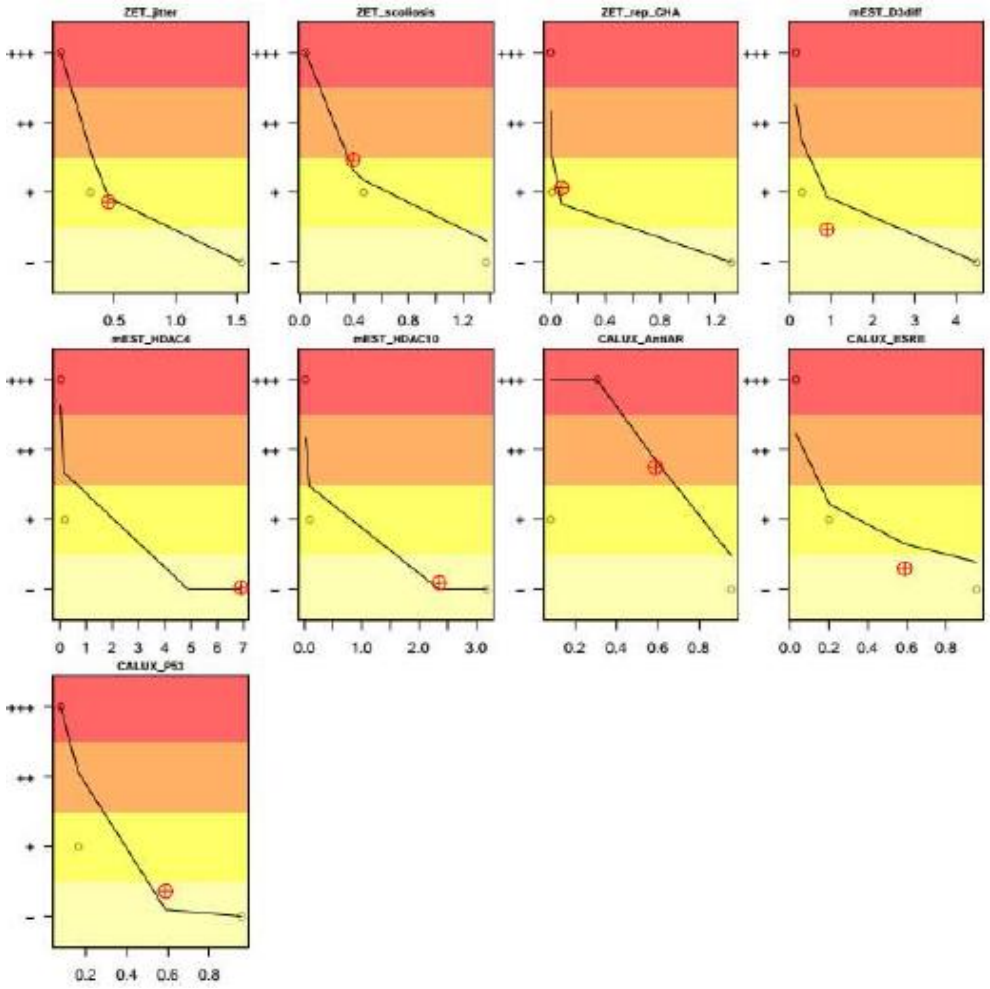

If only the best tests and relevant to neurodevelopmental toxicity are used (ZET_pericardial, ZET_eyes, ZET_jitter, UKN1_viability), the classifier assigns MHA to category negative with probability 69%, positive with probability 18%, and strongly positive with probability 3%. See Figure X3 for the assignment of MHA by those classifiers.

If only the best tests and relevant to neurodevelopmental and developmental toxicity are used (All five ZET read outs, ZET reporter for cranio-facial deformation, mEST cell viability at day 3, UKN1 cell viability and all 14 CALUX assays), the classifier assigns MHA to category negative with probability 50%, mildly positive with probability 41%, positive with probability 8%, and strongly positive with probability 1%. See Figure X3 for the assignment of MHA by those classifiers.

Results for MPA classification

A/ On the basis of in vitro measurements

Once trained, the classifier assigns MPA to category negative (which is the correct classification according to the *in vivo* data available in fact) with probability 93% of the case and strongly positive with probability 7%. Figure X4 shows the assignment of MPA by the best classifiers. The strongly positive assignments come again from only two tests which responded strongly to MPA.

Figure X4: Results of automatic classification of MPA (red crossed circle) given its response in the various assays relevant to the underlying AOP.

The black dots mark the positions of the source chemicals used for training the classifier.

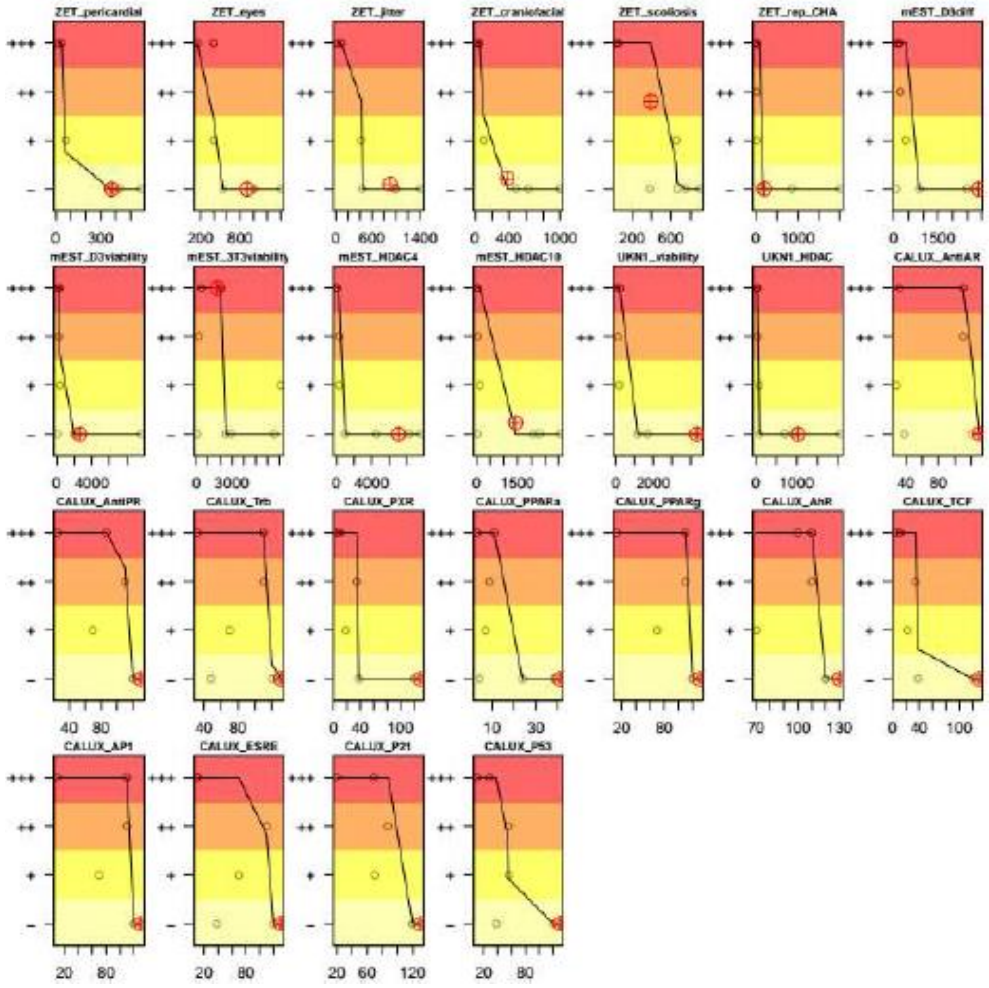

If only the best tests and relevant to neurodevelopmental toxicity are used (ZET_pericardial, ZET_eyes, ZET_jitter, UKN1_viability), the classifier assigns MPA to category negative with probability 99% of the case and strongly positive with probability 1%. See Figure X4 for the assignment of MPA by those classifiers.

If only the best tests and relevant to neurodevelopmental and developmental toxicity are used (All five ZET read outs, ZET reporter for cranio-facial deformation, mEST cell viability at day 3, UKN1 cell viability and all 14 CALUX assays), the classifier assigns MPA to category negative with probability 96% of the case and strongly positive with probability 4%. See Figure X4 for the assignment of MPA by those classifiers.

B/ On the basis of in vitro measurements corrected for mouse pharmacokinetics

Once trained on this specific data, the classifier assigns MPA to category negative with probability 89%, and mildly positive with probability 11%. Figure X5 shows the assignment of MPA by the best classifiers. The low number of training chemicals (only three) is probably responsible for the uncertainty in the predictions. The pharmacokinetic correction also seems to increase the predicted toxicity (although MPA appears negative *in vivo*, in fact).

Figure X5: Results of automatic classification of MPA (red crossed circle) given its response in the various assays relevant to the underlying AOP, after pharmacokinetic correction for the mouse.

The black dots mark the positions of the source chemicals used for training the classifier.

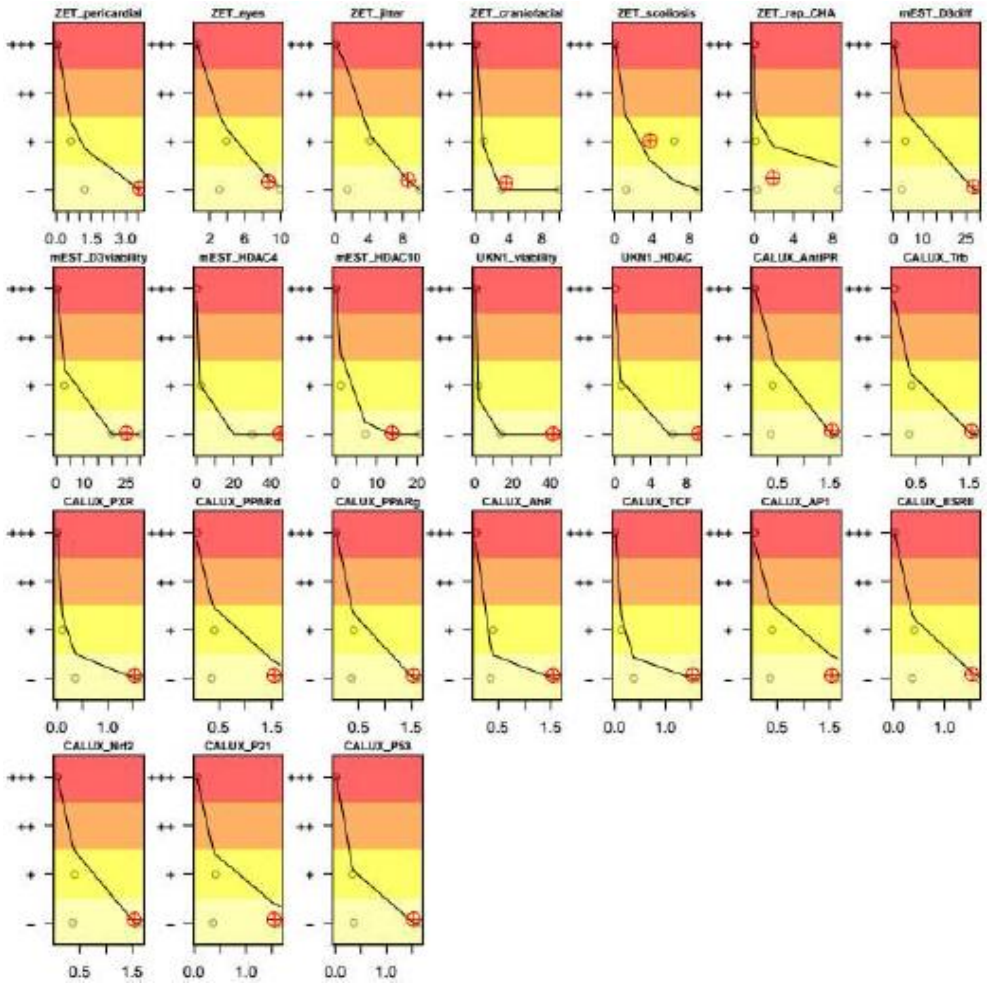

If only the best tests and relevant to neurodevelopmental toxicity are used (ZET_pericardial, ZET_eyes, ZET_jitter, UKN1_viability), the classifier assigns MPA to category negative with probability 90%, mildly positive with probability 10%. See Figure X5 for the assignment of MPA by those classifiers.

If only the best tests and relevant to neurodevelopmental and developmental toxicity are used (All five ZET read outs, ZET reporter for cranio-facial deformation, mEST cell viability at day 3, UKN1 cell viability and all 14 CALUX assays), the classifier assigns MPA to category negative with probability 87%, mildly positive with probability 13%. See Figure X5 for the assignment of MPA by those classifiers.

C/ On the basis of in vitro measurements corrected for human pharmacokinetics

Once trained on this specific data, fewer tests appear predictive, and the classifier assigns MPA to category negative with probability 85%, mildly positive with probability 14%, positive with probability 1%. Figure X6 shows the assignment of MPA by the best classifiers. The low number of training chemicals (only three) is probably responsible for

the uncertainty in the predictions. The pharmacokinetic correction also seems to increase the predicted toxicity.

Figure X6: Results of automatic classification of MPA (red crossed circle) given its response in the various assays relevant to the underlying AOP, after pharmacokinetic correction for the mouse.

The black dots mark the positions of the source chemicals used for training the classifier.

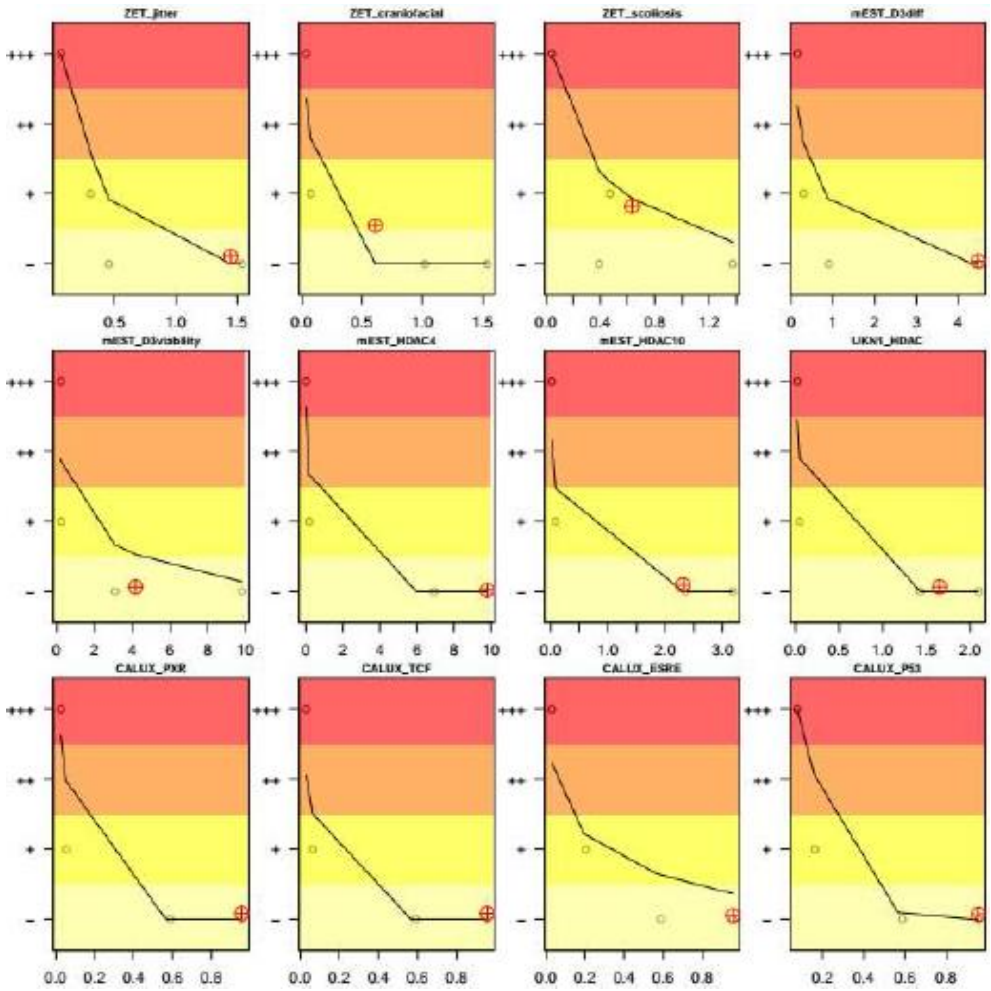

If only the best tests and relevant to neurodevelopmental toxicity are used (ZET_pericardial, ZET_eyes, ZET_jitter, UKN1_viability), the classifier assigns MPA to category negative with probability 58%, mildly positive with probability 37%, positive with probability 4%, and strongly positive with probability 1%. See Figure X6 for the assignment of MPA by those classifiers.

If only the best tests and relevant to neurodevelopmental and developmental toxicity are used (All five ZET read outs, ZET reporter for cranio-facial deformation, mEST cell viability at day 3, UKN1 cell viability and all 14 CALUX assays), the classifier assigns MPA to category negative with probability 79%, mildly positive with probability 19%, positive with probability 2%, and strongly positive with probability 1%. See Figure X6 for the assignment of MPA by those classifiers.

Training of the Bayesian consensus method

In vitro based predictors

With *in vitro* based predictors (EC10s or similar) are used, all seven chemicals of the training set have data.

Figure A1: Best fits (red lines) of a linear model (truncated in y between 0, no effect, and 3, strong effect) obtained by Bayesian calibration.

Ten thousand samples of parameter values (intercept and slope) were obtained by MCMC sampling. The 20 grey lines correspond to fits obtained with 20 random intercepts and slopes drawn from their joint posterior distribution. They give an idea of the uncertainty in the model after calibration. The data point for MHA is indicated by a red triangle (it was not used for training).

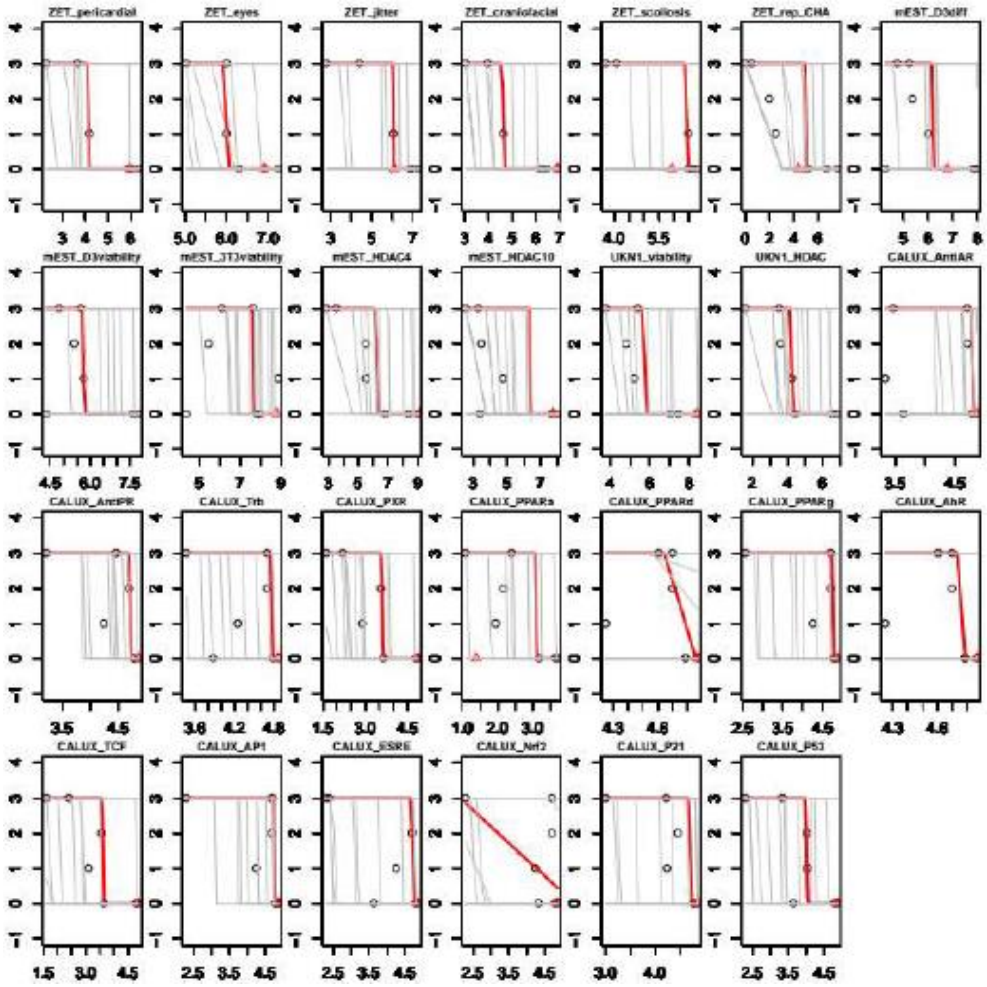

The fitted models were used to predict the classification of the seven training (source) chemicals. The average accuracy of those predictions (exact prediction of the training chemical by the model) was computed for each of the 10000 intercepts and slopes drawn from their joint posterior distribution. The following Table gives the average accuracy of the various tests. For example, the zebrafish embryo test for jitters classifies correctly the training chemicals 88% of the times. With four toxicity classes, random allocation would be correct 25% of the times. We chose to retain the test having a more stringent than 50%

average accuracy. With that criterion, only the CALUX_PPARd test was not retained as a good predictor (underlined in the Table).

Test name	Accuracy
ZET_pericardial	0.88
ZET_eyes	0.78
ZET_jitter	0.88
ZET_craniofacial	0.88
ZET_scoliosis	0.89
ZET_rep_CHA	0.73
mEST_D3diff	0.58
mEST_D3viability	0.58
mEST_3T3viability	0.55
mEST_HDAC4	0.76
mEST_HDAC10	0.58
UKN1_viability	0.71
UKN1_HDAC	0.75
CALUX_AntiAR	0.53
CALUX_AntiPR	0.71
CALUX_Trb	0.54
CALUX_PXR	0.73
CALUX_PPARa	0.71
CALUX_PPARd	0.18
CALUX_PPARg	0.68
CALUX_AhR	0.68
CALUX_TCF	0.72
CALUX_AP1	0.68
CALUX_ESRE	0.69
CALUX_Nrf2	0.40
CALUX_P21	0.71
CALUX_P53	0.65

In vitro based predictors corrected for mouse pharmacokinetics

With *in vitro* based predictors corrected for mouse pharmacokinetics (oral equivalent doses in mmoles/kg) are used, only three chemicals of the training set have data.

Figure A2: Best fits (red lines) of a linear model (truncated in y between 0, no effect, and 3, strong effect) obtained by Bayesian calibration.

Ten thousand samples of parameter values (intercept and slope) were obtained by MCMC sampling. The 20 grey lines correspond to fits obtained with 20 random intercepts and slopes drawn from their joint posterior distribution. They give an idea of the uncertainty in the model after calibration. The data point for MHA is indicated by a red triangle (it was not used for training).

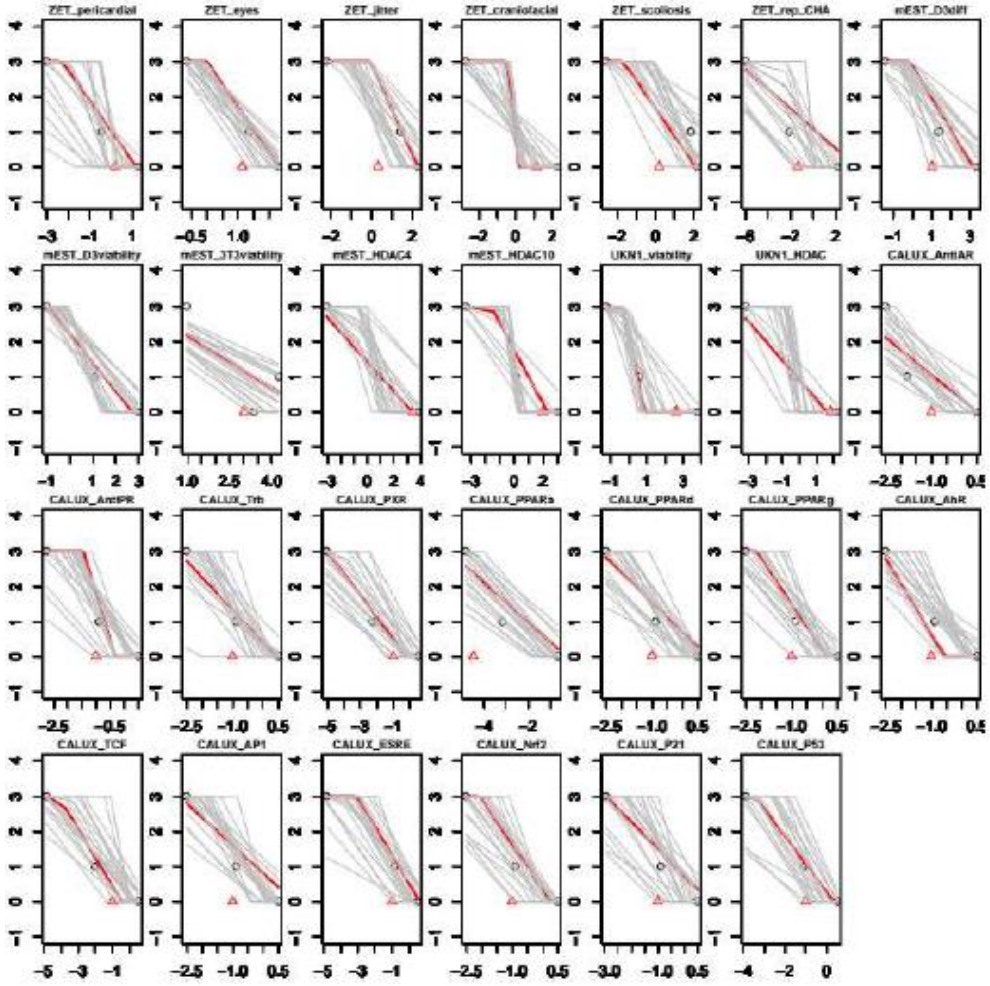

The following Table gives the average accuracy of the various tests, calculated as above. The mEST_3T3viability test was not retained as a good predictor in this case (underlined in the Table) because it had less than 50% average accuracy.

Test name	Accuracy
ZET_pericardial	0.88
ZET_eyes	0.89
ZET_jitter	0.89
ZET_craniofacial	0.87
ZET_scoliosis	0.76
ZET_rep_CHA	0.80
mEST_D3diff	0.86
mEST_D3viability	0.83
mEST_3T3viability	0.20
mEST_HDAC4	0.87
mEST_HDAC10	0.87
UKN1_viability	0.85
UKN1_HDAC	0.88
CALUX_AntiAR	0.52
CALUX_AntiPR	0.84
CALUX_Trb	0.83
CALUX_PXR	0.79
CALUX_PPARa	0.63
CALUX_PPARd	0.83
CALUX_PPARg	0.83
CALUX_AhR	0.83
CALUX_TCF	0.80
CALUX_AP1	0.83
CALUX_ESRE	0.87
CALUX_Nrf2	0.83
CALUX_P21	0.85
CALUX_P53	0.86

In vitro based predictors corrected for human pharmacokinetics

With *in vitro* based predictors corrected for human pharmacokinetics (oral equivalent doses in mmoles/kg) are used, only three chemicals of the training set have data.

Figure A3: Best fits (red lines) of a linear model (truncated in y between 0, no effect, and 3, strong effect) obtained by Bayesian calibration.

Ten thousand samples of parameter values (intercept and slope) were obtained by MCMC sampling. The 20 grey lines correspond to fits obtained with 20 random intercepts and slopes drawn from their joint posterior distribution. They give an idea of the uncertainty in the model after calibration. The data point for MHA is indicated by a red triangle (it was not used for training).

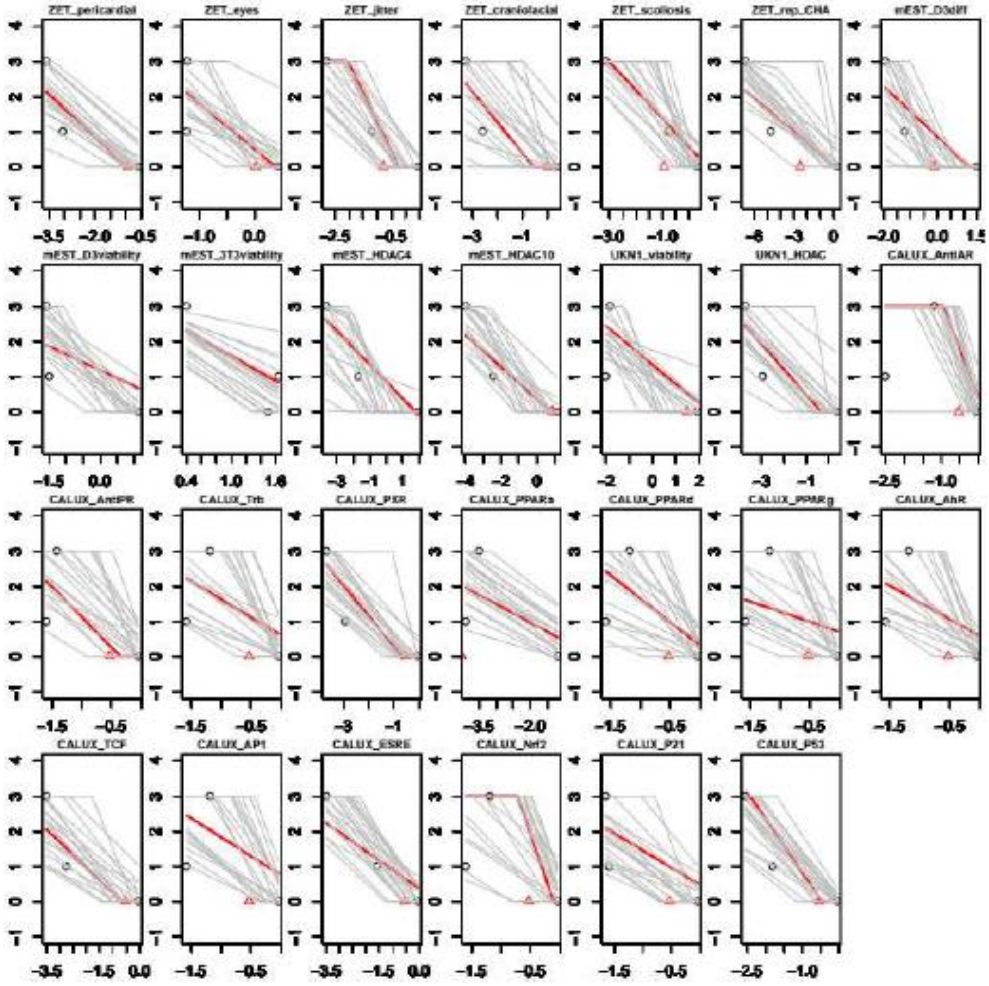

The following Table gives the average accuracy of the various tests with this predictor, calculated as above. Only nine test were retained as good predictors in this case (not underlined in the Table) having more than 50% average accuracy. This is due to the poorer model fit to the data (Figure A3 above).

Test name	Accuracy
ZET_pericardial	0.42
ZET_eyes	0.36
ZET_jitter	0.81
ZET_craniofacial	0.43
ZET_scoliosis	0.87
ZET_rep_CHA	0.55
mEST_D3diff	0.61
mEST_D3viability	0.38
mEST_3T3viability	0.27
mEST_HDAC4	0.75
mEST_HDAC10	0.61
UKN1_viability	0.38
UKN1_HDAC	0.47
CALUX_AntiAR	0.55
CALUX_AntiPR	0.35
CALUX_Trb	0.40
CALUX_PXR	0.47
CALUX_PPARa	0.25
CALUX_PPARd	0.40
CALUX_PPARg	0.39
CALUX_AhR	0.40
CALUX_TCF	0.48
CALUX_AP1	0.39
CALUX_ESRE	0.82
CALUX_Nrf2	0.39
CALUX_P21	0.36
CALUX_P53	0.55

9. Class-3: Biological Fingerprint Classification model description

Dice Distance Classification:

Clustering compounds on basis of biological fingerprints (FPs) generated from assay readouts

Method:

A semiautomatic workflow has been generated in KNIME in order to read in categorical (binary) assay readouts, transform them into FP representations in Bit Vector format (by using the "Create Bit Vector Node" in KNIME), calculate similarity indices on basis of these biological FPs ("Distance Matrix Calculate" node; Dice similarity coefficient), and visualize the calculated similarities/distances in heat maps and hierarchical cluster views (dendrogram). First, all CALUX assays served as input for generating the described visualizations and in order to retrieve a "consensus vote" for classifying CS-2 compounds into positives (1) and negatives (0) according to these assays. In more detail, (dis)similarity to the target compound (as determined by all CALUX assay readouts as biological FP) served as a new categorical input variable for the subsequent calculations/visualisations, where dissimilarity <0.5 was annotated to be an "inactive (0)" consensus FP, and dissimilarity >0.5 was annotated to be an "active (1)" consensus FP. Further, this consensus CALUX readout was combined with binary readouts from single readout values mEST, UKN1, and ZET reporter plus 1) pericardial/yolk oedema effects value for ZET classic, 2) single neurodevelopmental effects value for ZET classic, and 3) single developmental effects value for ZET classic. These combinations of binary readouts were combined into biological FP representations respectively, and the above described visualizations were retrieved.

Results

Analysis CALUX battery:

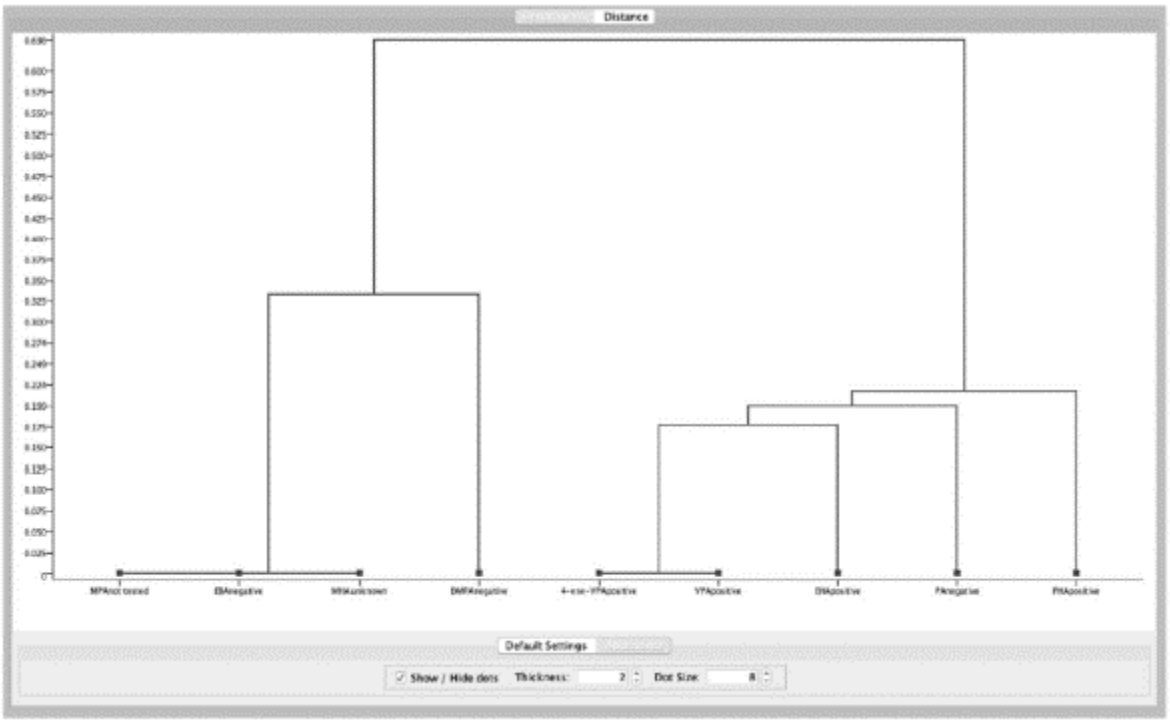

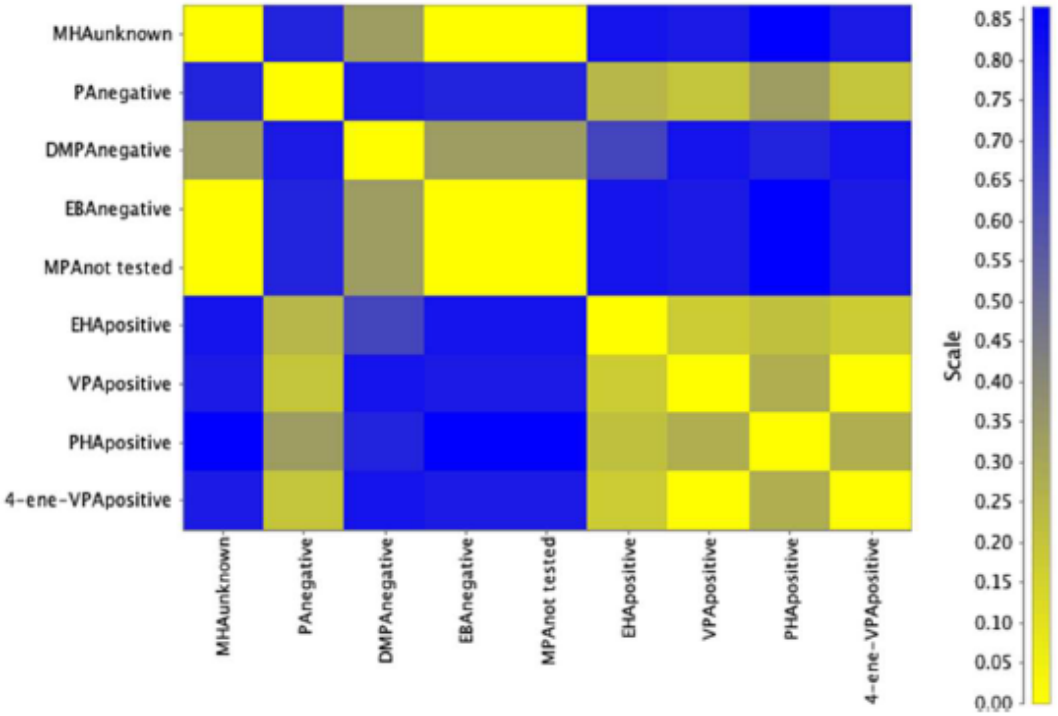

Scale….distance (Dice)

Key	MHAunknown	PAnegative	DMPAnegative	EBAnegative	MPAnot tested	EHApositive	VPApositive	PHApositive	4-ene-VPApositive
MHAunknown	0.00	0.75	0.33	0.00	0.00	0.80	0.78	0.87	0.78
PAnegative	0.75	0.00	0.78	0.75	0.75	0.25	0.20	0.33	0.20
DMPAnegative	0.33	0.78	0.00	0.33	0.33	0.64	0.80	0.75	0.80
EBAnegative	0.00	0.75	0.33	0.00	0.00	0.80	0.78	0.87	0.78
MPAnot tested	0.00	0.75	0.33	0.00	0.00	0.80	0.78	0.87	0.78
EHApositive	0.80	0.25	0.64	0.80	0.80	0.00	0.58	0.22	0.18
VPApositive	0.78	0.20	0.80	0.78	0.78	0.18	0.00	0.27	0.00
PHApositive	0.87	0.33	0.75	0.87	0.87	0.22	0.27	0.00	0.27
4-ene-VPApositive	0.78	0.20	0.80	0.78	0.78	0.18	0.00	0.27	0.00

Analysis 1:

Using single CALUX value + **pericardial and/or yolk oedema** (=most sensitive) effects value for ZET classic + single read out values mEST, UKN1, and ZET reporter

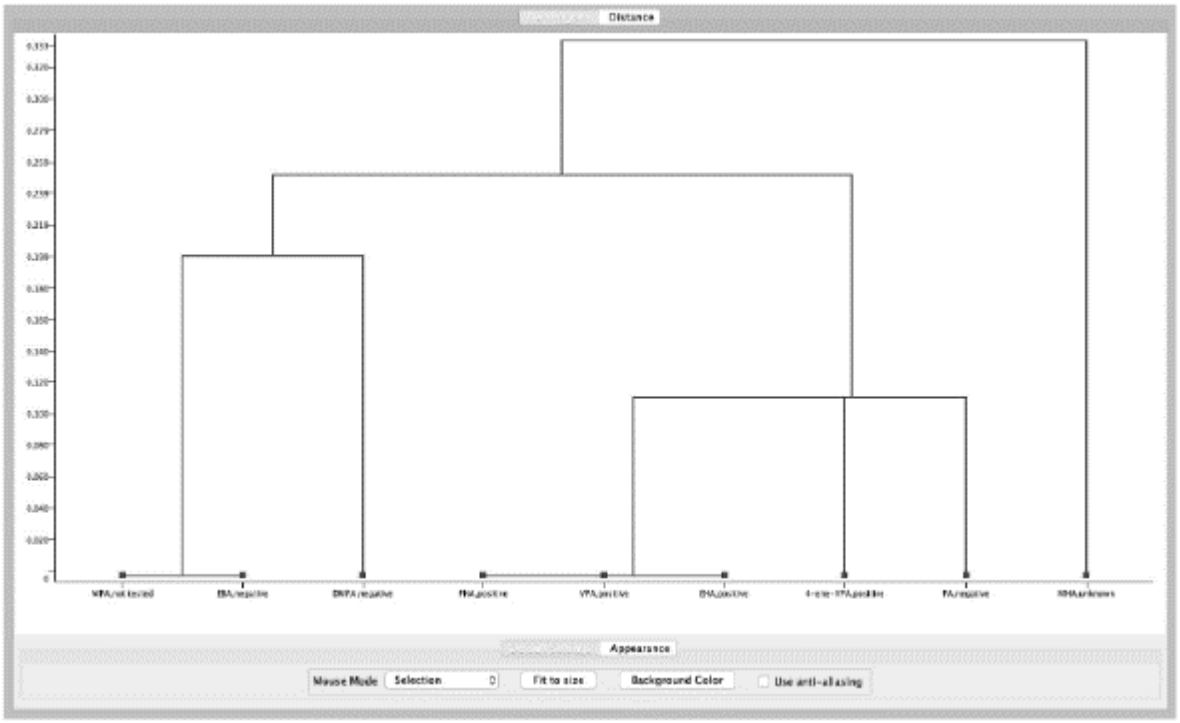

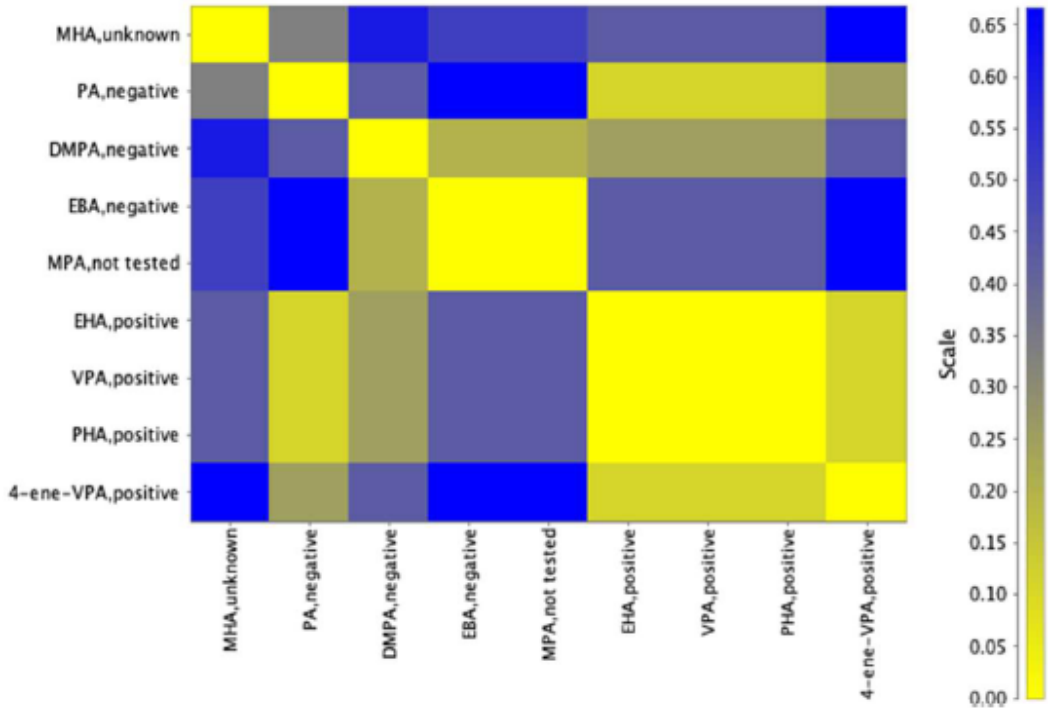

Scale….distance (Dice)

Key	MHAunknown	PAnegative	DMPAnegative	EBAnegative	MPAnot tested	EHApositive	VPApositive	PHApositive	4-ene-VPApositive
MHAunknown	0.00	0.33	0.60	0.50	0.50	0.43	0.43	0.43	0.67
PAnegative	0.33	0.00	0.43	0.67	0.67	0.11	0.11	0.11	0.25
DMPAnegative	0.60	0.43	0.00	0.20	0.20	0.25	0.25	0.25	0.43
EBAnegative	0.50	0.67	0.20	0.00	0.00	0.43	0.43	0.43	0.67
MPAnot tested	0.50	0.67	0.20	0.00	0.00	0.43	0.43	0.43	0.67
EHApositive	0.43	0.11	0.25	0.43	0.43	0.00	0.00	0.00	0.11
VPApositive	0.43	0.11	0.25	0.43	0.43	0.00	0.00	0.00	0.11
PHApositive	0.43	0.11	0.25	0.43	0.43	0.00	0.00	0.00	0.11
4-ene-VPApositive	0.67	0.25	0.43	0.67	0.67	0.11	0.11	0.11	0.00

Analysis 2:

Using single CALUX value + single **neurodevelopmental effects** value for ZET classic + single read out values mEST, UKN1, and ZET reporter

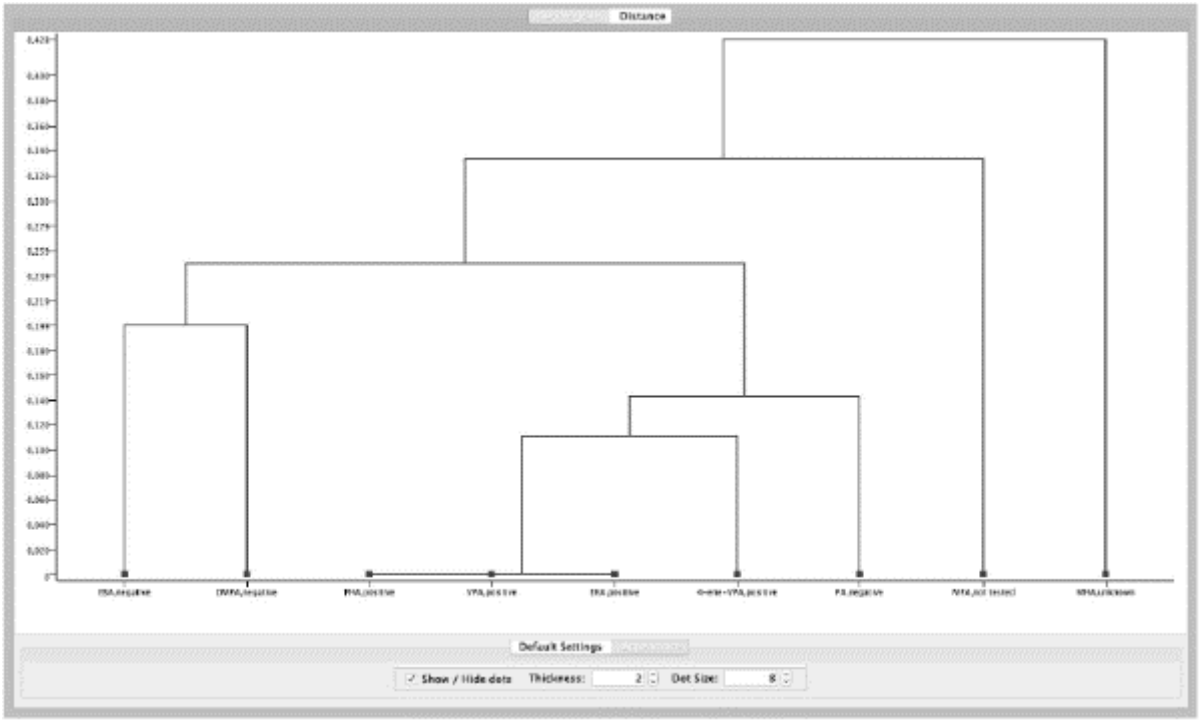

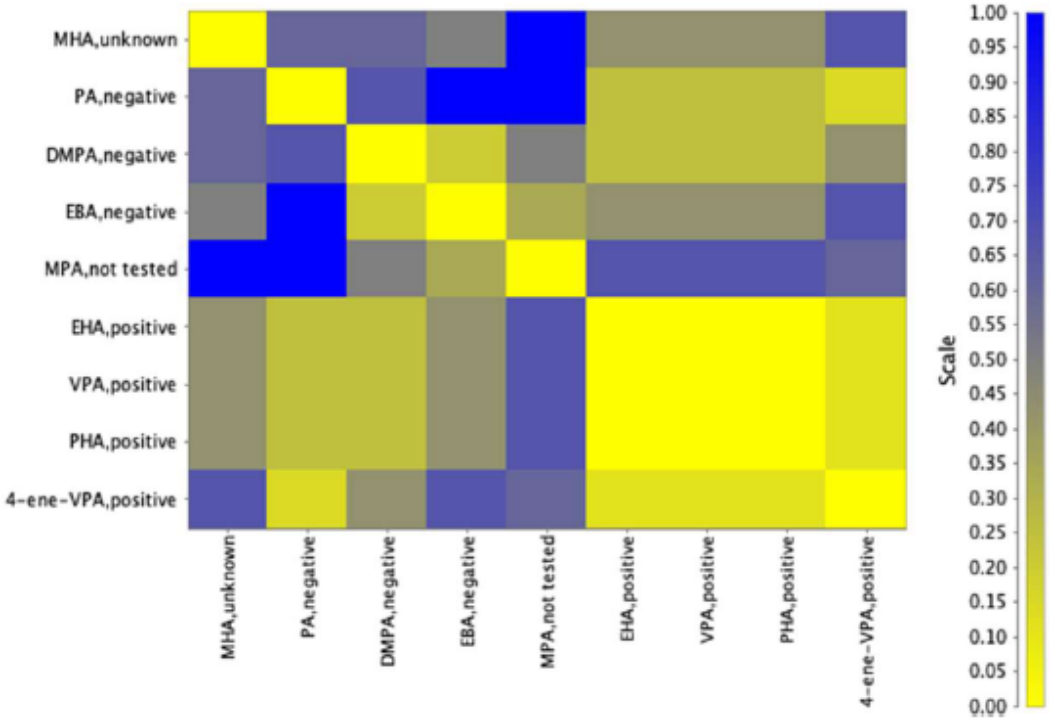

Scale….distance (Dice)

Key	MHAunknown	PAnegative	DMPAnegative	EBAnegative	MPAnot tested	EHApositive	VPApositive	PHApositive	4-ene-VPApositive
MHAunknown	0.00	0.60	0.60	0.50	1.00	0.43	0.43	0.43	0.67
PAnegative	0.60	0.00	0.67	1.00	1.00	0.25	0.25	0.25	0.14
DMPAnegative	0.60	0.67	0.00	0.20	0.50	0.25	0.25	0.25	0.43
EBAnegative	0.50	1.00	0.20	0.00	0.33	0.43	0.43	0.43	0.67
MPAnot tested	1.00	1.00	0.50	0.33	0.00	0.67	0.67	0.67	0.60
EHApositive	0.43	0.25	0.25	0.43	0.67	0.00	0.00	0.00	0.11
VPApositive	0.43	0.25	0.25	0.43	0.67	0.00	0.00	0.00	0.11
PHApositive	0.43	0.25	0.25	0.43	0.67	0.00	0.00	0.00	0.11
4-ene-VPApositive	0.67	0.14	0.43	0.67	0.60	0.11	0.11	0.11	0.00

Analysis 3:

Using single CALUX value + single **developmental effects** value for ZET classic + single read out values mEST, UKN1, and ZET reporter

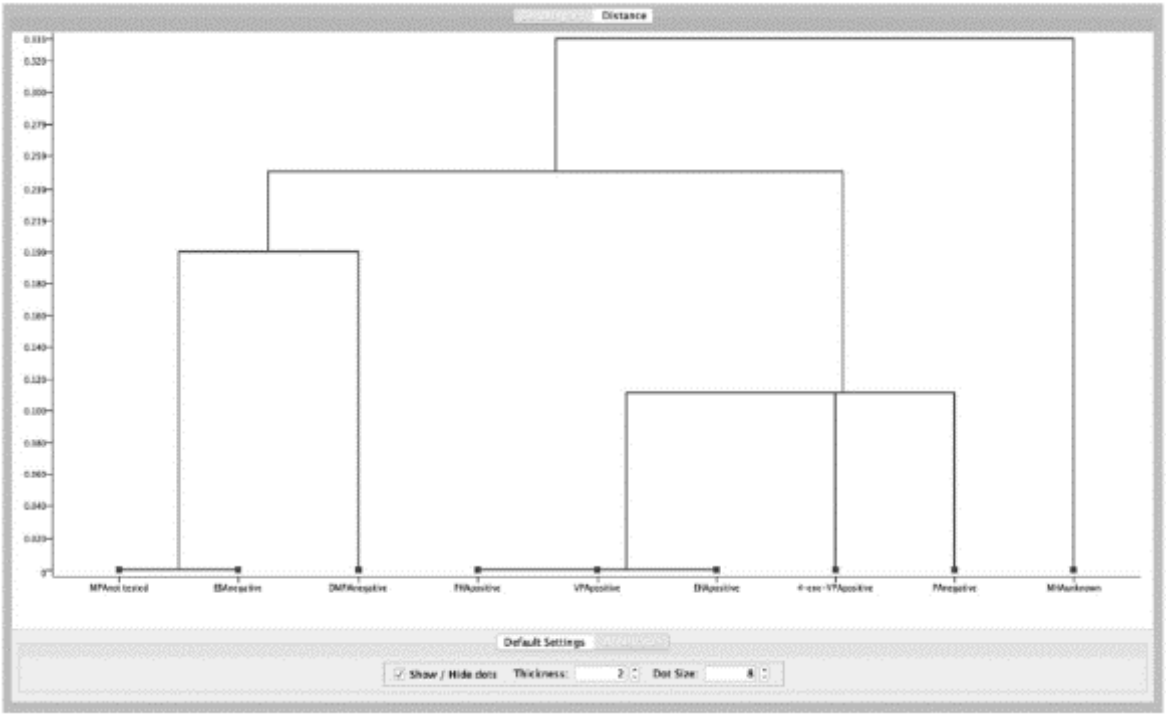

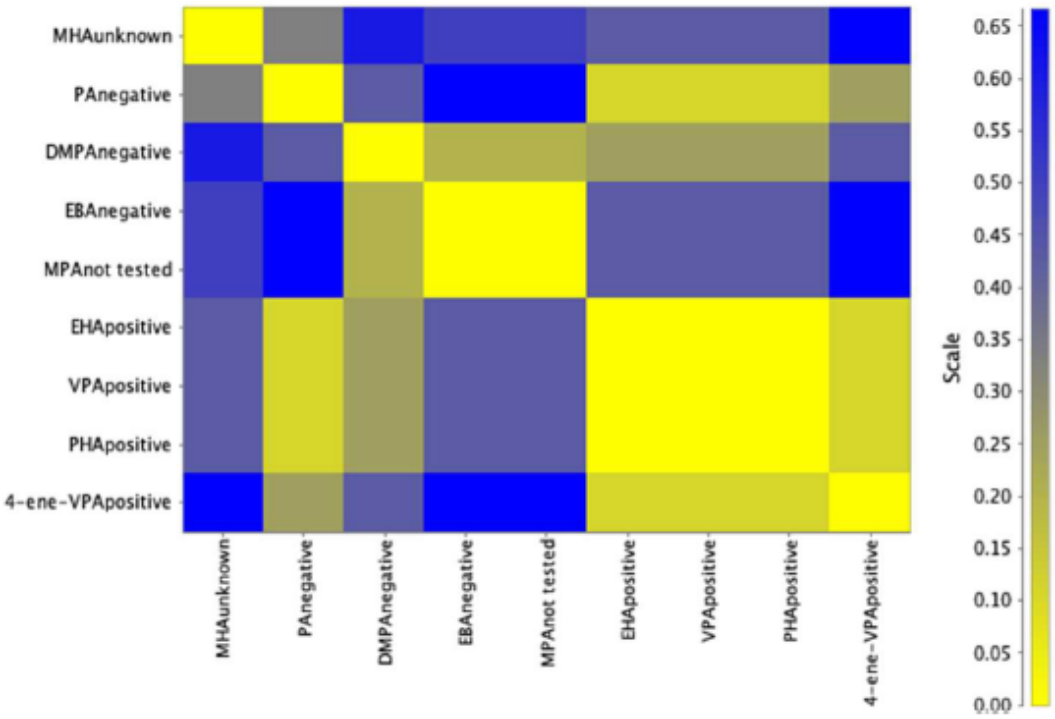

Scale….distance (Dice)

Key	MHAunknown	PAnegative	DMPAnegative	EBAnegative	MPAnot tested	EHApositive	VPApositive	PHApositive	4-ene-VPApositive
MHAunknown	0.00	0.33	0.60	0.50	0.50	0.43	0.43	0.43	0.67
PAnegative	0.33	0.00	0.43	0.67	0.67	0.11	0.11	0.11	0.25
DMPAnegative	0.60	0.43	0.00	0.20	0.20	0.25	0.25	0.25	0.43
EBAnegative	0.50	0.67	0.20	0.00	0.00	0.43	0.43	0.43	0.67
MPAnot tested	0.50	0.67	0.20	0.00	0.00	0.43	0.43	0.43	0.67
EHApositive	0.43	0.11	0.25	0.43	0.43	0.00	0.00	0.00	0.11
VPApositive	0.43	0.11	0.25	0.43	0.43	0.00	0.00	0.00	0.11
PHApositive	0.43	0.11	0.25	0.43	0.43	0.00	0.00	0.00	0.11
4-ene-VPApositive	0.67	0.25	0.43	0.67	0.67	0.11	0.11	0.11	0.00